Theoretical Studies on Microscopic Solvation for Complicated Systems: Reactions with Transition Metal Complexes and Chemical Phenomena in Ionic Liquids

Seigo Hayaki

2013

Preface

Solution is a typical phase in which many chemical processes proceed. Microscopic information on solution plays an important role to understand chemical phenomena. Nowadays various functional molecules are developed and chemical systems become complicated. The more complex reaction systems are, the more important realistic models to represent the system, especially solvation at the molecular level are. This is because the molecularity of solvent is often essential to describe complex chemical phenomena. In this thesis, based on real-system model the author studies solvation in complicated chemical systems: reactions with transition metal complexes and chemical phenomena in ionic liquids. These systems are representative in terms of their wide range of application and complexity. The theoretical description for these systems at the molecular level, however, has been very limited due to their complexity.

This thesis is composed of two parts and contains seven chapters. Chapter 1 and 7 are the general introduction and conclusions, respectively. In part I, with the aid of an integral equation theory, a.k.a. RISM, solvation effects in a catalytic reaction with transition metal complex is explored at the molecular level. In Chapter 2, the liquid structures of neat nitromethane, which is one of the typical reaction medium in catalytic reactions are investigated using RISM theory with the aid of molecular orbital theory. Chapter 3 presents a molecular level of study on solvation effects in the reaction of Pt(II) complex via S_N2 mechanism based on RISM-SCF-SEDD method. In part II, *ab initio* studies on chemical reactions in ionic liquids are exhibited. The extension of RISM-SCF-SEDD method to multi-component system realizes the treatment of a Diels-Alder (chapter 4) and S_N2 (chapter 5) reactions in ionic liquids, which consist bulky cation and anion. In chapter 6, the theoretical procedure is developed to incorporate the flexibility of side chains in constituent ions in conjunction with flexible-RISM and

applied to investigate an excited state intramolecular proton transfer reaction in ionic liquids.

The studies presented in this thesis were carried out at Department of Molecular Engineering, Graduate School of Engineering, Kyoto University from 2007 to 2013. The author wishes to express his sincere gratitude to Professor Hirofumi Sato for invaluable suggestions, fruitful discussions and shrewd advice on not only theoretical chemistry but also philosophies for science. All studies in this thesis could not be possible without his full cooperation. The author would like to express his deepest appreciation to Emeritus Professor Shigeyoshi Sakaki for his helpful advice and warm encouragement. Various comments based on theoretical, physical, and inorganic chemistry were invaluable for this study. The author also expresses gratitude to Associate Professor Yoshihide Nakao for his kind help on computational techniques and electronic structure theory. He also expresses sincere acknowledgement to Professor Yoshifumi Kimura (Hosei University) and Ms. Kayo Suda (Kyoto University) for their collaboration and kind discussions in Chapter 6.

The author is also grateful to Dr. Daisuke Yokogawa, Dr. Atsushi Ishikawa, Mr. Hideo Ando, Dr. Kentaro Kido, and Dr. Kenji Iida. Scientific talks with them on various occasions were very enjoyable and fruitful. Acknowledgment is also made to all members of the research group of Professor Hirofumi Sato and Emeritus Professor Shigeyoshi Sakaki. The discussions and school life with them were enjoyable and generated his motivation of this study.

The author would like to thank Emeritus Professor Hiroshi Nakatsuji and all members of his research group in Undergraduate School of Industrial Chemistry, Faculty of Engineering, Kyoto University. The author studied valence ionization of transition metal complexes to get bachelorship under the instruction for fundamental knowledge and techniques to research theoretical chemistry. The author wishes to express my gratitude for Professor Andriy Kovalenko and all members of his research group in National Institute for Nanotechnology (NINT), Alberta, Canada. Prof. Kovalenko gave me an invaluable opportunity to study the aggregation of huge aromatic compounds using 3D-RISM solvation theory and the author never forget the kind hospitality during his visit. Although these studies are not included in this thesis, the experiences and instructions are indispensable to complete it.

The author thanks Japan Society for the Promotion of Science (JSPS) for financial support (Fellowship for Japanese Junior Scientists) and the Global COE program “International Center for Integrated Research and Advanced Education in Material Science” for financial aid to visit NINT, Canada.

Finally, the author sincerely thanks his grandmother, Setsuko Arizono, his parents, Kimiyuki Hayaki and Yoko Hayaki, and his brothers, Hiroyuki Hayaki and Nobuyuki Hayaki for their understanding, encouragement, and continuous support from all sides.

Seigo Hayaki

December 2012

Contents

Chapter 1

General Introduction

Solution is a typical phase in which various chemical events occur. The surrounding solvent molecules play important roles to determine the reaction kinetics, yields, photo properties and so on. [1] Information on microscopic solvation is essential to understand chemical phenomena. Various functional molecules have been developed in recent years and their geometric and electronic structures have been more and more complicated. The more complex reaction systems are, the more realistic model to represent the system becomes important, especially solvation at the molecular level. This is because the molecularity of solvent is often essential to describe complicated chemical phenomena properly.

Because chemical systems in solution are composed of solute and solvent, the complexity is attributed to solute and/or solvent molecules. As examples of the complex solute systems, transition metal complexes, biomolecules, and photo-functional materials can be conceivable as shown in Figure 1.1. For solvent systems, ionic liquid, acid/base solution, and supercritical fluids can be exemplified. In this thesis, I wish to focus on two representative systems: transition metal complexes as solute and ionic liquid as solvent.

Transition metal complexes are utilized in the wide range of applications such as large scale industrial catalysts and fine systhetic tools in laboratory. In many cases of reaction with transition metal complex, changes in flexible electronic structure due to the *d* electrons in the metal center occur, accompanied with complex bond formation/dissociation, charge transfer, and coodination of solvent. [2–4] Ionic liquids are expected to be a kind of novel reaction media because various kinds of compounds are soluble, [5–8] though dielectric constant is not

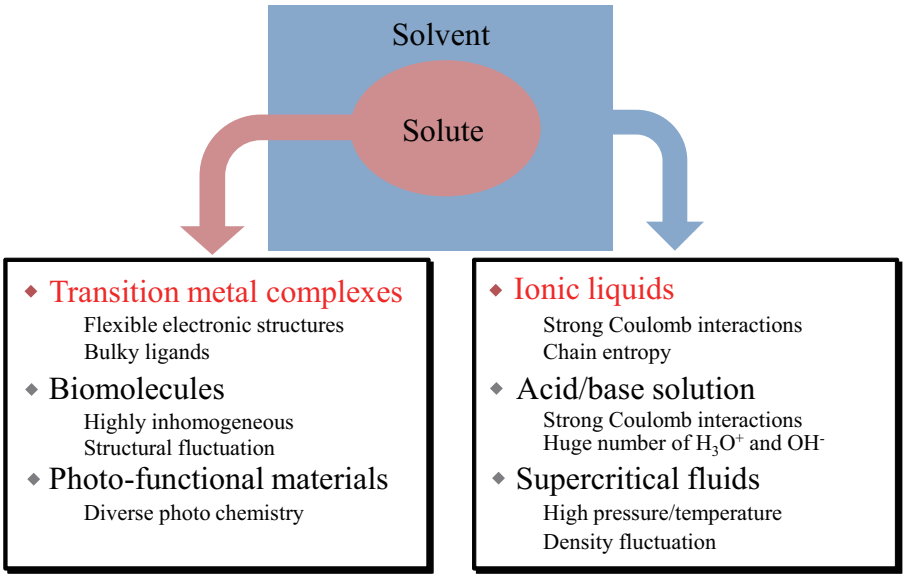

Figure 1.1: Examples for complex solute and solvent systems.

consistent with thermodynamic properties observed in reactions in ionic liquids. [6, 9]

Therefore in the chemical system composed of complicated solute and/or solvent, realistic models which reproduce molecularity of solvent are required. These complexity in the chemical systems, however, make it difficult to treat solvent with explicit model such as molecular simulations and thus studies based on realistic models have been very limited.

Before exhibiting brief surveys on reactions with transition metal complexes in solution and features of solvation in ionic liquids, I wish to introduce theoretical fundamentals and their characteristics in the present theoretical chemistry.

1.1 Methodologies for Chemical Phenomena in Solution

Because solution systems are composed of solute molecules (or reaction centers) and vast majority of solvent molecules, different level of theories are used to treat chemical phenomena in solution: The electronic structure solute molecule is described by Schrödinger equation. Solute–solvent and solvent–solvent interactions are expressed with electrostatic and Lennard-Jones interactions in the framework of classical physics. In this section, theoretical techniques on electronic structure theory, solvation models, and their hybrid methods are briefly summa-

rized.

1.1.1 Electronic structure theories

In order to obtain accurate electronic energy of many-electron system, electronic structure theories of wave function have been developed. Beyond Hartree-Fock (HF) method, in which the mean field approximation is assumed, [10, 11] the various kinds of highly accurate (post-HF) theories have been developed such as Møller-Plesset (MP) method, in which perturbation terms are added for the Fock operator, configuration interaction (CI) method, in which different electronic configurations are systematically introduced, and coupled cluster (CC) method, in which electronic configurations are efficiently incorporated with excitation operator acting on HF wave function (Figure 1.2)。

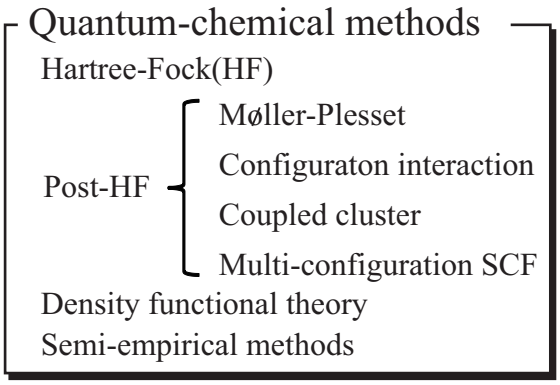

Figure 1.2: Representative quantum chemical methods.

The perturbations related to excitation configuration interaction are incorporated such as MPn($n = 2, 3, \dots$) methods, more accurate energy can be obtained in many cases as increasing n. * Taking into consideration of the higher terms demands larger computational cost.

Density functional theory (DFT) describes many-electron systems with its electron density instead of the wave function. [12] Owing to the introduction of molecular orbital concept by Kohn and Sham and the development of exchange-correlation functionals such as B3LYP, [12] the method becomes capable of providing reasonable energy and electronic properties compa-

*MP method often shows oscillating behavior in energy convergence as the perturbation order.

Table 1.1: Limiting scaling in terms of basis set size M_{BS} for various methods. [11] [a]

scaling	CI methods	MP methods	CC methods
M_{BS}^5	CIS	MP2	CC2
M_{BS}^6	CISD	MP3	CCSD
M_{BS}^7		MP4	CC3, CCSD(T)
M_{BS}^8	CISDT	MP5	CCSDT
M_{BS}^9		MP6	
M_{BS}^{10}	CISDTQ	MP7	

[a] The standard scaling of HF and DFT is M_{BS}^4.

rable to those by MP2 method with cheaper cost. Thus DFT is adopted in many computational studies in the present chemistry.

The above-mentioned methods assume single-configuration wave function. But it is often invalid in the case of the first period transition metal complexes. In this situation, multi-configuration method such as complete active space self-consistent field (CASSCF), in which not only the coefficients of the linear combination of the Slater determinants but also the molecular orbitals used for constructing the determinansts are optimized, is required. The theories explained so far are free from empirical parameter and thus called *ab initio* theory. The computational demands, however, tend to be large in *ab initio* calculations. Several semi-empirical methods, in which for example two-electron integrals are parametrized to reproduce experimental thermodynamic quantities, have been also proposed.

The computational cost of the electronic structure theories depends on the number of basis sets M_{BS} to describe wave functions (Table 1.1). Because the accuracy and cost are trade-off, CCSD(T) is practically utilized as the most sophisticated method.[†] HF and DFT methods, which need relatively small computational cost, are applied to π–π stacking systems composed of 200 atoms. [14] Several huge computations on a whole protein in a quantum fashion are also reported. [13]

[†]CCSD(T) method can be applied to molecules composed of at most 30 atoms at the present.

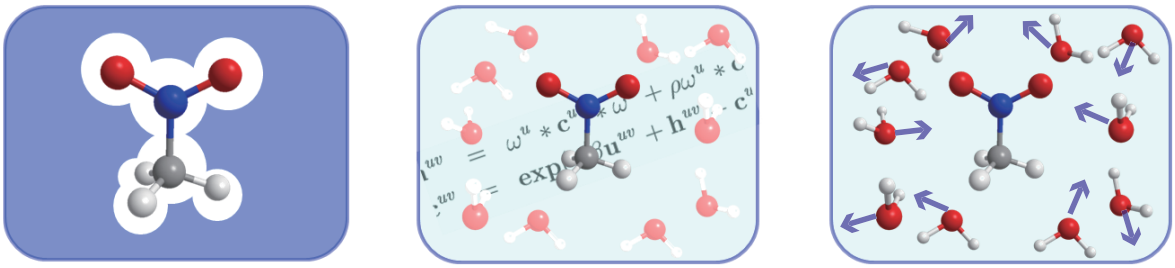

(a) (b) (c)

Figure 1.3: Schematic illustrations for solvation models. (a) dielectric continuum model, (b) integral equation theories, and (c) molecular simulation.

Table 1.2: Features of the solvation models.

	dielectric continuum model	IET	MS
computational cost	small	relatively small	large
molecularity of solvent	ignored	incorporated	incorporated

1.1.2 Solvation models

Because the vast majority of solvent molecules constitute solution systems, it is formidable to treat all molecules in a quantum mechanics. Hence various kinds of models based on diverse approximations have been proposed and utilized to describe the system. They can be classified into three categories: (a) dielectric continuum model, (b) integral equation theories (IETs), and (c) molecular simulation (MS) as shown in Figure 1.3. The features of the models are also summarized in Table 1.2.

Dielectric continuum model is the most concise one, in which molecularity of solvent is ignored and solvent is considered as continuum media with dielectric constant ϵ . [15–17] Due to the simplicity the model demands extremely cheap cost. On the other hand, local interaction such as hydrogen bond can not be taken into account in the model. For some solvents their dielectric constants ϵ do not reflect the polarity of solvation as discussed below.

The most straightforward approach is MS such as molecular dynamics or Monte Carlo methods, in which solvent configurations are generated in the framework of classical physics. [18]

The merit of the method is capability to provide both microscopic and macroscopic physical quantities by calculating ensemble average over solvent configurations. As an example, Figure 1.4 shows radial distribution functions (RDFs) representing liquid (or solvation) structure. RDFs describe how the density of atoms changes as a function of the distance r from a focused atom. The probability distributions in solid phase are expressed with very sharp spikes since atoms are fixed at a specific positions of crystal structure, while the functions in vapor phase show small change from a certain value because of their random movement. In solution, however, the functions are broaden because of thermal fluctuation as in the Figure. The peak positions of RDFs tell us insight into the structure of hydrogen bond network in pure water.

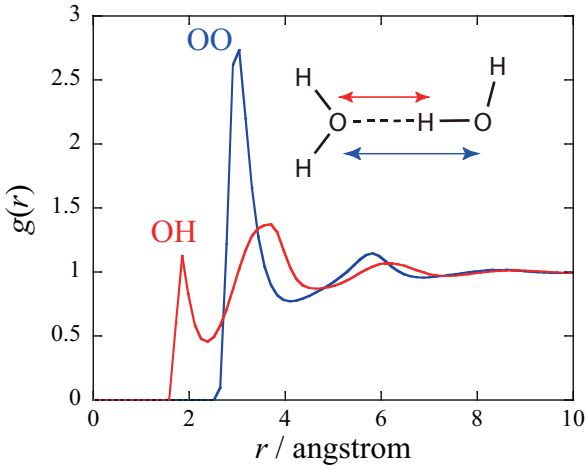

Figure 1.4: RDFs around a water oxygen atom. Red and blue indicate O–H and O–O RDFs, respectively.

In the procedure of MS, RDFs are obtained by calculating number of particles $\Delta N(r)$ in a spherical shell the distance between r and $r + \Delta r$, averaging it over the number of solvent configurations M.

$$g(r) = \frac{1}{4\pi r^2 \Delta r} \frac{V}{N} \langle \Delta N(r) \rangle = \frac{1}{4\pi r^2 \Delta r} \frac{V}{N} \frac{1}{M} \sum_{i}^{M} \Delta N_i(r), \tag{1.1}$$

where V is the box volume and N is the number of particles. When N and M are sufficiently large, MS calculation gives correct results in principle. In practice, $N(10^2 \sim 10^4)$ and

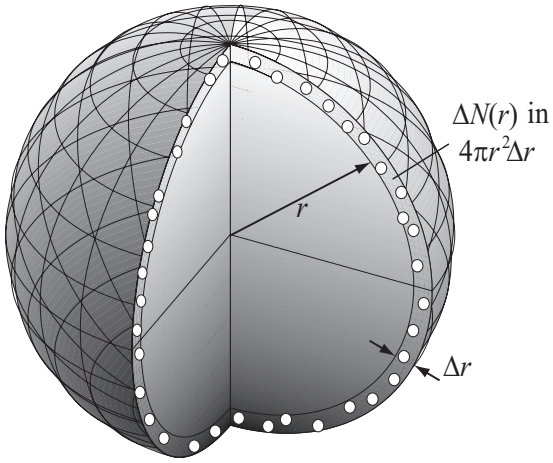

Figure 1.5: Schematic illustration for evaluation of RDFs in MS.

$M(10^6 \sim 10^8)$ are set to finite but computational demand is generally high. So-called sampling problem is inherent in MS.

The third model, IET, has intermediate character between dielectric continuum model and MS. In the framework of IET, certain solvent configurations are not explicitly generated but RDFs $g(r)$ are analytically calculated under approximation. [19, 20] Among IETs for molecular solvation, reference interaction site model (RISM) is the most prevailing one: [21, 22]

$$\boldsymbol{h} = \boldsymbol{\omega} * \boldsymbol{c} * \boldsymbol{\omega} + \boldsymbol{\omega} * \boldsymbol{c} * \boldsymbol{\rho h}, \tag{1.2}$$

where $\boldsymbol{h}$ and $\boldsymbol{c}$ denote the total and direct correlation functions, respectively. The former function is connected to RDF through the equation, $h(r) = g(r) - 1$. $\boldsymbol{\rho}$ is the number density and $\boldsymbol{\omega}$ is the intramolecular correlation function, which defines geometry of molecule. Thanks to its analytical treatment of correlation functions, the computational demand is relatively small and the method is free from the sampling problem.

1.1.3 Free energy based on hybrid method between electronic structure theory and solvation model

In order to handle chemical events with bond formation, dissociation or changes in electronic states in solution system, several hybrid methods of the electronic structure theory and solvation model have been proposed. A hybrid method of MS is called QM/MM (quantum

mechanical/molecular mechanical) method. [23, 24] The most popular hybrid with IETs is RISM-SCF [25–27] and one of the most sophisticated continuum model is PCM. [15–17] Each method inherits the characteristics of the corresponding solvation model described in the previous subsection. In particular, QM/MM method requires $10^6 \sim 10^8$ times electronic structure calculations, whose cost is huge. Because of the computational demands, semi-empirical methods are often adopted in QM/MM calculations. On the other hand, highly accurate *ab initio* theories such as CCSD(T) or CASSCF are applicable to PCM model or RISM-SCF.

Free energy, which is of primary importance to understand chemical phenomena in solution, can be calculated with different manners. In the framework of the hybrid methods, free energy $\mathscr{A}$ is defined as the sum of electronic energy of solute molecule in solution E_{sol} and solvation free energy $\Delta\mu$,

$$\begin{aligned} \mathscr{A} &= E_{\mathrm{sol}} + \Delta\mu & (1.3) \\ &= \left\langle \Psi_{\mathrm{sol}} | \hat{H} | \Psi_{\mathrm{sol}} \right\rangle + \Delta\mu, & (1.4) \end{aligned}$$

where Ψ_{sol} and $\hat{H}$ are wave function and electronic Hamiltonian of the solute, respectively.

For example, solvation free energy of PCM is defined as follows: [17]

$$\Delta\mu_{\mathrm{PCM}} = E_{\mathrm{es}} + E_{\mathrm{cav}} + E_{\mathrm{dis}} + E_{\mathrm{rep}}, \tag{1.5}$$

where E_{es}, E_{cav}, E_{dis}, and E_{rep} denote the electrostatic, cavaitation, dispersion, and repulsion energy, respectively. $\Delta\mu_{\mathrm{PCM}}$ can be easily computed since geometries and configurations of solvent molecules do not have to be considered explicitly.

In the framework of QM/MM method, solvation free energy $\Delta\mu_{\mathrm{QM/MM}}$ is defined in the same manner as MS: [18]

$$\Delta\mu_{\mathrm{QM/MM}} = -\frac{1}{\beta} \ln \int \mathrm{d}\mathbf{r}^N \exp\left\{-\beta U_{\mathrm{int}}(\mathbf{R}, \mathbf{r})\right\}, \tag{1.6}$$

where β is the inverse of the product of Boltzmann constant k_{B} and temperature T. U_{int} stands for the solute–solvent and solvent–solvent interaction potential energy. $\mathbf{R}$ and $\mathbf{r}$ denote the geometry and configuration of solute and solvent, indicating that the calculation demands huge cost because configuration integral over N solvent molecules is necessary. In the computation

of free energy, thermodynamic integration, in which changes between two states are sequencially calculated along the coupling parameter λ, and perturbation method, in which energy difference is calculated via sampling for only a reference state, are often adopted. More effective sampling approaches such as averaged solvent electrostatic potential from molecular dynamics (ASPD/MD), in which quantum chemical calculations are performed not in every solvent configurations but only in mean field potential generated by solvent (or surrounding molecules), have been developed. [17, 28]

In the case of RISM-SCF several formulae of solvation free energy in terms of correlation functions are analytically given. [26, 29] The most prevailing form is,

$$\Delta\mu_{\mathrm{RISM}} = -\sum_{\alpha}\sum_{\gamma}\frac{4\pi\rho_{\gamma}}{\beta}\int \mathrm{d}r r^2 \left\{\frac{1}{2}\left(h_{\alpha\gamma}(r)\right)^2 - c_{\alpha\gamma}(r) - \frac{1}{2}h_{\alpha\gamma}(r)c_{\alpha\gamma}(r)\right\}. \qquad (1.7)$$

α and γ correspond to the site in solute or solvent molecules, respectively. $h_{\alpha\gamma}(r)$ and $c_{\alpha\gamma}(r)$ can be obtained by analytically solving RISM equation. Therefore solvation free energy is free from statistical error and its computatonal demand is modest.

1.2 Reactions with Transition Metal Complexes in Solution

Transition metal complexes exhibit varieties of geometry, bonding nature, and reaction behavior, which often require quantum mechanical treatments. They are often ascribed to flexible electronic structure due to *d* electrons in transition metals. Theoretical studies of them are considerably important nowadays. [3, 4] In exploring the catalytic reactions with transition metal complexes, oxidative addition and reductive elimination play an essential role. [30, 31] As a simple example, the catalytic reactions composed of oxidative addition and reductive elimination to ketonize acyl chloride with rhodium complexes are known as shown in Scheme 1.1. [30]

Oxidative addition reaction can be classified three mechanics: concerted, S_N2-like, and radical mechanisms as shown in Scheme 1.2. [2, 30] It is well-known that solvation effects are significant in S_N2-like mechanism because of the polarization in transition metal complexes due to back donation from metal center to ligand. There are, however, two difficulties in theoreti-

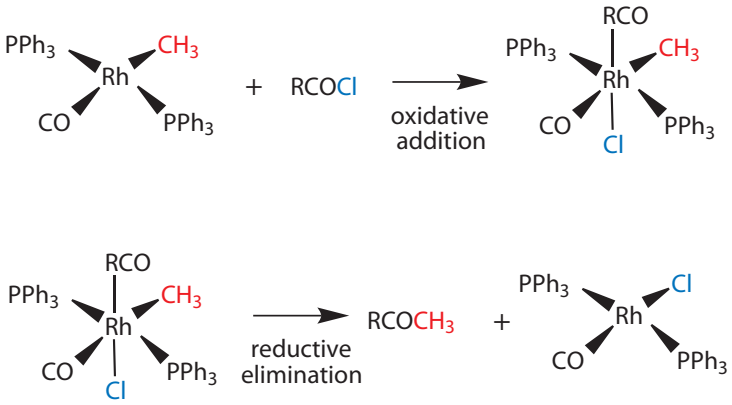

Scheme 1.1: Simple catalytic examples composed of oxidative addition and reductive elimination steps.

cal treatment of reactions with transition metal complxes: (i) complex eletctronic structure and bulky ligands tend to require high cost computations. (ii) Because the metal center is buried in the ligands, it is difficult to assign the effective charge that determines solute–solvent electrostatic interaction. In most preceding theoretical studies on reactions via S_N2-like mechanisms, solute molecule is treated in the isolated state or in dielectric continuum model. Theoretical investigation which explicitly treats solvent molecule has been very limited.

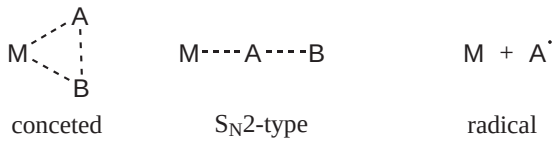

Scheme 1.2: Classification of oxidative addition reaction.

1.3 Solvation in Ionic Liquids

Ionic liquid, which consists of cation and anion as shown in Figure 1.3, is defined as a molten salt that melts below 100 °C. Experimental studies elucidate that ionic liquids have the following features: [5] (i) liquid phase in a wide range of temperature, (ii) due to their negligible vapor pressure, ionic liquids are applicable even in vacuum, (iii) incombustibility and stable in high temperature, (iv) high viscosity compared with conventional molecular liquids,

Table 1.3: Dielectric constants of several molecular liquids and ionic liquids.

	ϵ
Methanol	32.6
Typical ionic liquids	11-13
Dichloromethane	8.9

(v) high ion conductivity, and (vi) polarity of typical ionic liquids is comparable to that of lower alcohol.

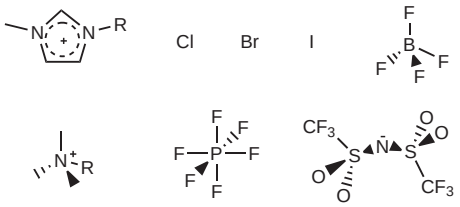

Scheme 1.3: Representative constituent ions of room-temperature ionic liquids.

Because various compound such as organometallics and cellulose are soluble in some ionic liquids in addition to the aforementioned features, [33] solvation mechanisms in ionic liquids attract many researchers both in experimental and theoretical fields. One of the most simple solvation model is dielectric continuum. It is, however, difficult to measure the dielectric constant of ionic liquid. While the dielectric constant of ionic liquid has been reported in recent years as shown in Table 1.3, their dielectric constants are ca. 12, which is close to dichloromethane. [5, 34] This contradicts the experimental observations that polarity of ionic liquids is comparable lower alcohol. Thus dielectric continuum model is oversimplified to mimic and discuss the solvation in ionic liquids. [6, 9]

Although molecularity of ionic liquids has to be incorporated, there are difficulty in theoretical treatment of ionic liquids. Ionic liquids are characterized by (i) strong Coulomb interactions among constituent ions and (ii) large entropic motion in flexible side chain inherent in many kinds of ionic liquids. Because of (i), mobility of the solvent molecules is much slower

than that of non-ionic solvent and due to (ii), it is difficult to obtain appropriate statistical average compared with conventional liquids. Furthermore, long-range electrostatic interaction makes the accurate evaluation difficult because a simple cutoff method is not applicable due to long Debye length. Although QM/MM studies with semi-empirical method have been performed, [35] theoretical studies based on *ab initio* theory is very limited.

1.4 Aims of This Thesis

In this thesis, the author wishes to report theoretical studies based on realistic molecular model for solvation mechanisms in complex chemical systems: reactions with transition metal complexes and chemical phenomena in ionic liquids.

In part I, chapter 2 and 3, the author investigated solvation effects in an oxidative addition reaction of Pt(II) complex in terms of microscopic liquid structure of nitromethane solvent media and solvation structure of nitromethane around the solute.

In chapter 2, liquid structure of neat nitromethane obtained by RISM theory was assigned to dimer structures obtained by MP2 method. Nitromethane is one of the polar organic solvent (ϵ = 37.5) and displayed significant solvation effects in the aforementioned reaction of Pt(II) complexes. It was argued that the high polarity is attributed to large dipole moment due to the strong electron withdrawing nature of nitro group. It was also disputed whether hydrogen bond between C–H$\cdots$O–N plays an important role in determining liquid structure or not. [36] The purposes of chapter 2 are to present detailed analysis on the liquid structure of nitromethane and to elucidate the factor governing the liquid structure.

In chapter 3, solvation effects of nitromethane solvent for the oxidative reaction of methyliodide to $PtMe_2(NH_3)_2$ were studied with RISM-SCF-SEDD method. Experimental studies have shown that the reaction proceeds via S_N2-like mechanisms as shown in Scheme 1.4 and is accelerated in polar solvent by 10 times compared in weakly polar solvent. [37] The reaction path, however, is still unclear, namely two different paths are plausible after the addition of methyl group: (i) the iodide anion dissociates from the reaction center or (ii) the iodide an-

ion moves around the platinum complex due to the strong Coulombic interaction between the charged species. The purposes of this chapter are to assess the solvation effects in determining not only barrier height but also reaction path and to clarify microscopic solvation mechanisms for the first time as a reaction with transition metal complex.

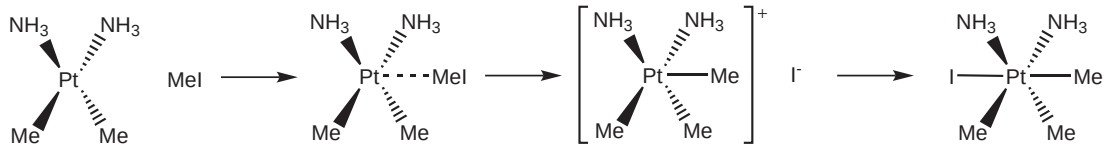

Scheme 1.4: Oxidative addition reaction of methyliodide to $PtMe_2(NH_3)_2$.

Part II consists of chapters 4, 5, and 6. In this part, the author explored the solvation mechanisms in chemical phenomena in ionic liquids using multi-component RISM-SCF-SEDD method utilized *ab initio* electronic structure theories.

In chapter 4, the Diels-Alder reaction of cyclopentadiene (CP) with methyl acrylate (MA) which provides *endo* and *exo* mixture (Scheme 1.5) in a standard ionic liquid, 1-3-dimethylimidazolium chloride ([mmim][Cl][‡]) is studied. The *endo-exo* selectivity is sensitive to solvent polarity and typical ionic liquids exhibit the modest polarity: the polarity of [mmim][Cl] is weaker than that of water and stronger than dimethyl ether. [38] It is nontrivial that ionic liquids show modest polarity regardless of their strong Coulomb interactions among constituent ions. The purposes of chapter 4 are to shed light on the origin of modest polarity of ionic liquids and mechanisms of *endo-exo* selectivity in the reaction.

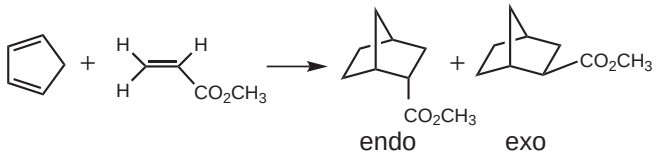

Scheme 1.5: Diels-Alder reaction of CP and MA.

[‡]In the thesis, the name of imidazolium cations are represented with the initial letters of alkyl chains as in ref. [5]: for example, 1-**m**utyl-3-**m**ethyl **im**idazolium and 1-**b**utyl-3-**m**ethyl **im**idazolium cations are abbreviated as [mmim] and [bmim], respectively.

Chapter 5 describes a study on an S_N2 reaction of *p*-nitrobenzenesulfonate (*p*-NBS) with chloride anion in [mmim][PF_6] (Scheme 1.6) employing highly sophisticated CCSD method. From the thorough measurement of thermodynamic properties and neutron diffraction studies, it is proposed that the de-solvation of chloride anion makes it possible to act as a nucleophile and give rise to the reaction. [39, 40] The purposes in chapter 5 are to elucidate the reaction mechanism by presenting the changes in solvation free energy and solvation structure along the reaction. The limitation of the rigid model inherent in conventional RISM theory is also examined.

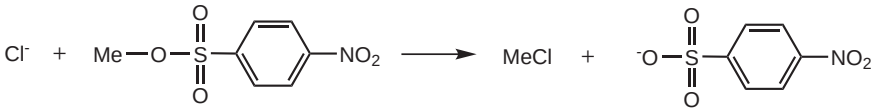

Scheme 1.6: S_N2 reaction of methyl *p*-NBS and chloride anion.

In chapter 6, the author investigated an excited-state proton transfer reaction of 4′-N,N-diethylamino-3-hydroxyflavone (DEAHF) in a typical ionic liquid, 1-butyl-3-methylimidazolium hexafluorophosphate ([bmim][PF_6]) by utilizing RISM-SCF-SEDD method in conjunction with flexible-RISM theory, in which geometrical fluctuation of solvent molecules is incorporated. It is well known that ionic liquids exhibit a wide range of solvation dynamics from sub ps to ns time scales and rapid reaction process such as electron or proton transfer reaction is affected by solvent relaxation. Basically the ESIPT kinetics of DMAHF in RTILs (Scheme 1.7) is similar to those in conventional solvent, however, it should be noted that the dependency of the proton-transfer rate on the excitation wavelength was observed. [41] Regardless of the advances in the experimental field, the microscopic view of proton transfer in ionic liquids is still unclear. The purposes of this chapter is to analyze the relation between solvent relaxation and proton transfer process at the molecular level.

Through these studies, the author wishes to present deep understanding of solvation effects in chemical systems composed of complex solute or solvent molecules and provide the microscopic view to their mechanisms.

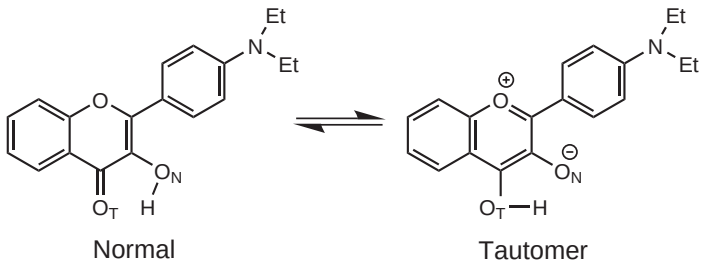

Scheme 1.7: Excited-state intramolecular proton transfer reaction of DEAHF.

Bibliography

[1] *Solvents and Solvent Effects in Organic Chemistry, 3rd ed.*; Reichardt, C.; Wiley-VCH; Weinheim, Germany, 2003.

[2] *Principles and Applications of Organotransition Metal Chemistry*; Collman, J. P.; Hegedus, L. S.; Norton, J. R.; Finke, R. G.; University Science Books: Mill Valley, CA, 1987.

[3] *Computational Modeling for Homogeneous and Enzymatic Catalysis*; Morokuma, K.; Musaev, J.; Wiley-VCH: Weinheim, Germany, 2008.

[4] Sakaki, S; Ohnishi, Y.; Sato, H. *Chem. Record* **2010**, *10*, 29.

[5] *Ionic Liquids in Synthesis* 2nd ed.; Welton, T.; Wasserscheid, P. Eds.; VCH-Wiley: Weinheim, Germany, 2008.

[6] Weingärtner, H. *Angew. Chem. Int. Ed.* **2008**, *47*, 654.

[7] Castner, E. D.; Wishart, J. F. *J. Chem. Phys.* **2010**, *132*, 120901.

[8] Castner, E. W. Jr.; Margulis, C. J.; Maroncelli, M; Wishart, J. F. *Annu. Rev. Phys. Chem.* **2011**, *62*, 85.

[9] Kobrak, M. N. *J. Phys. Chem. B* **2007**, *111*, 4755.

[10] *Modern Quantum Chemistry: Introduction to Advanced Electronic Structure Theory*; Szabó, A.; Ostlund, N. S.; Dover; New York, U.S.A. 1989.

[11] *Introduction to Computational Chemistry* 2nd ed.; Frank, J.; Wiley: Weinheim, Germany, 2007.

[12] *A Chemist's Guide to Density Functional Theory* 2nd ed.; Koch, W.; Holthausen, M. C.; Wiley: Beinheim, Germeny, 2001.

[13] Inaba, T.; Tsunekawa, N.; Hirano, T.; Yoshihiro, T.; Kashiwagi, H.; Sato F. *Chem. Phys. Lett.* **2007**, *434*, 331.

[14] Grimme, S.; Antony, J.; Ehrlich, S.; Krieg, H. *J. Chem. Phys.* **2010**, *132*, 154104.

[15] Tomasi, J.; Persico, M. *Chem. Rev.* **1994**, *94*, 2027.

[16] Cramer, C; Truhlar, D. *Chem. Rev.* **1999**, *99*, 2161.

[17] *Continuum Solvation Models in Chemical Physics: From Theory and Applications*; Mennucci, B.; Cammi, R.; Wiley: West Sussex, England, 2007.

[18] *Understanding Molecular Simulation* 2nd ed.; Frenkel, D.; Smit, B.; Academic Press: London, England, 2002.

[19] *Theory of Simple Liquids* 3rd ed.; Hansen, J.-P.; McDonald, I. R.; Academic Press: London, England, 2005.

[20] *Molecular Theory of Solvation* ; Hirata, F. Eds.; Kluwer Academic Publishers: Netherlands, 2003.

[21] Chandler, D.; Anderson, H. C. *J. Chem. Phys.* **1972**, *57*, 1930.

[22] Hirata, F.; Rossky, P. J. *Chem. Phys. Lett.* **1981**, *83*, 329.

[23] Gao, J. *Acc. Chem. Res.* **1996**, *29*, 298.

[24] Senn, H. M.; Thiel, W. *Angew. Chem. Int. Ed.* **2009**, *48*, 1198.

[25] (a) Ten-no, S.; Hirata, F.; Kato, S. *Chem. Phys. Lett.* **1993**, *214*, 391. (b) Ten-no, S.; Hirata, F.; Kato, S. *J. Chem. Phys.* **1994**, *100*, 7443.

[26] Sato, H.; Hirata, F.; Kato, S. *J. Chem. Phys.* **1996**, *105*, 1546.

[27] (a) Yokogawa, D.; Sato, H.; Sakaki, S. *J. Chem. Phys.* **2007**, *126*, 244054. (b) Yokogawa, D.; Sato, H.; Sakaki, S. *J. Chem. Phys.* **2009**, *131*, 214504.

[28] Sanchez, M. L.; Aguilar, A.; Olivares del Valle, F. J. *J. Comput. Chem.* **1997**, *18*, 313.

[29] Singer, S. J.; Chandler, D. *Mol. Phys.* **1985**, *55*, 621.

[30] *Inorganic Chemistry*; Shriver, D. F.; Atkins, P. W.; UOxford University Press: England, 1999.

[31] (a) Low, J. J.; Goddard, W. A, III *J. Am. Chem. Soc.* **1984**, *106*, 6928. (b) Low, J. J.; Goddard, W. A, III .*J. Am. Chem. Soc.* **1984**, *106*, 8321. (c) Low, J. J.; Goddard, W. A, III *Organometallics* **1986**, *5*, 609. (d) Low, J. J.; Goddard, W. A, III .*J. Am. Chem. Soc.* **1986**, *108*, 6115.

[32] (a) Griffin, T. R.; Cook, D. B.; Haynes, A.; Pearson, J. M.; Monti, D.; Morris, G. E. *J. Am. Chem. Soc.* **1996**, *118*, 3029. (b) Cheong, M.; Ziegler, T. *Organometallics* **2005**, *24*, 3053. (c) Feliz, M.; Freixa, Z.; van Leeuwen, P. W. N. M.; Bo, C. *Organometallics* **2005**, *24*, 5718. (d) Kégl, T.; Kollár, L. *J. Organomet. Chem.* **2007**, *692*, 1852.

[33] Swatloski, R. D.; Spear, S. K.; Holbrey, J. D.; Rogers, R. D. *J. Am. Chem. Soc.* **2002**, *124*, 4974.

[34] Weingartner, H.; Sasisanker, P.; Daguenet, C.; Dyson, P. J.; Krossing, I.; Slattery, J. M.; Schubert, T. *J. Phys. Chem. B* **2007**, *111*, 4775.

[35] (a) Acevedo, O. ; Jorgensen, W. L.; Evanseck, J. D. *J. Chem. Theor. Comput.* **2007**, *3*, 132. (b) Sambasivarao, S. V.; Acevedo, O. *J. Chem. Theor. Comput.* **2009**, *5*, 1038. (c) Arantes, G. M.; Ribeiro, M. C. C. *J. Chem. Phys.* **2008**, *128*, 114503. (d) Yockel, S.; Schatz, G. C. *J. Phys. Chem. B* **2010**, *114*, 14241. (e) Li, X.; Schatz, G. C.; Nesbitt, D. J. *J. Phys. Chem. B* **2012**, *116*, 3587.

[36] (a) Seminario, J. M.; Concha, M. C.; Politzer, P. *J. Chem. Phys.* **1995**, *102*, 8281. (b) Alper, H. E.; Abu-Awwad, F.; Politzer, P. *J. Phys. Chem. B* **1999**, *103*, 9738. (c) Sorescu,

D. C.; Rice, B. M.; Thompson, D. L. *J. Phys. Chem. A* **2001**, *105*, 9336. (d) Megyes, T.; Bálint, S.; Grósz, T.; Radnai, T.; Bakó, I. *J. Chem. Phys.* **2007**, *126*, 164507.

[37] (a) Jawad, J. K.; Puddephatt, R. J. *J. Organomet. Chem.* **1976**, *117*, 297. (b) Rendina, L. M.; Puddephatt, R. J. *Chem. Rev.* **1997**, *97*, 1735.

[38] (a) Jaeger, D. A.; Tucker, C. E. *Tetrahedron Lett.* **1989**, *30*, 1785. (b) Fischer, T.; Sethi, A. R.; Welton, T.; Woolf, J. *Tetrahedron Lett.* **1999**, *40*, 793. (c) Aggarwal, A.; Lancaster, N. L.; Sethi, A. R.; Welton, T. *Green Chem.* **2002**, *4*, 517. (d) Vidiš, A.; Ohlin, C. A.; Laurenczy, G.; Küsters, E.; Sedelmeier, G.; Dyson, P. J. *Adv. Synth. Catal.* **2005**, *347*, 266.

[39] (a) Lancaster, N. L.; Welton, T.; Young, G. B. *J. Chem. Soc., Perkin Trans.* **2001**, *2*, 2267. (b) Lancaster, N. L.; Salter, P. A.; Welton, T.; Young, G. B. *J. Organomet. Chem.* **2002**, *67*, 8855. (c) Lancaster, N. L.; Welton, T. *J. Organomet. Chem.* **2004**, *69*, 5986.

[40] Hardacre, C.; Holbrey, J. D.; McMath, S. E. J.; Bowron, D. T.; Soper, A. K. *J. Chem. Phys.* **2003**, *118*, 273.

[41] (a) Fukuda, M.; Terazima, M.; Kimura, Y. *Chem. Phys. Lett.* **2008**, *463*, 364. (b) Kimura, Y.; Fukuda, M.; Suda, K.; Terazima, M *J. Phys. Chem. B* **2010**, *114*, 11847. (c) Suda, K.; Terazima, M; Kimura, Y. *Chem. Phys. Lett.* **2012**, *531*, 70.

Part I

Microscopic Solvation in Reactions of Transition Metal Complexes

Chapter 2

A Theoretical Study of the Liquid Structure of Nitromethane with RISM Method

2.1 Introduction

Nitromethane is one of the simplest nitro-compounds and is liquid at ordinary condition. The substance is extremely versatile: Not only a typical solvent used for cleaning process and reaction media but also an intermediate in organic synthesis of various chemicals. The liquid has been extensively used for many industrial applications deeply related to our lives. Furthermore, nitromethane is known as its explosive properties: it burns easily and used as fuel. Due to its high-performance and reduced-toxicity, it has been known as a storable monopropellant having a prospects of use for space thrusters [1]. Because of these factors, the cellular structure of detonations in liquid nitromethane [2], and burning behaviour have been reported by means of computational modelling. But the molecular level information of the liquid has not been provided from these studies.

Concerning physicochemical character of this molecule, it is highly polar solvent (ε=37.5), which is slightly smaller than dimethyl sulfoxide (47.2), glycerol (46.5) and comparable to acetonitrile (36.6). A high ε may attribute to higher dipole moment of the molecule (μ=3.46D). It is conceivable that the nitro group draws electron and this intramolecular charge-deviation is responsible for the intermolecular interaction. It has been argued that the existence of the hydrogen boding between C–H$\cdots$O–N in liquid nitromethane. At the same time, it is likely that the dispersion interaction between nitro groups might also contribute to the characterization of the liquid structure. Very recently, a direct observation of the liquid structure was achieved by

x-ray and neutron diffraction, together with Car-Parrinello simulation [3]. There are also a few molecular simulation studies [4–6], but the detailed characterization of the liquid structure is still unclear.

Reference interaction site model (RISM) is an integral equation theory for molecular liquids [7,8]. Unlike molecular simulation methods such as molecular dynamics and Monte Carlo, the integration over the configurational space of liquid in RISM theory is performed in an analytic way and the computational cost is dramatically reduced compared to the simulations. It is more important that integral equation theory can offer constructional and systematic understanding of solvation phenomena. RISM has been also combined with *ab initio* molecular orbital (MO) theory (RISM-SCF) [9–11]. It determines the electronic structure of a solute and the solvent distribution around it in a self-consistent manner, successfully applied to various chemical processes in solution phase such as organometallic reaction in solution phase [12].

In the present study, the liquid structure of nitromethane is discussed by means of RISM theory. Results from *ab initio* MO computations are also incorporated to analyze the liquid structure. Note that RISM and MO computations were separately employed in this study.

2.2 Method

In this work, two set of parameters ("Set A" and "Set B") were examined for the intermolecular interaction. One of them is the same as that in our previous study [12], where nitromethane was used as solvent. The standard Lennard-Jones 12-6 potential plus Coulombic interaction was used and the parameters were determined from the OPLS parameter set [13] and from the set reported by Alper et al. [5].

$$E = \frac{qq'}{r} + 4\epsilon \left[\left(\frac{\sigma}{r} \right)^{12} - \left(\frac{\sigma}{r} \right)^{6} \right]. \tag{2.1}$$

The venerable Lorentz-Berthelot mixing rule ($\sigma_{AB} = (\sigma_A + \sigma_B)/2$ and $\epsilon_{AB} = \sqrt{\epsilon_A \epsilon_B}$) was employed to construct the potential as collected in Table 2.1. The main difference between the two is the charge assigned on carbon atom.

The number density (ρ) was assumed to be 0.0112464 molecules/Å^3, equal to the exper-

Table 2.1: Lennard-Jones parameters for nitromethane solvent.

	Set A			Set B		
Atom	σ/Å	ϵ/kcal mol^{-1}	$q/\|e\|$	σ/Å	ϵ/kcal mol^{-1}	$q/\|e\|$
N	3.250	0.120	0.540	3.562	0.200	0.717
O	2.960	0.170	-0.370	2.999	0.120	-0.406
C	3.500	0.066	0.020	3.809	0.080	-0.331
H	2.500	0.015	0.060	2.327	0.022	0.142

imental value (1.14 g/cm^3), and temperature was set to 298.15 K. RISM calculations were carried out to obtain the structure of liquid nitromethane on a grid of 4096 points using the hyper netted chain (HNC) closure approximation. In the RISM calculation, the rotation of methyl group around C–N bond can not be treated and the dihedral angles of H–C–N–O are fixed at 0°(H_A) and $\pm$120°(H_B). As shown below, however, the rigid-molecule approximation seems to have no affect on the discussion. All the RISM computations were performed by our own developing program package.

On the analysis of liquid structure obtained from RISM computations, standard *ab initio* MO computations were performed by using the Gaussian 03 suite of programs [14]. Several geometrical structures of nitromethane dimer were optimized at MP2 level using 6-31++G** basis set.

2.3 Results and Discussion

2.3.1 Optimized Structure of Dimer

To understand the mutual orientation of nitromethane molecules, standard *ab initio* MO calculations of the dimer system were performed. Two optimized structure (I and II) were obtained in gas phase as shown in Figure 2.1. Structure I is antiparallel arrangement of the dimer, while in structure II nitromethanes arrange in head-to-tail conformation. The potential energy difference between them is not so large and the structure I is more stable than II by 3.88 kcal/mol. The free energy difference between them is further small, no more than 0.52 kcal/mol. The reduction of the free energy difference arises from entropic contribution, espe-

cially from vibrational correction term. Li and co-workers have been reported a DFT (B3LYP) study for the same dimer [15], in which the four different structures were shown as possible stable geometries. In our case, optimization by MP2 method eventually arrive at the aforementioned one of two structures even when starting from their reported structures. Megyes et al. also showed optimization result [3], but only the structure I was reported.

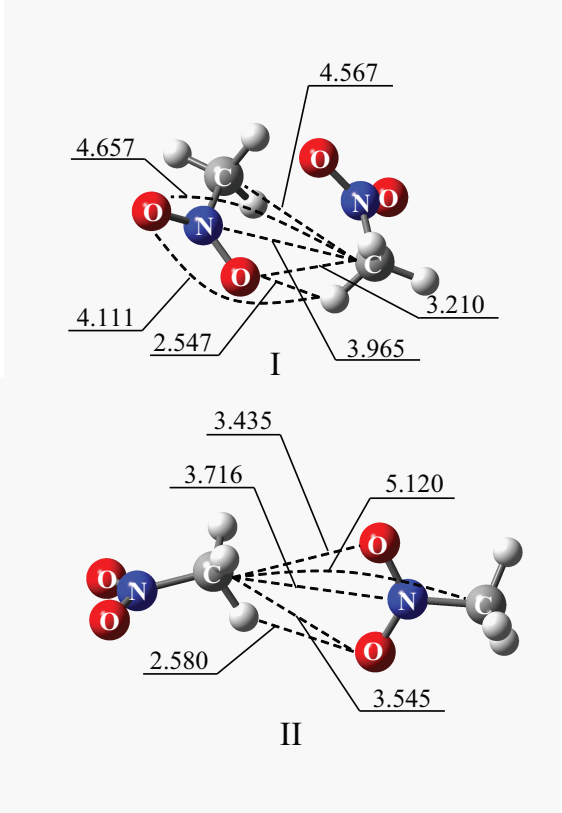

Figure 2.1: Optimized structures of nitromethane dimers. I and II are the antiparallel arrangement and head-to-tail conformation, respectively. Important interatomic distances are given in Å.

2.3.2 Structure of Liquid Nitromethane

In the framework of RISM theory, solvation structure is described in terms of radial distribution functions (RDFs). Note that the same function is also called as pair correlation function (PCF) because site-site pair is treated in RISM theory. The PCF represents the probability to find two atoms at a distance r and provides insight into the specific interactions in liquids.

The PCF computed with Set A is shown in Figure 2.2. The profiles of the function resemble the results of previous simulation studies [3–6]. The interatomic distances in these optimized structures are indicated in the figure with the white arrows (I) and black arrows (II). Almost all peak positions in PCFs coincide with the interatomic distances either one or two optimized structures mentioned above.

The C–C PCF

The C–C PCF rises around 3.0 Å and gradually reaches the bleary peak (5.2 Å). A shoulder is also seen around 4.0 Å. In the optimized structures, distances between two carbon atoms are respectively 4.6 and 5.1 Å, being slightly deviated from the PCF peak.

Compared to the previous simulations, the height of the shoulder look slightly lower. In the present work, there are two sources that makes the PCFs different from the previous ones. One is to perform RISM, in which different concept and procedure are used from standard molecular simulations. The statistical ensemble in RISM is appropriate but the theory is, at the same time, an approximation because the HNC is regarded as a truncated form of the $\log[\rho^{(1)}(1|\phi)/z^{*}(1)]$ expansion [16]. The other is a difference in the parameter set describing the solvent. In Figure 2.3, the same PCFs by using Set B are plotted [5]. The positions of peaks are not changed and liquid structures look very similar. However, the peak heights are slightly elevated at C–O and C–N pairs compared to Set A. The shoulder of C–C pair at 4.0 Å is obviously enhanced.

By integrating the C–C PCF up to the first minimum, the coordination number is computed as 14.1 both from Set A and B, which shows reasonable agreement with the previous report by Sorescu and co-workers; 12.8 [6]. Note that their parameters were originally prepared for crystalline nitromethane.

The O–H PCF

O–H PCF shows a peak around 2.5 Å (Figure 2.2), which is close to the sum of Lennard-Jones parameters, (σ_{O}+σ_{H})/2=2.73 Å. This indicates that oxygen and hydrogen atoms are directly contacted, but the peak height is lower than that of typical hydrogen bonding found in

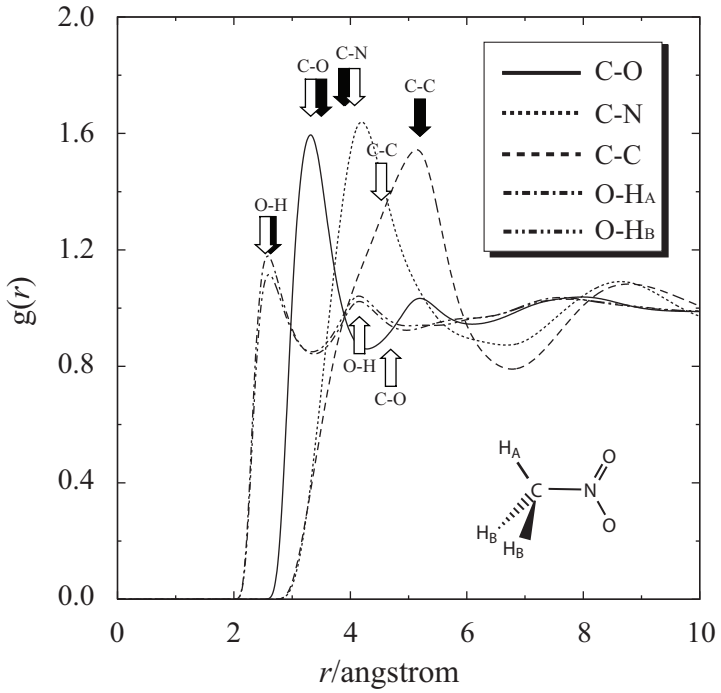

Figure 2.2: PCFs for the C–O, C–N, C–C, and O–H. White arrows and black arrows indicate the interatomic distances in structure I and structure II, respectively. See text for details.

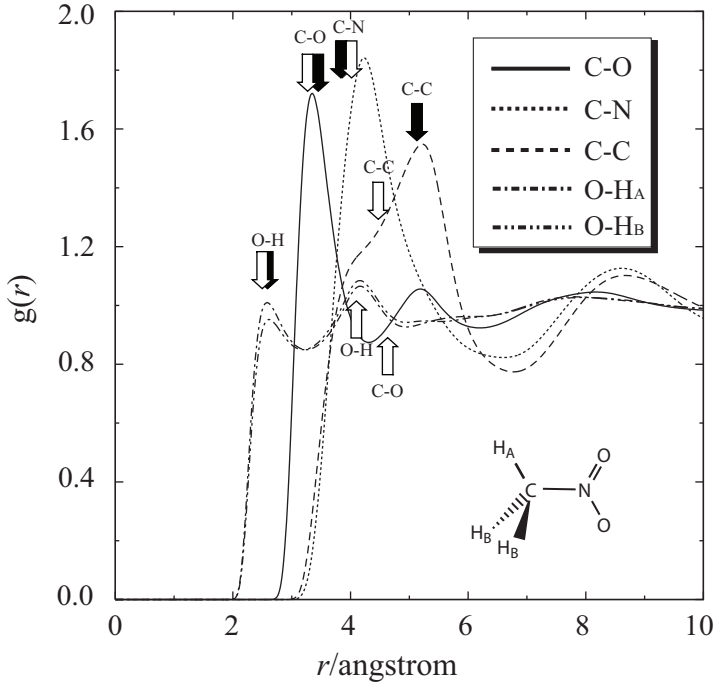

Figure 2.3: PCFs for the C–O, C–N, C–C, and O–H computed with the parameter set by Alper et al. [5] (Set B). See the caption in Figure 2.2

protic solvents. The same interaction in Set B (Figure 2.3) is more drastic and the peak height is less than 1.0. One might consider that the weak interaction between oxygen and hydrogen in Set A mainly attributes to the small charge assigned on hydrogen atom (+0.06$|e|$, see Table 1). However, the charge on hydrogen is much greater in Set B (+0.142 $|e|$) and a repulsive interaction between oxygen atom ($-0.406|e|$) and negatively charged carbon ($-0.331|e|$) should be the reason to weaken the O–H interaction. The second peak of O–H PCF (4.2 Å) is assigned to the contribution from the other oxygen atom in nitro group (4.1 Å in I). The O–H pair distance is longer than a typical hydrogen-bonding even for the first peak, consequently indicating that hydrogen bonding is very weak nor does not exist in this system, independently of the parameters. In the present study, the rotation around C–N bond was not treated. From the PCFs, the two sets of hydrogen atoms (H_A and H_B) are virtually equivalent and effect from the rotation is not significant.

Then, is the electrostatic interaction not important? Figure 2.4 compares the normal PCFs

and those computed by removing all the charges in Set A. Note that since the two different O–H PCFs are very similar, only H_B PCFs are shown for brevity. While C–O and O–H PCFs are not changed by turning off the electrostatic interaction, the peak positions are drastically changed in C–N and C–C PCFs. This result suggests that the electrostatic interaction between heavy atoms is primarily important to determine the liquid structure. Remember that the DFT computes several bound structures but some of them disappear in MP2 computations, which can treat dispersion interaction. This paradoxical result might suggest the importance of electrostatic interaction in the present nitromethane system.

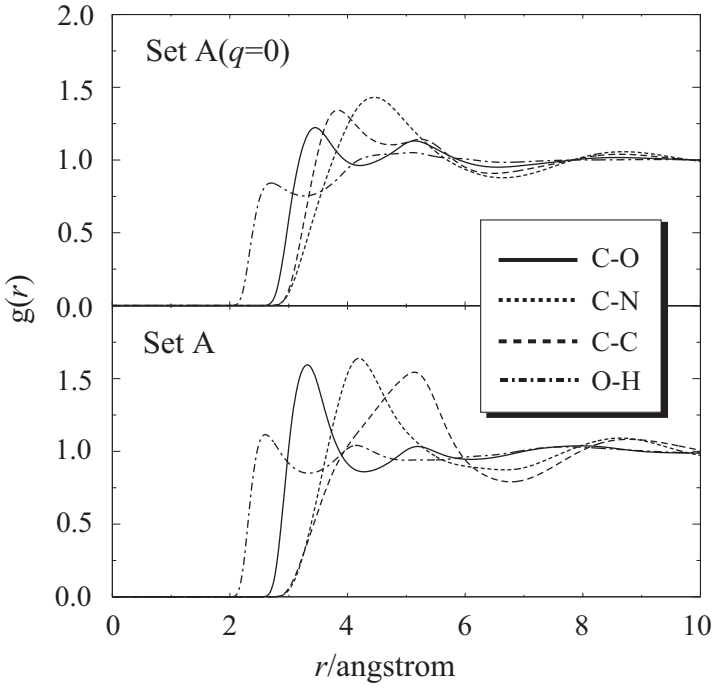

Figure 2.4: PCFs for the C–O, C–N, C–C, and O–H computed with (lower panel) Set A and (upper panel) all the charges were removed.

By the recently performed x-ray diffraction study by Megyes et al., the experimental RDF is available [3]. Figure 2.5 shows the comparison between the RDF and the present RISM calculation. Using the same scattering weighting factors (C-C, 0.04; C-N, 0.08; C-O, 0.18; N-O, 0.21; N-N, 0.05; and O-O, 0.25), total RDF ($g(r)$) was computed by averaging over PCFs obtained from RISM theory. The contributions from hydrogen atoms were omitted. Both of

RDFs show a good agreement though a very slight difference is seen in the shoulder around 2.5 Å.

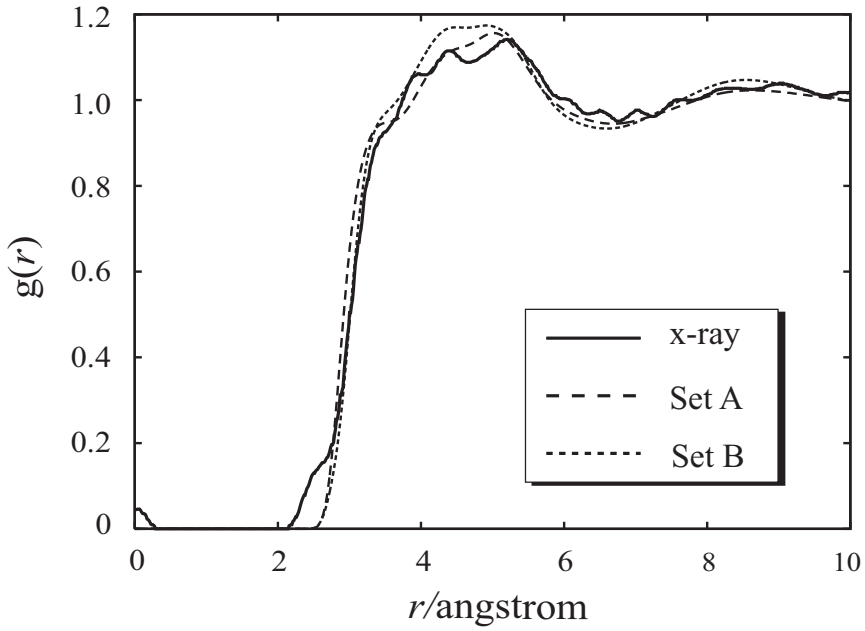

Figure 2.5: Intermolecular total radial distribution functions obtained by x-ray diffraction (solid line) and RISM calculations with set A (dashed line) and set B (dotted line).

Before closing the section, we would like to call attention to the readers that the analysis based on dimer cluster is just an expedient: we never support the existence of the association pair with certain life time. In reality, all the molecules move around and the "clusters" – regardless of whether it can be meaningfully defined – shown in the figures would disappear immediately. Actually, the atomic distances are not perfectly fit to the peak positions due to the contribution from molecular fluctuation. But the analysis through the optimized structure could offer pictorial understanding of liquid structure.

2.4 Concluding Remarks

The liquid structure of nitromethane was studied by means of RISM theory. The obtained solvation structures, namely RDFs, are consistent with the previous simulation studies. The reliability of the present computation can be also confirmed by the agreement with the exper-

imentally obtained RDF. We have examined two sets of intermolecular parameters. Although some differences were seen in PCFs, the coordination number and total RDF were almost identical in both of the parameter sets.

With the aid of the optimized structures computed by *ab initio* MO method (MP2), the peaks of RDFs can be clearly assigned. We found that antiparallel arrangemant and head-to-tail forms can be regarded as representative conformation. As previously pointed out, hydrogen bonding is weak or does not exist in liquid nitromethane.

Bibliography

[1] Boyer, E.; Kuo, K. K. *Proc. Combust. Inst.* **2007**, *31*, 2045.

[2] Oran, E. S.; Kailasanath, K. *Combust. Flame* **1986**, *65*, 339.

[3] Megyes, T.; Bálint, S.; Grósz, T.; Radnai, T.; Bakó, I. *J. Chem. Phys.* **2007**, *126*, 164507.

[4] Seminario, J. M.; Concha, M. C.; Politzer, P. *J. Chem. Phys.* **1995**, *102*, 8281.

[5] Alper, H. E.; Abu-Awwad, F.; Politzer, P. *J. Phys. Chem. B* **1999**, *103*, 9738.

[6] Sorescu, D. C.; Rice, B. M.; Thompson, D. L. *J. Phys. Chem. A* **2001**, *105*, 9336.

[7] Chandler, D.; Andersen, H. C. *J. Chem. Phys.* **1972**, *57*, 1930.

[8] Hirata, F.; Rossky, P. J. *Chem. Phys. Lett.* **1981**, *83*, 329.

[9] Ten-no, S.; Hirata, F.; Kato, S. *J. Chem. Phys.* **1994**, *100*, 7443.

[10] Sato, H.; Hirata, F.; Kato, S. *J. Chem. Phys.* **1996**, *105*, 1546.

[11] Yokogawa, D.; Sato, H.; Sakaki, S. *J. Chem. Phys.* **2007**, *126*, 244054.

[12] Hayaki, S.; Yokogawa, D.; Sato, H.; Sakaki, S. *Chem. Phys. Lett.* **2008**, *458*, 329.

[13] Price, M. L. P.; Ostrovsky, D.; Jorgensen, W. L. *J. Comput. Chem.* **2001**, *22*, 1340.

[14] Gaussian 03, Revision D.02; Pople, J. A. et al, Gaussian, Inc., Wallingford CT.

[15] Li, J.; Zhao, F.; Jing, F. *J. Comput. Chem.* **2003**, *24*, 345.

[16] For example; *Theory of Simple Liquids* 3rd ed.; Hansen, J.-P.; McDonald, I. R.; Academic Press: London, England, 2005.

Chapter 3

Solvation Effects in Oxidative Addition Reaction of Methyliodide to Pt(II) Complex: A Theoretical Study with RISM-SCF Method

3.1 Introduction

Oxidative addition of organic molecules to low-valent transition metal complexes is one of essential processes in organometallic chemistry because it plays key roles in many synthetic reactions [1]. As well known, the oxidative addition is classified into three categories; i.e., concerted process, S_N2-like process, and radical process. Though the concerted oxidative addition has been theoretically investigated well [2], theoretical studies of the S_N2-type oxidative addition have been limited except for several pioneering works [3–6]. One of the reasons is the difficulty to incorporate solvation effects in electronic structure calculation; remember that S_N2-type reaction is significantly affected by solvation. In previous theoretical studies of the S_N2-type oxidation addition, the reaction mechanisms was mainly discussed but solvation structure was not. Considering the importance of solvation effects in this type of oxidation addition, it is worth investigating the solvation effects on the reaction in detail. However, details such as microscopic solvation structure have not been clarified yet since dielectric continuum model treats solvent molecules in an implicit way.

In the present communication, we wish to report the solvation effects and solvation structures in the S_N2-type oxidative addition of MeI to model complex, $PtMe_2(NH_3)_2$. We selected this reaction because Puddephatt et al. thoroughly investigated S_N2-type oxidative addition of many substrates to platinum(II) complexes in various solvents, and reported thermodynamic

data of these reactions [7, 8]. Here RISM-SCF method [9, 10], in which solvent molecules are taken into consideration in a statistical manner, is applied to the oxidative addition of MeI to $PtMe_2(NH_3)_2$ in nitromethane. RISM-SCF method has been successfully applied to various reactions including S_N2 reaction and is believed to be a powerful means to evaluate solvation effects [11]. This is the first theoretical study of the solvation effects and solvation structures on S_N2-type oxidative addition to transition metal complexes, to our knowledge.

3.2 Method

All calculations were performed with density functional theory by using the GAMESS program package [12], where B3LYP functional was employed for exchange-correlation term. The core electrons of Pt (up to 4f) and I (up to 4d) were replaced with effective core potentials (ECPs) of LANL2DZ and valence electrons of Pt and I were represented by (341/321/21) and (21/21/1) basis sets, respectively. We employed 6-31G* basis sets for C, N, and H. The RISM integral equations were solved with hyper netted chain (HNC) closure relation. The Lennard-Jones parameters and effective charges for solute and solvent were collected in Table 3.1. The OPLS parameters were used for nitromethane [13, 14]. The density of nitromethane was assumed to be 1.14 g cm^{-3}=0.0112464 molecules $Å^{-3}$. Temperature was taken to be 313 K which was employed in experimental condition [8]. In this study, we employed the new-generation of RISM-SCF, in which the spatial electron density distribution (SEDD) is directly treated [15]. The great advantage of this procedure is the removal of the grid dependency that is inherent in the original RISM-SCF. It is also noted that the RISM-SCF-SEDD method is numerically very stable even if buried atoms are involved in the solute molecule such as transition metal complex. Since we wish to focus on the solvation effect, gas-phase geometries were adopted to exclude the contribution from the geometrical difference.

Table 3.1: Lennard-Jones parameters for solute and solvent.

Molecule	Site	σ/Å	ϵ/kcal mol^{-1}	$q/\|e\|$
Solute	Pt	4.780	0.056	
	C	3.800	0.050	
	N	3.250	0.170	
	H	1.000	0.056	
	I	4.320	0.633	
Nitromethane	N	3.250	0.120	0.540
	O	2.960	0.170	-0.370
	Me	3.775	0.207	0.200

3.3 Results and Discussion

3.3.1 Free energy changes

The reaction profile is shown in Figure 3.1. Species **1** is the sum of reactants at infinite separation. Methyliodide approaches the platinum complex to form adduct **2**. Transition state **TS$_{23}$** takes a linear Pt–C–I arrangement and the CH_3 moiety is planar, corresponding to Walden inversion of methyliodide seen in typical S_N2-type reaction. In gas phase, intermediate **3** was optimized after **TS$_{23}$**. However, **1** seems unlikely in solution because the methyl group is almost planar and Pt–C distance is considerably long, as will be discussed below. Two different paths are plausible after the inversion. In one path, the iodide anion dissociates from the reaction center (**4a**). In the other path, the iodide anion moves around the platinum complex through the midpoint between two methyl ligands (**4b**).

Free energy changes along these paths are given in Figure 3.2. In gas phase, **4b** is more favorable than **4a**. The reaction via **4b**, however, may not occur in gas phase because the barrier is too high. The situation is quite different in nitromethane. Because solvation effects play significant role to stabilize **4a**, **4a** is more stable than **4b**. As discussed below, this arises from the remarkable solvation of separated cationic and anionic species. Activation free energy $\Delta G^{\ddagger}$ in nitromethane (ϵ=37.5) is 20.7 kcal/mol, which is very close to the experimental value (18.1 kcal/mol) [8]. Thus the reaction can proceed only by the aid of solvation effects. It is noted that the concerted path is ruled out because Kégl and Kollar recently reported a high barrier in the concerted oxidative addition of MeI to $PtMe_2$(bdpp) (bdpp=(2*S*,4*S*)-2,4-

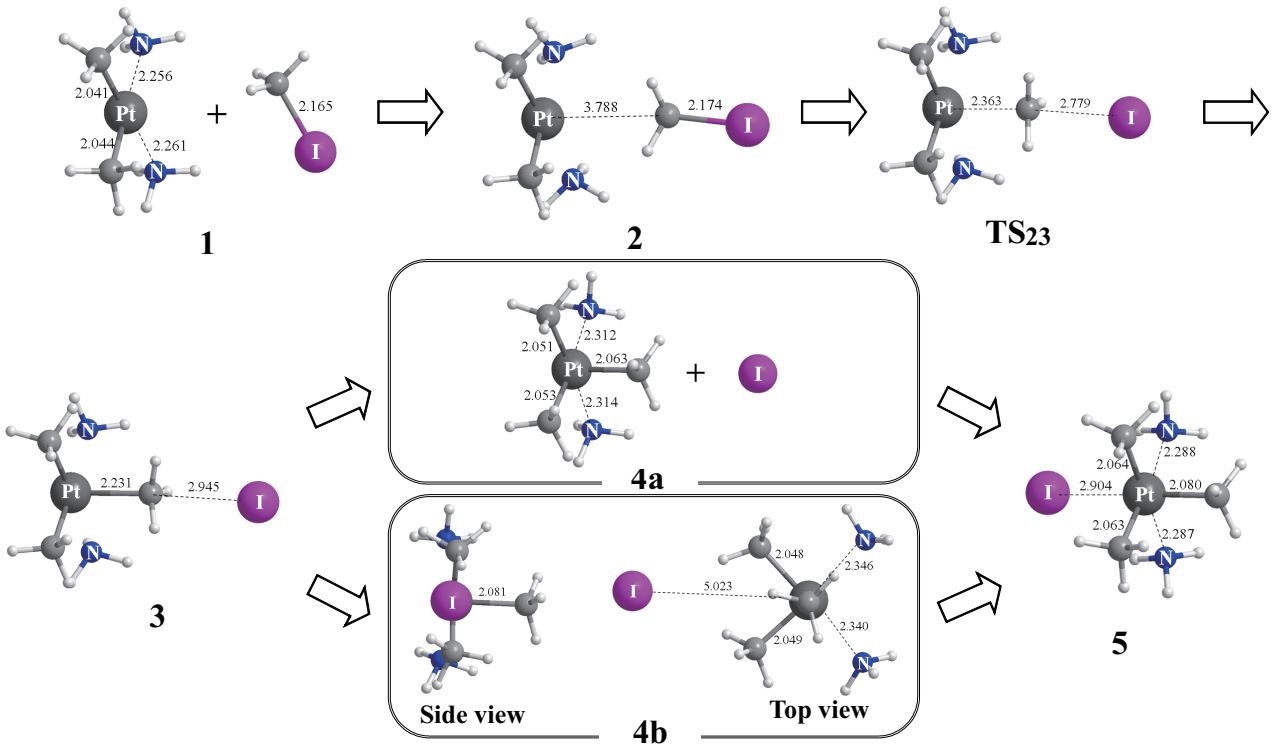

Figure 3.1: Geometry changes in oxidative addition of MeI to Pt(II) complex in gas phase. Bond lengths are in angstrom.

bis(diphenylphosphino)pentane) by DFT method [6].

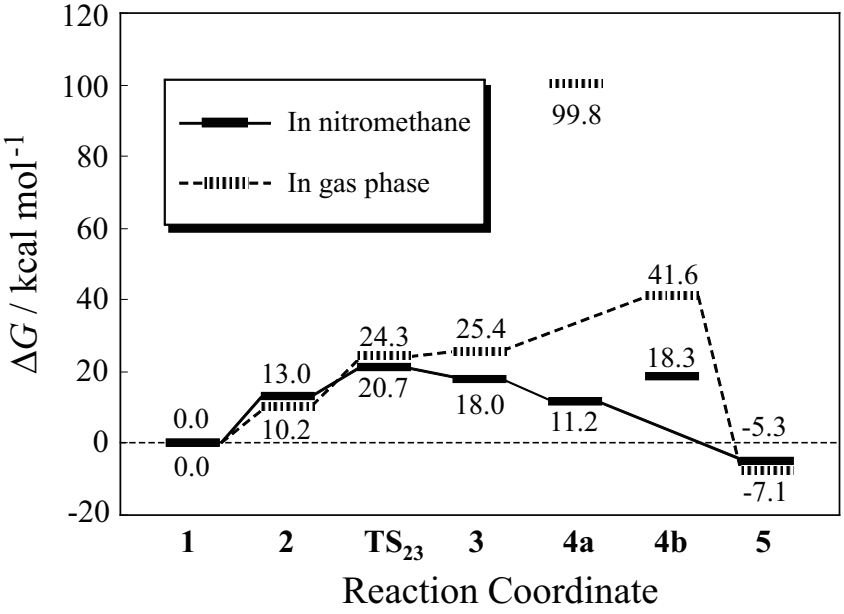

Figure 3.2: Free energy changes in nitromethane (solid line) and in gas phase (dashed line).

3.3.2 Reorganization energy and solvation free energy

The total energy of solvation system is defined as follows:

$$\mathscr{A} = E_{\text{solute}} + \Delta\mu = E_{\text{isolated}} + E_{\text{reorg}} + \Delta\mu. \tag{3.1}$$

E_{reorg} is defined as the difference in energy between the solute in solvent (E_{solute}) and that in isolated state (E_{isolated}).

$$E_{\text{reorg}} = E_{\text{solute}} - E_{\text{isolated}} = \langle \Psi \left| H \right| \Psi \rangle - \langle \Psi_0 \left| H \right| \Psi_0 \rangle , \tag{3.2}$$

where $|\Psi\rangle$ and $|\Psi_0\rangle$ are wave functions in solution and in gas phase, respectively. E_{reorg} is a measure of the stabilization energy by solvation effects to the electronic structure of the solute. Solvation free energy $\Delta\mu$ in the present theory is given by

$$\Delta\mu^{\text{HNC}} = \frac{\rho}{2\beta} \sum_{\alpha}^{\text{solute}} \sum_{\gamma}^{\text{solvent}} \int_0^{\infty} 4\pi r^2 (h_{\alpha\gamma}^2 - 2c_{\alpha\gamma} - h_{\alpha\gamma} c_{\alpha\gamma}) dr, \tag{3.3}$$

$$\beta = \frac{1}{k_B T}, \tag{3.4}$$

where h, c, and ρ are the total correlation functions, direct correlation functions, and density of solvent. k_{B} and T are the Boltzmann constant and temperature, respectively. $\Delta\mu$ can be "formally" divided into the contribution from each atom labeled α [16].

$$\Delta\mu^{\mathrm{HNC}} = \frac{\rho}{2\beta} \sum_{\gamma}^{\text{solvent}} \int_0^{\infty} 4\pi r^2 (h_{\alpha\gamma}^2 - 2c_{\alpha\gamma} - h_{\alpha\gamma} c_{\alpha\gamma}) dr. \tag{3.5}$$

This quantity represents how much the contribution from each site is. Figure 3.3 shows the change of E_{reorg} and $\Delta\mu$ along the reaction path. Particularly, the solvation free energy of **4a** is remarkably large; E_{reorg} and $\Delta\mu$ for **4a** are 1.5 kcal/mol and -78.8 kcal/mol, respectively. $\Delta\mu$ values of Pt and I sites is -49.1 kcal/mol and -43.8 kcal/mol, respectively. Both of them dominantly contribute to stabilization of **4a**.

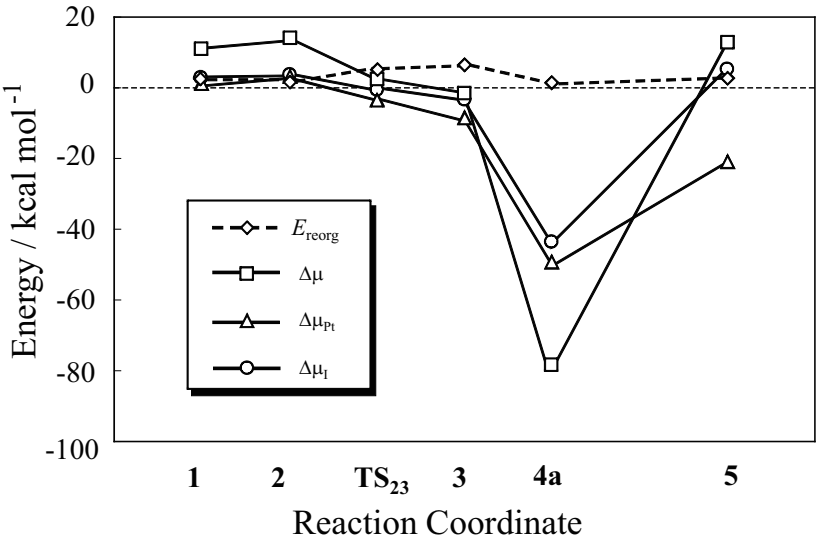

Figure 3.3: Reorganization energy (dashed line) and solvation free energy (solid line) changes along the reaction coordinate.

3.3.3 Solvation structure

The solvation structure is described in terms of a set of radial distribution functions (RDFs) in RISM-SCF method. Figure 3.4 shows the RDFs of nitromethane solvent molecules around

the platinum. In the RDFs of Pt–Me, the peak located around 4.0 Å corresponds to direct contact of the methyl group of nitromehtane with the platinum center, which becomes lower as the reaction proceeds. The peak found around 5.9 Å represents that the methyl group of nitromethane is distant from the platinum center. This peak becomes larger. In the Pt–O RDFs, the peak around 4.3 Å, which corresponds to the distribution of the oxygen atom around the platinum center, becomes larger. A shoulder found around 5.0 Å in the Pt–O RDFs of **4a** is assigned to the distribution of the other oxygen atom of nitromethane. All these results indicate that the coordination structure of nitromethane solvent around the platinum atom changes as depicted in the inset of Figure 3.4. This change of solvation structure can be understood in terms of the effective charge. The changes in the effective charge on several important atoms of the solute molecule are shown in Figure 3.5. Though the effective charges on a methyl and an amine ligand little change, those on the platinum and the iodine atom considerably change. In the initial stage of the reaction, the effective charge assigned to the platinum atom is -0.50 $|e|$, which becomes 0.90 $|e|$ in **4a**; note that the charge of the platinum atom significantly changes upon the reaction. The solvation structure reflects strong interaction between the platinum and the oxygen in **4a**, indicating the notable contribution of the platinum center to the solvation free energy, as shown in Figure 3.3.

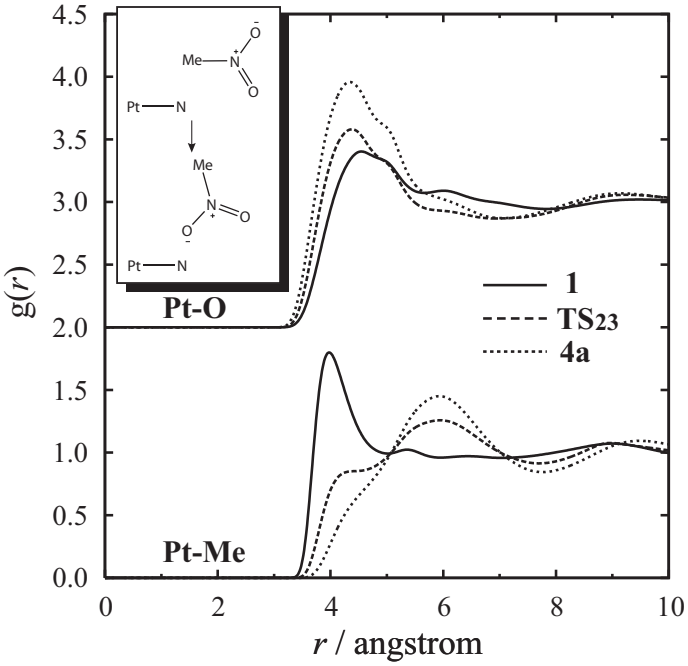

Figure 3.4: RDFs of Me and O around the Pt atom in species **1**, **TS$_{23}$**, and **4a**. The representative solvation structures are depicted in the inset.

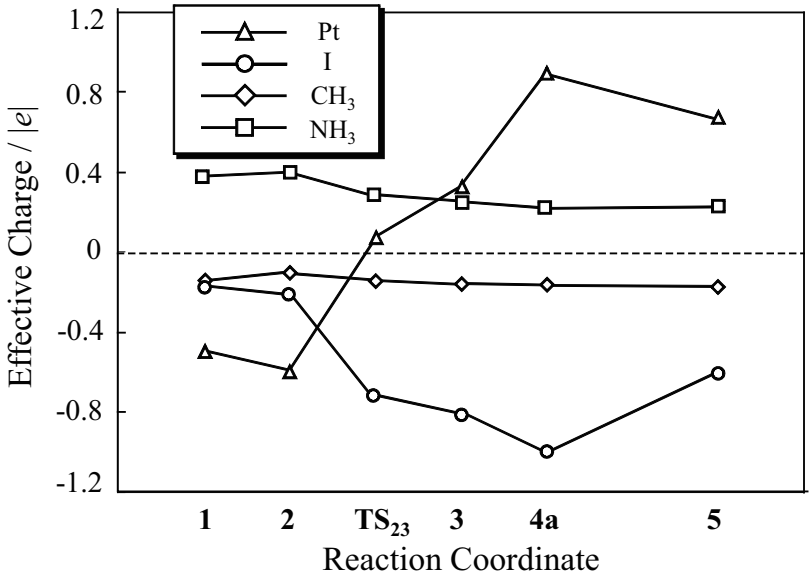

Figure 3.5: The effective charges of species **1**–**5** assigned to Pt, I, CH_3, and NH_3. CH_3 and NH_3 represent the sum of the charges on the atoms of a methyl and an amine ligand, respectively.

The RDFs between solvent nitromethane and the iodine atom are shown in Figure 3.6. One may first notice that the peak height of the I–Me RDFs dramatically increases as the reaction proceeds, indicating that the iodide anion is more and more strongly solvated. This is because the effective charge of the iodine atom changes from -0.18 $|e|$ to -1.00 $|e|$ upon going from **1** to **4a**, due to the electron transfer from the platinum complex to the iodine atom. Since the iodide anion becomes more repulsive with the solvent oxygen atom than the neutral iodine atom, the peak of the I–O RDFs located at 4.0 Å disappears and a small peak appears around 6.0 Å as the reaction proceeds. It is important that the attractive interaction between the iodide anion and solvent molecules becomes stronger, which leads to the stabilization of **4a**.

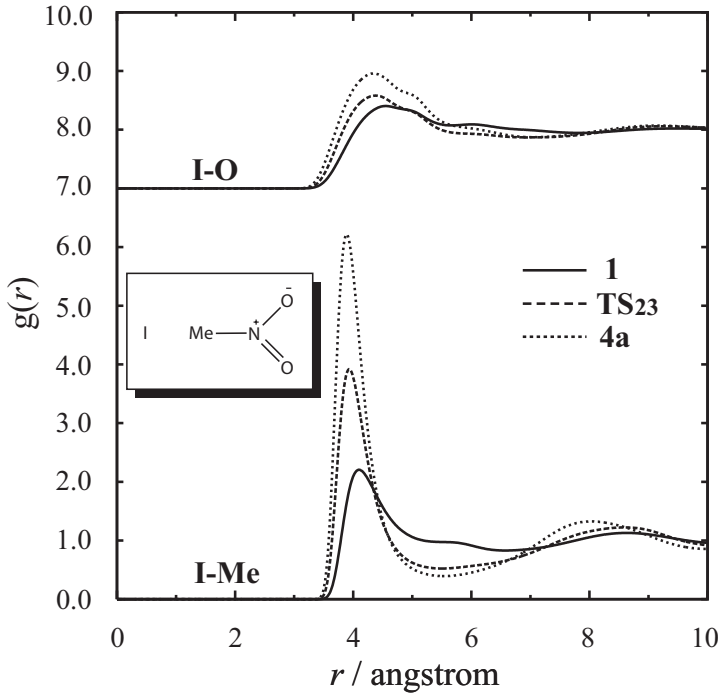

Figure 3.6: RDFs of Me and O around the I atom in species **1**, **TS$_{23}$**, and **4a**. The representative solvation structure is depicted in the inset.

3.4 Concluding Remarks

We have theoretically studied the solvation effects in the oxidative addition reaction of MeI to $PtMe_2(NH_3)_2$ via S_N2 mechanism in nitromethane solvent by means of RISM-SCF-SEDD

method. The reaction may not occur in gas phase due to the high barrier because iodide anion can not dissociate from methyl group in the reaction. In nitromethane solvent, on the other hand, solvation stabilizes the iodide anion and thus the dissociation can easily occur. Detailed analysis of the solvation free energy indicates that the solvation of the platinum and the iodine sites is main factor for the stabilization. The RDFs which RISM-SCF method provides clearly show that the solvation structure around the platinum center considerably changes and solvation around the iodide anion becomes stronger as the reaction proceeds.

Bibliography

[1] Collman, J. P.; Hegedus, L. S.; Norton, J. R.; Finke, R. G.; *Principles and Applications of Organotransition Metal Chemistry* ; University Science Books: Mill Valley, CA, 1987.

[2] Sakaki, S. *Theoretical Aspects of Transition Metal Complex* Ed. by Frenking, G. P31, Springer; Berlin, Germany 2005.

[3] Griffin, T. R.; Cook, D. B.; Haynes, A.; Pearson, J. M.; Monti, D.; Morris, G. E. *J. Am. Chem. Soc.* **1996**, *118*, 3029.

[4] Cheong, M.; Ziegler, T. *Organometallics* **2005**, *24*, 3053.

[5] Feliz, M.; Freixa, Z.; van Leeuwen, P. W. N. M.; Bo, C. *Organometallics* **2005**, *24*, 5718.

[6] Kégl, T.; Kollar, L. *J. Organomet. Chem.* **2007**, *92*, 1852.

[7] Rendina, L. M. ; Puddephatt, R. J. *Chem. Rev.* **1997**, *97*, 1735.

[8] Jawad, J. K.; Puddephatt, R. J. *J. Organomet. Chem.* **1976**, *117*, 297.

[9] Ten-no, S.; Hirata, F.; Kato, S. *J. Chem. Phys.* **1994**, *100*, 7443.

[10] Sato, H.; Hirata, F.; Kato, S. *J. Chem. Phys.* **1996**, *105*, 1546.

[11] Sato, H.; Sakaki, S. *J. Phys. Chem. A* **2004**, *108*, 1629.

[12] Schmidt, M. W.; Baldridge, K. K.; Boatz, J. A.; Elbert, S. T.; Gordon, M. S.; Jensen, J. H.; Koseki, S.; Matsunaga, N.; Nguyen, K. A.; Su, S. Windus, T. L.; Dupuis, M.; Montgomery J. A. *J. Comput. Chem.* **1993**, *14*, 1347.

[13] Price, M. L. P.; Ostrovsky, D.; Jorgensen, W. L. *J. Comput. Chem.* **2001**, *22*, 1340.

[14] Jorgensen, W. L.; Madura, J. D.; Swenson, C. J. *J. Am. Chem. Soc.* **1984**, *106*, 6638.

[15] Yokogawa, D.; Sato, H.; Sakaki, S. *J. Chem. Phys.* **2007**, *126*, 244504.

[16] Sato, H.; Hirata, F. *J. Mol. Struct.* (THEOCHEM) **1999**, *461*, 113.

Part II

Chemical Phenomena in Ionic Liquids

Chapter 4

A Theoretical Analysis of a Diels-Alder Reaction in Ionic Liquids

4.1 Introduction

Room-temperature ionic liquids (RTILs) are expected to be the novel class of solvents for a wide range of possible applications as a reaction medium due to their inherent properties. [1] The first study of the Diels-Alder reaction in an ionic liquid was performed by Jaeger, followed by a number of reports [2]. The reaction of cyclopentadinene (CP) with methyl acrylate (MA) leads to a mixture of *endo* and *exo* products (Figure 4.1) and it has been observed that imidazolium ionic liquids show the *endo*-selectivity to be comparable to that in ethanol . It is surprising that, regardless of the strong charge of components of ionic liquids, their solvation effects are weaker than water. The explanation on the standpoint of hydrogen bonding donation has been made [3] but the mechanism is still unclear. In view of the growing number of applications, study of the effects of ionic liquids have on chemical reactions is of primary importance. Nevertheless, the strong electrostatic interaction of solvent molecules in RTILs makes it difficult to describe the solvation properly by molecular simulations such as molecular dynamics. Furthermore, quantum chemistry must be combined to treat chemical reactions. However, QM/MM method requires a considerable amount of computational resources and it is not feasible to apply it to RTILs system.

We extended the current RISM-SCF method, which is regarded as an alternative to QM/MM method, to allow for a two-component solvent, namely RTILs. RISM is an approximate integral equation theory and has been developed for the study of molecular liquids whose structure

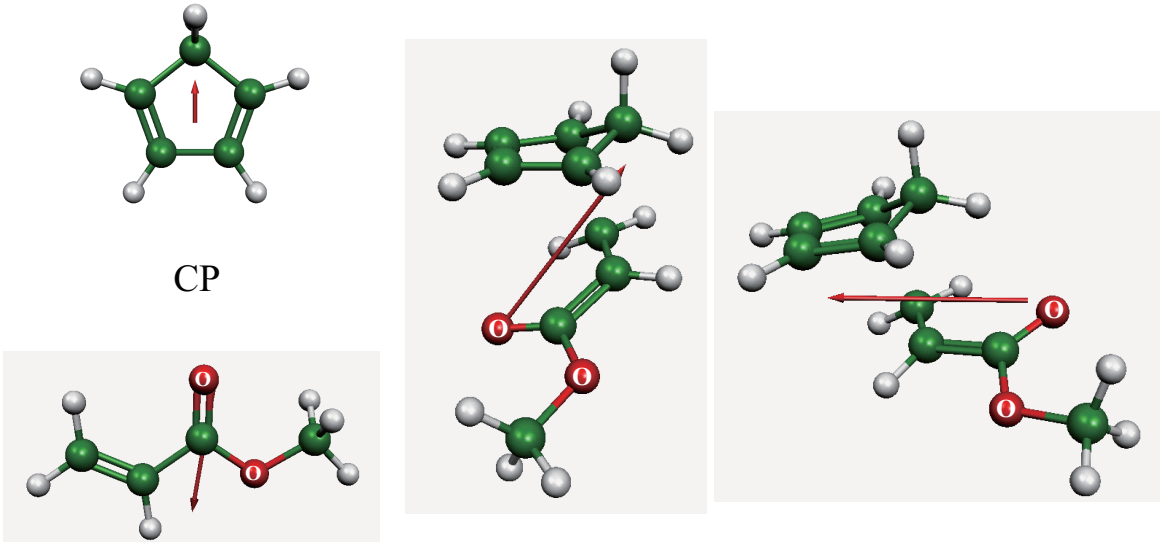

Figure 4.1: *endo* and *exo* forms of the Diels-Alder reaction. Directions of dipole moment are also depicted.

is dominated by short-range intermolecular repulsive forces. RISM was then extended to include Coulombic long ranged site-site interactions for polar solvents as well as solvent-solute interactions [4]. The hybrid approach, referred to as the RISM self-consistent field (SCF) procedure, combines RISM theory and *ab initio* molecular orbital theory and enables us to simultaneously determine the electronic structure of solute in solution and the statistical distribution of solvent molecules around it. The electronic and the solvation distributions are coupled through the electrostatic interactions between the interaction sites assigned to solute and solvent and allowed to be optimized in a self-consistent manner [5] within the framework of a microscopic mean-field approximation. RISM-SCF has been proved to be a powerful tool to calculate the change in free energy of chemical reactions in solution such as the Diels-Alder reaction in aqueous environment [6].

In the present study, we focused on the origin of the relatively moderate solvation effects of RTILs and the mechanism of *endo-exo* selectivity of the Diels-Alder reaction of CP with MA. Thanks to the analytical treatment of the ensemble, RISM is free from statistical error, which is a serious difficulty in the description of the strong Coulombic interaction in RTILs. However, the application is still very limited to a simple, classical solvation phenomenon [7]. This is the first study to treat a chemical reaction in ionic liquids theoretically, to our best knowledge.

4.2 Method

It is our intent here to only describe what we have added to the preexisting theory of RISM-SCF and assume the readers familiarity of the standard theory of molecular liquids. A more detailed discussion can also be found in our supporting information. The RISM integral equation is written as

$$\boldsymbol{h} = \boldsymbol{\omega} * \boldsymbol{c} * \boldsymbol{\omega} + \boldsymbol{\omega} * \boldsymbol{c} * \boldsymbol{\rho}\boldsymbol{h}\boldsymbol{\rho}, \tag{4.1}$$

where $\boldsymbol{h}$ and $\boldsymbol{c}$ are the matrix of total and direct correlation functions, respectively. $\boldsymbol{\omega}$ denotes the matrix of intramolecular correlation functions and $\boldsymbol{\rho}$ is that of number density of solvent. In order to apply the RISM theory to ionic liquids, which is multi-component solvent composed

of cation and anion, these matrices are extended to embrace the information on both cation and anion [7, 8]

$$\boldsymbol{\rho}_{\mathrm{multi}} = \begin{pmatrix} \boldsymbol{\rho}_{\mathrm{C}} & \mathbf{0} \\ \mathbf{0} & \boldsymbol{\rho}_{\mathrm{A}} \end{pmatrix}, \boldsymbol{\omega}_{\mathrm{multi}} = \begin{pmatrix} \boldsymbol{\omega}_{\mathrm{C}} & \mathbf{0} \\ \mathbf{0} & \boldsymbol{\omega}_{\mathrm{A}} \end{pmatrix}, \tag{4.2}$$

where subscript C and A stand for cation and anion, respectively. We combined this multi-component RISM theory [7, 8] with the new generation of RISM-SCF, in which the spatial electron density distribution (SEDD) is explicitly treated. It is noted that the applicability to chemical reactions covered by this theory is very wide-ranging, because RISM-SCF-SEDD is numerically stable compared to the original method, [5] even if the buried atoms are involved in the solute molecule.

In this study, we chose 1-3-dimethylimidazolium chloride ([mmim][Cl]), which is the standard solvent in RTILs' studies. [9] All hydrogen atoms were fused on the carbon atoms and these atoms were treated as a single site, since little significant differences were found between explicit description and united-atom model by previous works. [7, 9] It is also noticed that the effects of inhomogeneity is negligible when the length of side chain is less than 4-5 units. [10] All the computations were performed by GAMESS program package [11] modified by us. The geometry of reactants, TSs, and products were fully optimized in gas phase at the B3LYP level by using 6-31+G* basis sets and vibrational frequencies were calculated at the same level. Since the determination of the *endo-exo* selectivity was a delicate problem, energy changes were calculated with CCSD(T) method by using the same basis set. In this work, three kinds of solvents were employed to compare the experimental results: [mmim][Cl], water, and dimethyl ether (DME). As the potential parameters for [mmim][Cl] and solute, the same parameters were employed in past studies. [6, 7] RISM equations were solved with hyper netted chain (HNC) closure relation and temperature was set to 298.15 K for water and DME, and to 400 K for the ionic liquid.

Table 4.1: Reaction ratio of *endo* and *exo* products in the variety of solvents.

solvent	$\Delta\Delta G^{\ddagger}$ / kcal mol^{-1}	*endo*:*exo* (calcd.)	*endo*:*exo* (exptl.)	V_{cav}/Å^3
water	-2.17	38.9	5.9-9.3	16.62
RTILs	-1.62	7.7[a]	3.3-4.8[b]	153.79
DME	-1.02	5.6	2.9[c]	56.23

[a] [mmim][Cl]. [b] Examined in [bmim][BF_4], [bm_2im][BF_4], and [bmim][PF_6] [2].
[c] Diethyl ether.

4.3 Results and Discussion

The dienophile, namely MA, can take two conformations; *cis* or *trans*, which may bind with the diene to make a transition structure in two possible conformations; *endo* or *exo*. Therefore, four possible structures, *endo-cis*, *endo-trans*, *exo-cis*, and *exo-trans* are conceivable for the TSs. We performed the calculations on all conformations and confirmed that the *cis* conformations are more stable than *trans* ones both in gas phase and in solution (see Table 4.4 in appendix). In the present study, the stereo-selectivity on only *cis* type transition states is discussed. The stereo-selectivity of *endo* or *exo* product evaluated with the Boltzmann distribution of the free energy difference of the reaction barriers, $\exp\left(-\Delta\Delta G^{\ddagger}/k_{\mathrm{B}}T\right)$, where $\Delta\Delta G^{\ddagger}$ represents the free energy difference between *endo*-TS and *exo*-TS, $\Delta\Delta G^{\ddagger} = \Delta G^{\ddagger}(endo) - \Delta G^{\ddagger}(exo)$. The calculated *endo-exo* reaction ratio and experimental data were summarized in Table 4.1, where the volume of each solvent V_{cav} was calculated with GePol algorithm [12] as used in Eqn. 4.5, which will be discussed later. The ratio along three solvents was correctly reproduced in a semi-quantitative sense, and thus the advantage of the procedure was verified. It is noteworthy that the selectivity in RTILs is lower than that in water.

Now, two questions may arise. One is why RTILs are weaker than water in solvent effects though they should have strong Coulombic interaction. The other is why the selectivity is weakened in RTILs. One of the advantages of RISM theory is its capability to provide the information on solvation structure and to perform investigations based on microscopic solvation. In order to evaluate the contribution from electrostatic interaction between solute and solvent,

the charge density is defined using the resultant solvation structures:

$$\rho_\alpha(r) = \sum_{\gamma}^{\text{solvent}} q_\gamma \rho_\gamma g_{\alpha\gamma}(r), \tag{4.3}$$

where q_γ is charges of solvent site γ, ρ_γ is number density of solvent. $g_{\alpha\gamma}(r)$ denotes radial distribution function between solute site α and γ. The function $\rho_\alpha(r)$ is a convenient way to see the strong electrostatic-interaction source located around the focused solute site, α. The charge densities around carbonyl oxygen (α =O) in *endo*-TS are shown in Figure 4.2. In water (- - -), the sharp peak at $r \sim 2$ Å is mainly the contribution from solvent hydrogen, corresponding to the hydrogen bonding. Contribution from the attached oxygen facing water is found around $r \sim 4$ Å. It is noted that the amplitude of the charge density of [mmim][Cl] was much smaller than that of water, rather resembled that of DME. This indicates the electrostatic interaction in [mmim][Cl] is smaller than that of water. The effective charges allocated to $[\text{mmim}]^+$ (+1.0) is greater than water (+0.41 in each hydrogen). Thus the difference between [mmim][Cl] and water is ascribed to number density from the Eqn 4.3 ; $\rho_{[\text{mmim}][\text{Cl}]}$ and ρ_{water} were 0.005291 molecules Å^{-3} and 0.033426 molecules Å^{-3}, respectively. [9] This does not mean the molecules are packed sparsely in [mmim][Cl]. Evaluating the packing fraction calculated from the volume of solvent molecules V_{cav}, [mmim][Cl] is greater than water, which corresponds to an intuitional picture that molecules in RTILs are densely packed presumably because of the strong Coulomb interaction.

In order to estimate the number of solvent molecules associating with the effective interaction, we considered running coordination number (coordination number) of solvent site around carbonyl oxygen in *endo*-TS. coordination number is defined as follows:

$$N_\gamma(r) = \rho_\gamma \int_0^r 4\pi r'^2 g_{\text{O}\gamma}(r')\mathrm{d}r'. \tag{4.4}$$

Figure 4.3 shows the running coordination number of the three kinds of solvents focused on the vicinity of the first solvation shell (see appendix Figure 4.9 for a wider region of r). Among many positively charged sites in $[\text{mmim}]^+$, the C_R site (see appendix Figure 4.5), to which the strongest positive charge is assigned, is shown in Figure 4.3 to be comparble to DME. With

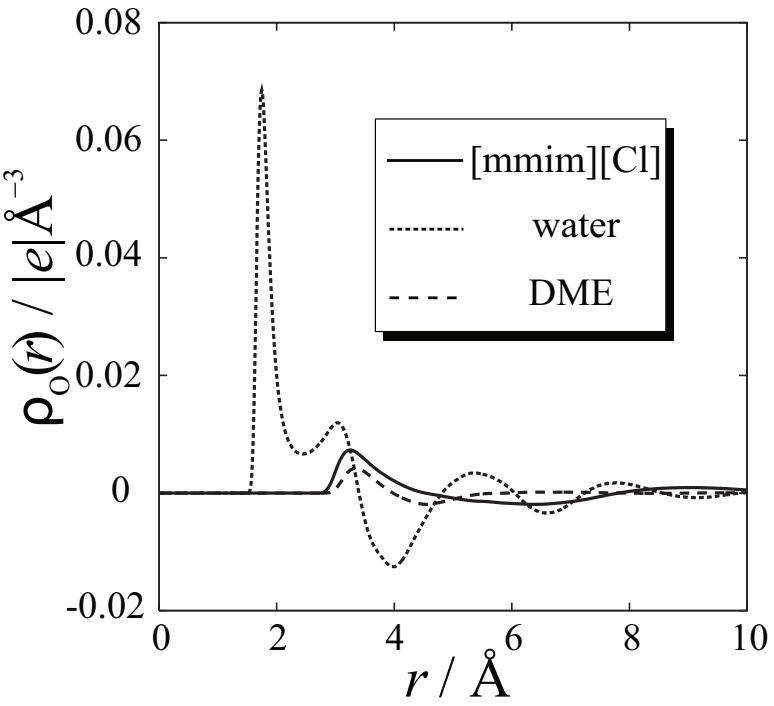

Figure 4.2: Comparison of the charge density due to [mmim][Cl], water, and DME.

increasing coordination number, water is the closest and [mmim][Cl] is the farthest from the carbonyl O of the solute, which reflects the size of solvent molecules.

To evaluate the quantity independent from molecular size, we introduced the scaled distance *r'* by the third root of V_{cav},

$$r' = r / \sqrt[3]{V_{\mathrm{cav}}}. \tag{4.5}$$

Scaled coordination number curves $N(r')$ reflect how closely solvent molecules coordinate to the solute within the occupied space, and the more rapidly $N(r')$ increases, the more strongly solvent coordinate. $N(r')$ is depicted in Figure 4.4. Comparing three different curves of positively charged sites (i.e. C_R, H, and Me), $N(r')$ of C_R site increases most rapidly. This indicates that [mmim][Cl] is packed more densely than water within the space allocated to each solvent molecule, which probably originate from the strong Coulomb interaction between charged components. [13] The discussion so far leads to the picture that although the electronic field from each ions of [mmim][Cl] (*i.e.,* $[mmim]^+$ and Cl^-) is never weak, the lower number

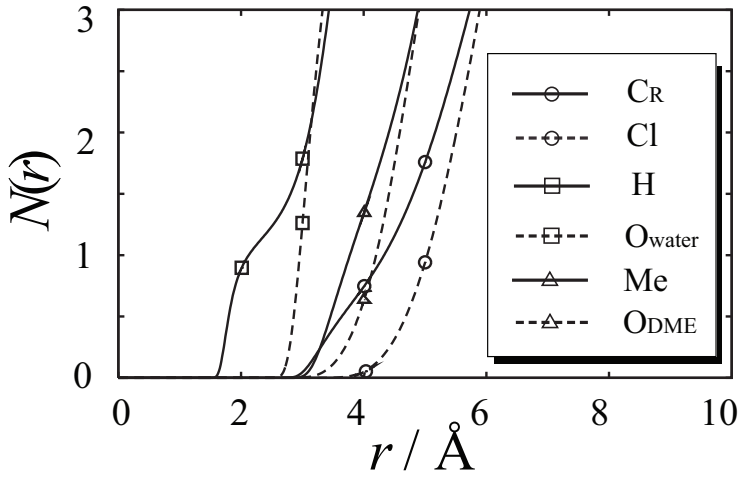

Figure 4.3: Running coordination number of [mmim][Cl], water, and DME.

density due to the bulkiness of imidazolium cation gives rise to weaker solvation effects than water. Note that this is the electrostatic part of the solvation effects. Other contributions such as hydrophobic effects may also explain the entire solvation process.

Finally, we would like to answer the second question, the mechanism of selectivity of the reaction. As explained above, the Coulombic field induced by RTILs is considered to be moderate in comparison to the water solvent. The difference in the activation barrier between two isomers (Table 4.1) is understood in terms of solvation structure and the electronic structure of the solute, but the explanation is not simple. In the present treatment, both of them are determined in a self-consistent manner: As the solvent coordination becomes greater, the polarization of the the solute is enhanced in general, namely, the distortion of the electronic structure with respect to the isolated state becomes larger. The free energy difference ($\Delta\Delta G^{\ddagger}$) is thus expressed as the sum of the difference in solvation free energy between the isomers, $\Delta\Delta\Delta\mu$, and the difference in the reorganization energy, $\Delta\Delta E_{\mathrm{reorg}}$ (see appendix for the details). Table 4.2 summarizes these two contributions. A considerable difference in the solvation free energy is found in water environment while it is much smaller in RTIL and in DME. Strong solvation, however, also induces large electronic distortion of solute molecule. One might think the difference of the solvation structure around the carbonyl oxygen is related because *exo*-TS

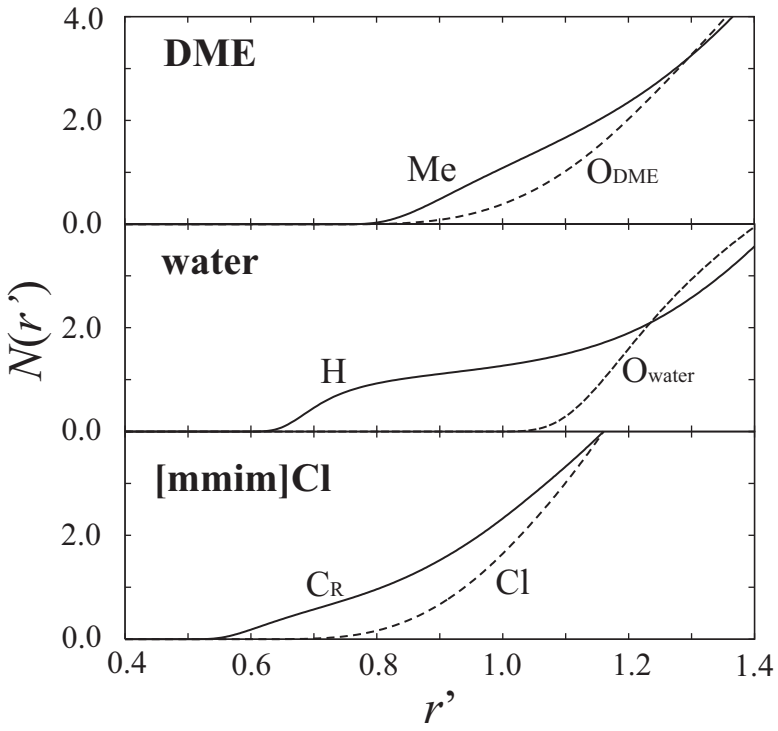

Figure 4.4: Scaled running coordination number of [mmim][Cl] (bottom), water (middle), and DME (top).

Table 4.2: *endo-exo* difference in contributions of solvation effects at TS.[a]

	$\Delta\Delta E_{\mathrm{reorg}}$	$\Delta\Delta\Delta\mu$	total
water	1.50	-2.97	-1.47
RTIL	-0.77	0.18	-0.59
DME	-0.07	-0.24	-0.31

[c] All the values in kcal/mol. Respective gas phase values must be added to obtain $\Delta\Delta G^{\ddagger}$.

would expose the carbonyl oxygen to polar solvent more than *endo*-TS. The hydration of water molecules is relatively strong (See Figure 4.7 in appendix), leading to the great stabilization of the solvation free energy. Dipole moment at TS is also expected to be correlated with the barrier height (Table 4.7 in appendix). However, none of them perfectly explains the reaction trend. The coupling between the solvation structure described by statistical RISM theory and the electronic structure by quantum chemistry is essential to understand the mechanism and the delicate balance between them governs the reaction profile.

4.4 Concluding Remarks

In summary, we have established the method to study chemical reactions in RTILs based on RISM theory. We compared the results in three different solvents obtained from RISM-SCF-SEDD method and elucidated that since the number of molecules interacting the solute is much smaller than that of water, the polarity of [mmim][Cl] is as strong as lower alcohols.

4.5 Appendix

In RISM-SCF, total energy of the system is defined as,

$$\mathscr{A} = E_{\mathrm{solute}} + \Delta\mu, \tag{4.6}$$

where E_{solute} is total energy of the solute molecule described in standard *ab initio* molecular orbital theory, corresponding to CP and/or MA in the present study. By using variational principle, a set of equation describing solution system is obtained. Hence, the electronic structure of the solute and solvent structure are obtained in a self-consistent manner.

Reorganization energy and solvation free energy are defined as follows:

$$E_{\mathrm{reorg}} = E_{\mathrm{solute}} - E_{\mathrm{isolated}} = \mathscr{A} - \Delta\mu - E_{\mathrm{isolated}}, \tag{4.7}$$

where E_{isolated} is total energy of the solute in isolated state, corresponding energy obtained by a standard *ab initio* molecular orbital method.

Solvation free energy $\Delta\mu$ (Eqn.4.6) can be "formally" divided into the contribution from each atom labeled α.

$$\Delta\mu = \sum_{\alpha} \Delta\mu_{\alpha}, \tag{4.8}$$

and

$$\Delta\mu_{\alpha} = -\frac{\rho}{\beta} \sum_{s} \int \mathrm{d}\mathbf{r} \left[c_{\alpha s}(r) - \frac{1}{2} h_{\alpha s}^2(r) + \frac{1}{2} h_{\alpha s}(r) c_{\alpha s}(r) \right]. \tag{4.9}$$

This quantity represents how much the contribution from each site is. Hence, solvation free energy can be formally decomposed to the contribution from cation and anion (Table 4.5),

$$\Delta\mu_{\mathrm{cation}} = -\frac{\rho}{\beta} \sum_{\alpha} \sum_{s}^{\mathrm{cation}} \int \mathrm{d}\mathbf{r} \left[c_{\alpha s}(r) - \frac{1}{2} h_{\alpha s}^2(r) + \frac{1}{2} h_{\alpha s}(r) c_{\alpha s}(r) \right]. \tag{4.10}$$

$$\Delta\mu_{\mathrm{anion}} = -\frac{\rho}{\beta} \sum_{\alpha} \sum_{s}^{\mathrm{cation}} \int \mathrm{d}\mathbf{r} \left[c_{\alpha s}(r) - \frac{1}{2} h_{\alpha s}^2(r) + \frac{1}{2} h_{\alpha s}(r) c_{\alpha s}(r) \right]. \tag{4.11}$$

The Lennard-Jones parameters of the solute were taken from literatures. SPC-like water was assumed for the solvent. All of them are summarized in Table 4.3.

Table 4.3: Lennard-Jones parameters adopted to solvents.[a]

species	site	σ / Å	ϵ / kcal mol^{-1}	$q/\|e\|$
[mmim][Cl]	C_R	3.880	0.10414	0.504
	N	3.250	0.16692	-0.267
	C_W	3.880	0.10414	0.199
	Me	3.775	0.20350	0.310
	Cl	4.401	0.09910	-1.000
water	O	3.166	0.155	-0.820
	H	1.000	0.056	0.410
DME	Me	3.0676	0.179	-0.500
	O	3.8609	0.181	0.250

[a] Number density was set to as following; 0.005291 molecules Å^{-3} for [mmim][Cl], 0.033426 molecules Å^{-3} for water, and 0.009608 molecules Å^{-3} for DME.

Table 4.4: Reaction barriers of TS-*cis-trans* conformations. All values are relative to the reactants at CCSD(T) level.[a]

species	$\Delta G^{\ddagger}$ (gas) / kcal mol^{-1}	$\Delta G^{\ddagger}$ ([mmim][Cl]) / kcal mol^{-1}	$\Delta G^{\ddagger}$ (water) / kcal mol^{-1}	$\Delta G^{\ddagger}$ (DME) / kcal mol^{-1}
endo-cis	29.7	22.3	24.8	30.0
endo-trans	31.6	24.3	27.0	31.7
exo-cis	30.4	23.9	26.9	31.0
exo-trans	32.1	25.0	28.7	32.4

[a] Temperature was set to 298.15 K except [mmim][Cl]. The values are at 400 K in [mmim][Cl].

Table 4.5: Solvation free energy in various solvents.

species	$\Delta\mu$(cation) / kcal mol^{-1}	$\Delta\mu$(anion) / kcal mol^{-1}	$\Delta\mu$([mmim][Cl]) / kcal mol^{-1}	$\Delta\mu$(water) / kcal mol^{-1}	$\Delta\mu$(DME) / kcal mol^{-1}
endo-TS	59.0	4.0	63.0	20.3	5.4
exo-TS	60.2	2.7	62.9	23.3	5.7
difference	-1.2	1.3	0.1	-3.0	-0.3

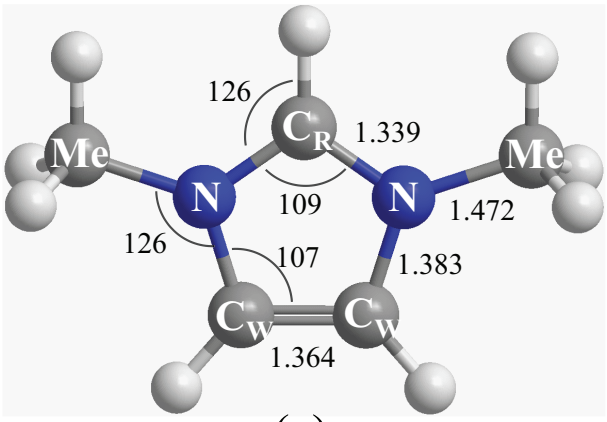

(a)

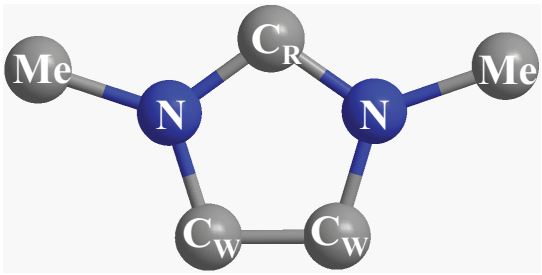

(b)

Figure 4.5: (a) explicit description and (b) united-atom model of $[mmim]^+$. The structure was optimized by computing at B3LYP/6-31++G** level. Bond lengths and angles are in angstrom and in degree, respectively.

Table 4.6: Reorganization energy in various solvents.

species	E_{reorg}([mmim][Cl]) / kcal mol^{-1}	E_{reorg}(water) / kcal mol^{-1}	E_{reorg}(DME) /kcal mol^{-1}
endo-TS	5.2	11.3	1.4
exo-TS	6.0	9.8	1.5
difference	-0.8	1.5	-0.1

Table 4.7: Dipole moments in the solvents. All the values are in Debye.

	water	[mmim]Cl	DME
CP	0.54	0.64	0.51
MA	2.72	2.42	2.05
endo-TS	4.39	3.37	3.06
exo-TS	4.17	3.34	2.90

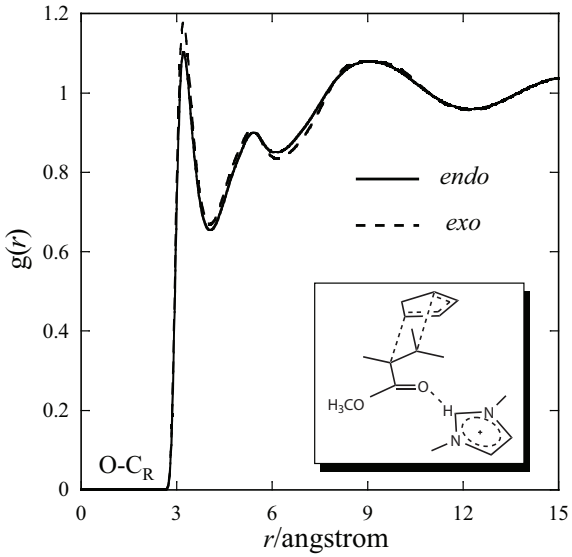

Figure 4.6: Comparison of RDFs of C_R between *endo*-TS (solid line) and *exo*-TS (dashed line) around carbonyl oxygen. Schematic picture of the interaction is shown in the inset. Note that the peak position of O-C_R is more distant than that of typical hydrogen bond because the C_R-H bond is fused as in the united-atom model.

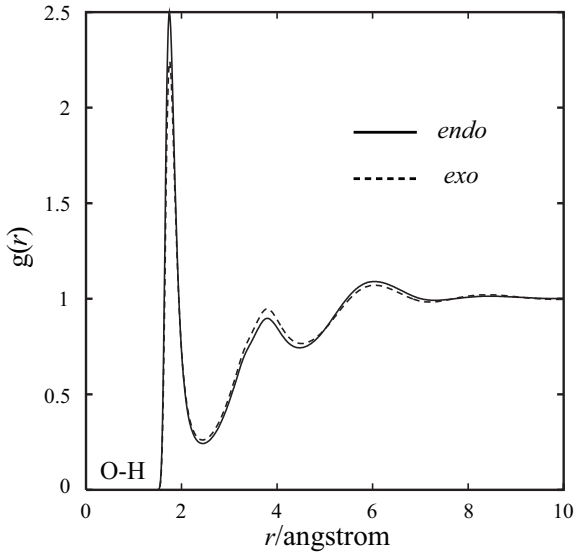

Figure 4.7: Comparison of RDFs of water hydrogen around carbonyl oxygen. Solid line and dashed line stand for *endo*-TS and *exo*-TS, respectively.

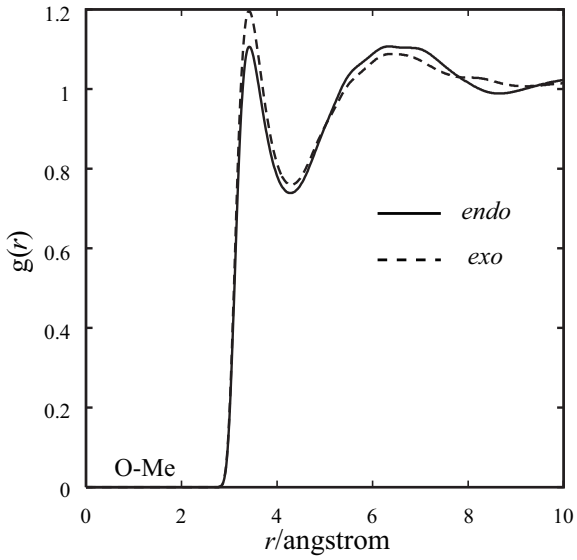

Figure 4.8: Comparison of RDFs of Me of DME around carbonyl oxygen. Solid line and dashed line stand for *endo*-TS and *exo*-TS, respectively.

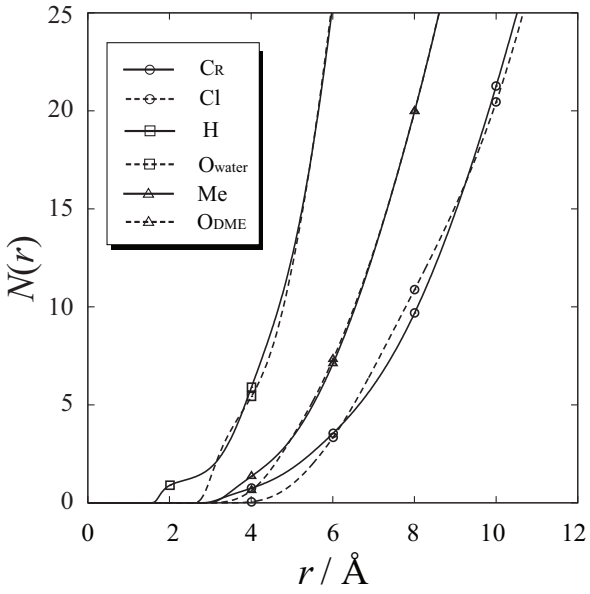

Figure 4.9: Running coordination number of [mmim][Cl], water, and DME.

Bibliography

[1] *Ionic Liquids in Synthesis*; Welton, T.; Wasserscheid, P. Eds.; VCH-Wiley: Weinheim, Germany, 2008.

[2] (a) Jaeger, D. A.; Tucker, C. E. *Tetrahedron Lett.* **1989**, *30*, 1785. (b) Fischer, T.; Sethi, A. R.; Welton, T.; Woolf, J. *Tetrahedron Lett.* **1999**, *40*, 793. (c) Aggarwal, A.; Lancaster, N. L.; Sethi, A. R.; Welton, T. *Green Chemistry* **2002**, *4*, 517. (d) Vidiš, A.; Ohlin, C. A.; Laurenczy, G.; Küsters, E.; Sedelmeier, G.; Dyson, P. J. *Adv. Synth. Catal.* **2005**, *347*, 266.

[3] Reichardt, C. *Green Chemistry* **2005**, *7*, 339.

[4] (a) Chandler, D.; Andersen, H. C. *J. Chem. Phys.* **1972**, *57*, 1930. (b) Hirata, F.; Rossky, P. J. *Chem. Phys. Lett.* **1981**, *83*, 329. (c) Hirata, F.; Rossky, P. J.; Pettitt, B. M. *J. Chem. Phys.* **1982**, *78*, 4133.

[5] (a) Ten-no, S.; Hirata, F.; Kato, S. *Chem. Phys. Lett.* **1993**, *214*, 391. (b) Ten-no, S.; Hirata, F.; Kato, S. *J. Chem. Phys.* **1994**, *100*, 7443. (c) Sato, H.; Hirata, F.; Kato, S. *J. Chem. Phys.* **1996**, *105*, 1546. (d) Yokogawa, D.; Sato, H.; Sakaki, S. *J. Chem. Phys.* **2007**, *126*, 244054.

[6] (a) Harano, Y.; Sato, H.; Hirata, F. *J. Am. Chem. Soc.* **2000**, *122*, 2289. (b) Harano, Y.; Sato, H.; Hirata, F. *Chem. Phys.* **2000**, *258*, 151.

[7] (a) Bruzzone, S.; Malvaldi, M.; Chiappe, C. *Phys. Chem. Chem. Phys.* **2007**, *9*, 5576. (b) Bruzzone, S.; Malvaldi, M.; Chiappe, C. *J. Chem. Phys.* **2008**, *129*, 074509.

[8] Kinoshita, M.; Hirata, F. *J. Chem. Phys.* **1997**, *106*, 5202.

[9] (a) Hanke, C. G.; Price, S. L.; Lynden-Bell, R. M. *Mol. Phys.* **2001**, *99*, 801. (b) Del Pópolo, M. G.; Lynden-Bell, R. M.; Kohanoff, J. *J. Phys. Chem. B* **2005**, *109*, 5895. (c) Buhl, M.; Chaumont, A.; Schurhammer, R.; Wipff, G. *J. Phys. Chem. B* **2005**, *109*, 18591. (d) Bhargava, B. L.; Balasubramanian, S. *Chem. Phys. Lett.* **2006**, *417*, 486.

[10] Canongia Lopes, J. N. A.; Pádua, A. A. H. *J. Phys. Chem. B* **2006**, *110*, 3330.

[11] Schmidt, M. W.; Baldridge, K. K.; Boatz, J. A.; Elbert, S. T.; Gordon, M. S.; Jensen, J. H.; Koseki, S.; Matsunaga, N.; Nguyen, K. A.; Su, S. Windus, T. L.; Dupuis, M.; Montgomery J. A. *J. Comput. Chem.* **1993**, *14*, 1347.

[12] Silla, E.; Villar, F.; Nilsson, O.; Pascual-Ahuir J. L.; Tapia, O. *J. Mol. Graphics* **1990**, *8*, 168.

[13] When the hydrogen atoms attached to carbon in [mmim] are explicitly treated, the difference in $\sqrt[3]{V_{\mathrm{cav}}}$ between the explicit model (5.26Å) and the united-atom model (5.34Å) is only 1.5 % and thus it is negligible.

Chapter 5

Ab Initio Study on S_N2 Reaction of Methyl *p*-nitrobenzenesulfonate and Chloride Anion in [mmim][PF_6]

5.1 Introduction

Ionic liquids (ILs), a unique class of solvents, are generally defined as a salt with melting points below 100 degrees [1]. Because their chemical property can be tuned by changing the combination of anion and cation, they are often called as 'designer solvent'. A wide range of applications has been developed so far, including electrochemistry, gas storage and so on. In particular, ILs are highly expected to serve as a green solvent to replace volatile organic solvents.

Nucleophilic substitution is one of typical reactions in organic system. A variety of the substitution reaction in ILs has been attracting many synthetic chemists' attentions and numerous studies such as S_N2 reaction have been extensively reported [2]. Meanwhile, Weingärtner stated as follows [3]; "The possibility to steer the nucleophilicity, or more generally, the solvent polarity, by variation of the couterion, reflects a unique feature of ILs. Theoretical models for nucleophilic substitution do not account for such effects." Quantum-chemical computational methods are now getting popular to analyze chemical reaction, especially in a system of isolated molecules. However, there are only few computational studies on chemical reaction in ILs. One of the obvious difficulty is how to treat the strong Coulombic interaction among ionic species. A extraordinary long computational time is required to obtain adequate statistical ensemble in molecular simulation. In addition, quantum chemistry is essential to

describe reaction and thus QM/MM simulation is a straightforward approach. But quantum chemical computation is very time-consuming and generally difficult to be performed with adequate statistical ensemble. In fact, semi-empirical or indirect treatment in quantum chemistry has been applied to reactions in ILs. Acevedo et al. reported Diels-Alder reaction based on semi-empirical PM3 hamiltonian [4]. Arantes et al. reported S_N2 reaction based on molecular dynamics simulation using pre-determined parameters [5].

An alternative to molecular simulation is a theory in statistical mechanics, reference interaction site model (RISM) [6], which is an integral equation theory for molecular liquid developed by Chandler et al. in 1970's. In the theory, radial distribution function describing solvation structure is directly computed in an analytical manner. Thanks to this feature of the theory, adequate statistical ensemble can be obtained with a reasonable computational cost. The treatment of ILs is realized by means of the extension to multicomponent system [7].

Chiappe et al. reported liquid structure at MOLECULAR LEVEL and thermodynamic properties of simple ions in ILs using RISM theory [8] and for the first time applied RISM-SCF method, which is a combination of RISM and electronic structure theory, [9] to predicting self-consistently electronic and classical solvation structure of ionic liquid. [10] Recently, we studied Diels-Alder reaction in ILs from the first principle [11] using RISM-SCF-SEDD method and it is noteworthy that very recently Chiappe and co-workers studied Diels-Alder reaction between cyclopendatiene and acrolein in [mmim][PF_6] with KS-DFT/3D-RISM-SCF theory. [12] RISM-SCF and its family have been successfully applied to a wide range of chemical phenomena in solution. It is our intent here to only describe the brief summary of the theory and assume the readers' familiarity of RISM-SCF as well as the statistical mechanics of molecular liquids. Some examples of recent studies are found in Refs. [13–17] More lengthy discssion can be found in several literatures. [18–20] It should be emphasized that highly sophisticated theory such as CCSD can be directly combined with statistical-mechanical solvation structure in a self-consistent manner. This point is a clear difference from conventional QM/MM simulation, in which semi-empirical electronic structure methods are still widely used.

In the present study, S_N2 reaction of methyl p-nitrobenzenesulfonate (p-NBS) and chloride anion is studied using RISM-SCF-SEDD method with CCSD level of theory.

5.2 Computational details

In RISM theory, solvation free energy ($\Delta\mu$) is given by, [21]

$$\Delta\mu = -\frac{\rho}{\beta}\sum_{\alpha s}\int \mathrm{d}\mathbf{r}\left[c_{\alpha s}(r) - \frac{1}{2}h_{\alpha s}^2(r)\Theta(-h_{\alpha s}(r)) + \frac{1}{2}h_{\alpha s}(r)c_{\alpha s}(r)\right], \tag{5.1}$$

where ρ is the number density and $\beta = 1/k_{\mathrm{B}}T$. Θ is Heaviside step function. $h_{\alpha s}(r)$ and $c_{\alpha s}(r)$ are respectively total and direct correlation functions between site α (in solute) and s (in solvent). Some selected features and advantages of RISM are summarized as following: (1) The theory provides adequate thermodynamic ensemble and is free from statistical error or so-called sampling problem. It deals with infinite number of solvent molecules and requires no 'simulation box'. (2) Since it is written in algebraic equation, computational cost is dramatically reduced compared to standard molecular simulation method. (3) The inputs of the computation are the same as those of simulations, and the outputs are very similar, too.

In RISM-SCF theory, conventional electronic structure theory is combined with RISM. The total energy of the system ($\mathscr{A}$) is defined as follows,

$$\mathscr{A} = E_{\mathrm{solute}} + \Delta\mu = E_{\mathrm{isolated}} + E_{\mathrm{reorg}} + \Delta\mu. \tag{5.2}$$

E_{solute} is total energy of the solute molecule (p-NBS with Cl^-) within the framework of *ab initio* MO theory including solvation effect. It is different from the total energy in gaseous phase (E_{isolated}) by E_{reorg}, which represents the distortion of electronic structure. In the theory, the influence of surrounding solvent is naturally taken into account and the electronic structure of the solute and the solvent structure are simultaneously obtained.

In quantum chemical aspect, 6-31+G(d) basis set was adopted through the study but the diffuse function was omitted in S atom since strongly positive charge was assigned for the atom. The geometries were optimized in gas phase using RHF method under the constraint of C_s structure, in which the dihedral angle of C–O_{S1}–S–C is in the mirror plane perpendicular

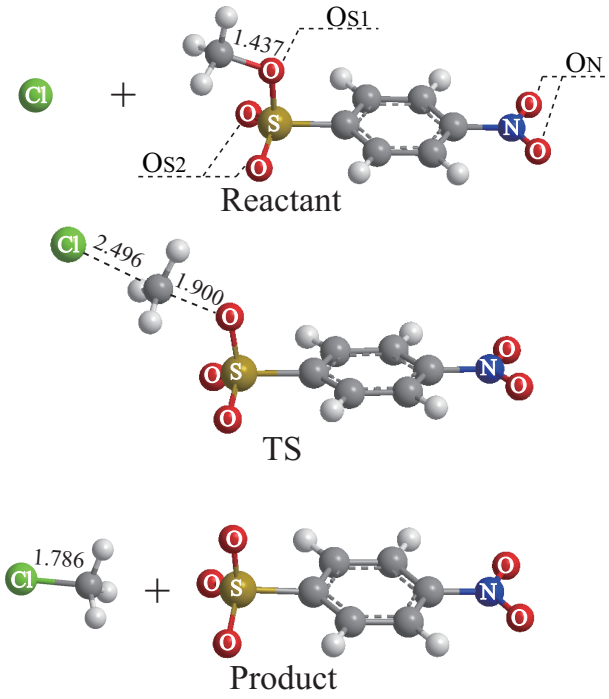

Figure 5.1: Optimized geometries of the reactant, TS, and product. Species are at infinite separation in the reactant and product. Distances are in angstrom.

to the benzene ring. The obtained structures were depicted in Figure 5.1. All the energy was then evaluated with CCSD method using the same basis set both in the gas phase as well as in solvent.

1-3-dimethylimidazolium hexafluorophosphate ([mmim][PF_6]) was chosen as the ionic solvent and a comparison was made with dichloromethane (DCM), which is one of the typical organic solvents. The RISM integral equation was solved with the Kovalenko-Hirata closure [21]. The temperature (T) and number density (ρ) were set to 400 K and 0.003704 molecules $Å^{-3}$ for [mmim][PF_6]. 298.15 K and 0.009339 molecules $Å^{-3}$ were used for DCM. The potential parameters for these solvents were taken from literatures. [22–25] All hydrogen and fluoride atoms were fused on the carbon and phosphate atoms, respectively, and these atoms were treated as a single site (see Table 5.1).

All the computations were performed by GAMESS program package [26] modified by us to implement RISM-SCF-SEDD method.

Table 5.1: Lennard-Jones parameters adopted to solute and solvents.

species	site	σ/Å	ϵ/kcal mol^{-1}	$q/\|e\|$
[mmim]$^+$	C_R	3.880	0.10414	0.504
	N	3.250	0.16692	-0.267
	C_W	3.880	0.10414	0.199
	CH_3	3.775	0.20350	0.310
PF_6	PF_6	5.600	0.39900	-1.000
DCM	C	3.400	0.10900	-0.363
	Cl	3.471	0.26500	-0.037
	H	2.293	0.01600	0.218
solute[a]	C	3.550	0.07000	-
	H	2.420	0.03000	-
	N	3.250	0.12000	-
	O_N	2.960	0.17000	-
	S	3.742	0.47000	-
	O_S	3.029	0.12000	-

[a] Effective charges of solute molecule are determined by RISM-SCF-SEDD method.

5.3 Results and Discussion

5.3.1 Energy profiles and activation barrier

The potential energy curve in gas phase and free energy curves in solution are shown in Figure 5.2, where the difference between the O_{S1}–CH_3 and CH_3–Cl bond lengths is chosen as the reaction coordinate R so as the reaction proceeds from the left hand side to right hand side,

$$R = r(\mathrm{O_{S1}}\text{–}\mathrm{CH_3}) - r(\mathrm{CH_3}\text{–}\mathrm{Cl}). \tag{5.3}$$

The energy curves were computed at fixed *R* by optimizing all the rest of degrees of freedom.

Since it is commonly believed that ILs can affect heavily the structure of transition states, [4, 12] the optimized TS structures in solution were checked. To be sure, the structural reorganization is noticeably large (see supporting information). While TS geometry is found at $R = -0.596$ Å in gas phase, that in [mmim][PF_6] is found at $R = -0.412$ Å. However, it does not greatly affect the discussion about the free energy around TS because the energy of the TS obtained in [mmim][PF_6] is approximately the same as that of the species at $R = -0.4$ Å.

Similar to the well-known S_N2 reaction system of Cl^-+CH_3Cl, [14] ion-dipole complex is found (marked with I) in gas phase around $R = -2$ Å and the barrier does not exist in effect.

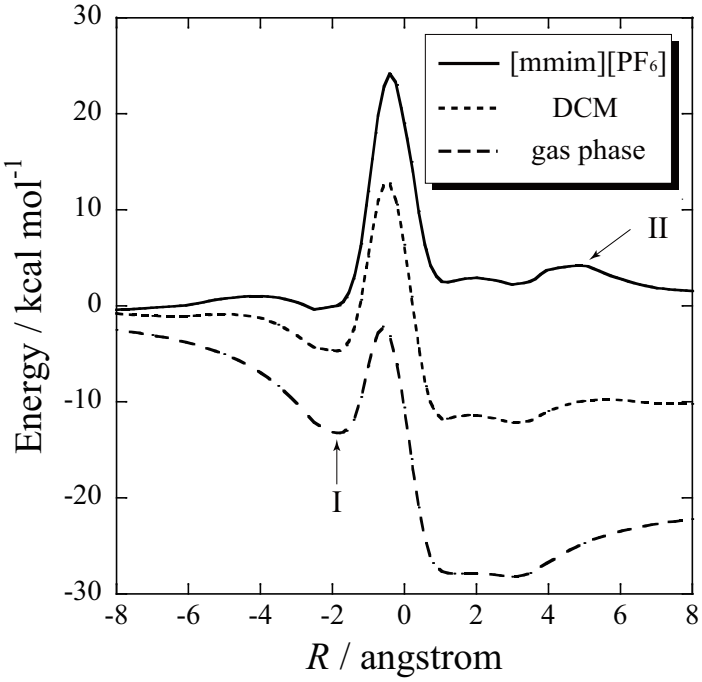

Figure 5.2: Potential energy curve in gas phase (dashed line) and free energy curves in [mmim][PF_6] (solid line) and in DCM (dotted line) along reaction coordinate *R*.

Due to the de-localization of electron, the product is considerably stabilized in gas phase. The profile is dramatically changed in solution phase. The stabilization of the ion-dipole complex with respect to the reactant is weakened in DCM and it virtually disappears in [mmim][PF_6]. The barrier in DCM (14.0 kcal mol^{-1}) is higher than that in gas phase, and the height is even higher for [mmim][PF_6] (27.3 kcal mol^{-1}). This is attributed to the difference in the stability of Cl^- at the reactant. Cl^- is strongly solvated by [mmim][PF_6] compared to the DCM. Since the baseline of the curves shown in the figure are standardized at the reactant state, the relative energy to the transition state (TS) becomes greater in [mmim][PF_6]. This means the stability in [mmim][PF_6] and in DCM are not significantly different at product state. In fact, the curvatures at the range from $+2$Å to longer region (marked with II) in [mmim][PF_6] and in DCM look very similar.

5.3.2 Changes in solvation free energy and effective charge

In order to elucidate the mechanism of the solvation, details of solvation energy are analyzed. Solvation free energy $\Delta\mu$ (Eq.5.1) can be "formally" divided into the contribution from each atom in the solute molecule labeled α.

$$\Delta\mu = \sum_{\alpha} \Delta\mu_{\alpha}, \tag{5.4}$$

where

$$\Delta\mu_{\alpha} = -\frac{\rho}{\beta} \sum_{s} \int \mathrm{d}\mathbf{r} \left[c_{\alpha s}(r) - \frac{1}{2} h_{\alpha s}^{2}(r) \Theta(-h_{\alpha s}(r)) + \frac{1}{2} h_{\alpha s}(r) c_{\alpha s}(r) \right]. \tag{5.5}$$

This quantity represents how much the contribution from each site is. For the sake of the convenience, $\Delta\mu$ is divided into four subsystems' contributions; Cl, methyl moiety (CH_3), SO_3, and nitrobenzene moiety ($NO_2C_6H_4$).

Figure 5.3 and 5.4 plot total $\Delta\mu$ and its components as function of *R* in [mmim][PF_6] and DCM, respectively. As discussed above, the reactant is strongly solvated and the total solvation free energy ($\Delta\mu$) gradually increase along R. After passing through the barrier, a plateau is found from *R* = 0 Å to *R* = 5 Å and the solute is stabilized with the formation of the product. (-6.8 kcal mol^{-1} in [mmim][PF_6] and -3.0 kcal mol^{-1} in DCM). Note that these features are similar in the two solvents, regardless the changes in their components are quite different.

In [mmim][PF_6], the significant changes are found in the curves of the energy component of Cl, CH_3, and SO_3 (Figure 5.3). These are directly related to the inversion in the S_N2 mechanism, where the bond formation and cleavage occur. The change in $\Delta\mu_{\mathrm{Cl}}$ is conspicuous and governs the total profile of changing. Clearly, the solvation of Cl plays a key role to determine the height of the reaction barrier, which makes the reactant side stable to be comparable to the product side as shown above. It is very likely that affinity of Cl^- for [mmim][PF_6] is strong enough and the anion is well solvated especially by $[mmim]^+$. The CH_3 and SO_3 curves show the opposite trends around $R = -4$ Å to -2Å, since the bond polarization occurs due to the the approaching chloride ion. After the substitution, *p*-NBS anion ($[SO_3\text{-}NO_2C_6H_4]^-$) is stabilized mainly due to the SO_3 component.

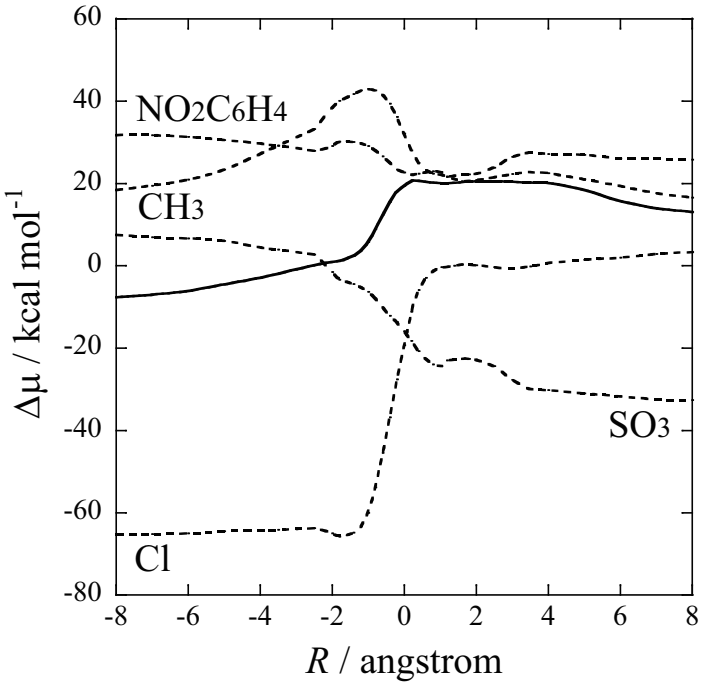

Figure 5.3: Solvation free energy in [mmim][PF_6] (solid line) and its components (dashed lines) as functions of *R*.

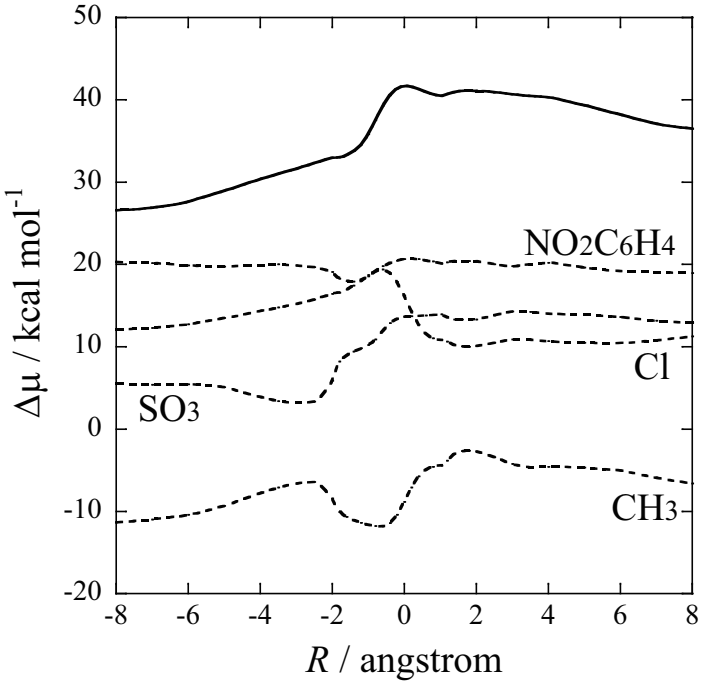

Figure 5.4: Solvation free energy in DCM (solid line) and its components (dashed lines) as functions of *R*.

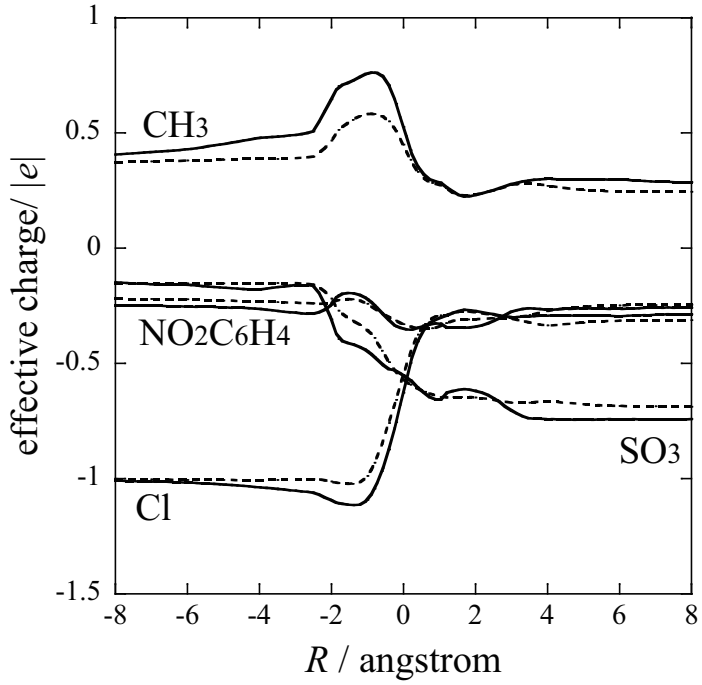

Figure 5.5: Changes in the effective charges assigned to each moiety in [mmim][PF_6] (solid lines) and in DMC (dashed lines) along the reaction coordinate *R*.

In DCM, the situation is quite different (Figure 5.4). There is no major player and all the free energy components are moderately changed. Note that the range of the vertical axis is half of the [mmim][PF_6] case. It is interesting that the changes in Cl, SO_3 and CH_3 are in opposite direction. $\Delta\mu_{\mathrm{Cl}}$ is positive at the reactant and then decreases along R. Presumably, the affinity of CH_3Cl for DCM at the product state is relatively strong compared to Cl^- appearing at the reactant state.

The effective charge provides valuable information to understand the solvation free energy. Figure 5.5 shows the effective charges assigned at each moiety. The components of Cl and SO_3 are considerably changed compared with others. As the reaction proceeds, electron transfer from Cl to *p*-NBS both in [mmim][PF_6] and DCM. This clearly shows the electron migrates from Cl mainly to SO_3 component. The change in the effective charge corresponds to the changing in the solvation free energy curves of [mmim][PF_6]. On the other hand, the solvation free energy in DCM is relatively insensitive to the changes in effective charge.

5.3.3 Solvation structure

Because of the large charge migration, the solvation structure drastically changes as the reaction proceeds, which can be seen through the radial distribution functions (RDFs). Figures 5.6 shows the RDFs around Cl atom in [mmim][PF_6]. The most positively charged site (C_R) in $[mmim]^+$ and the anionic element $[PF_6]^-$ are plotted in the figure. In the RDFs of Cl–C_R, the peak located around 3.5 Å corresponds to direct contact of C_R of $[mmim]^+$ with Cl anion. Cl–PF_6 RDF for I shows a broad peak around 6–8 Å, caused by the repulsive interaction between anions. These indicate that Cl^- is strongly solvated almost only by $[mmim]^+$ at the initial stage of the reaction. The feature is already pointed out in previous works by Welton et al.; [2] neutron diffraction study on the structurally related compound [mmim][Cl] showed that the anion is coordinated by 6 cations within 6.5 Å. [27] The coordination number calculated from the computed C_R–Cl RDF at the reactant is 5.6, showing good agreement with the experimental result. As the reaction proceeds, the peak of the RDF becomes lower and the coordination number decreases to 4.7 at TS. This indicates the occurrence of partial de-solvation of Cl^-, making it possible to act as a nucleophile and giving rise to the reaction. These results support the experimental information. [2]

The RDFs around Cl in DCM solvent is shown in Figure 5.7. Both in the RDFs of Cl–C and Cl–H, distinct peaks are found in I, which are weakened after producing CH_3Cl. The interaction between H atom in DCM and Cl^- contributes to the stabilization, but at the same time, the negatively charged site C in DCM becomes closer to Cl^-, which makes the interaction unfavorable. This may be one of the reasons that the reactant state in DCM is not strongly stabilized regardless of the strong charge of Cl^-.

5.4 Concluding Remarks

In the present article, S_N2 reaction of methyl p-nitrobenzenesulfonate (p-NBS) and chloride anion in ionic liquid ([mmim][PF_6]) was studied using RISM-SCF-SEDD theory. Solvation structure as well as energy profile along the reaction were discussed by comparing with dichloromethane system. To the best of our knowledge, this is the first attempt to elucidate the

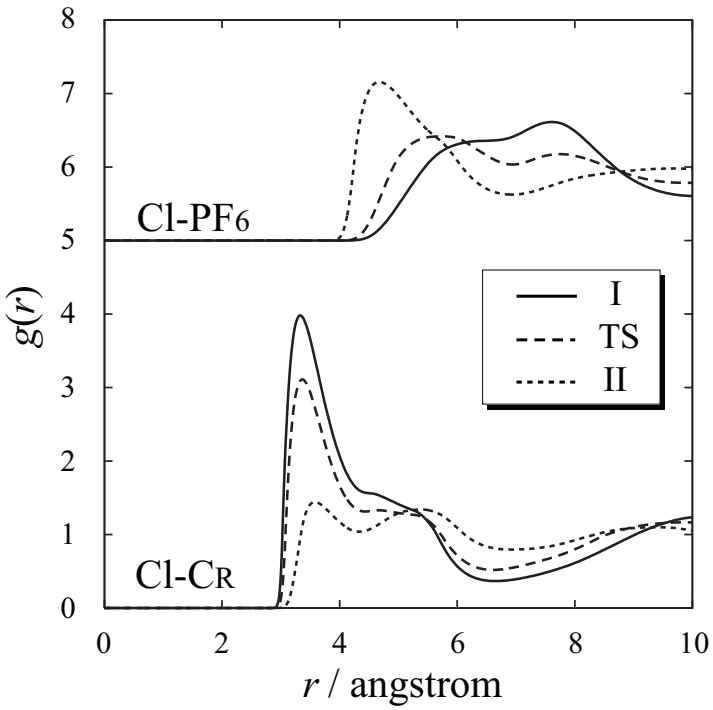

Figure 5.6: RDFs around the Cl atom at I, TS, and II: C_R and PF_6 in [mmim][PF_6]

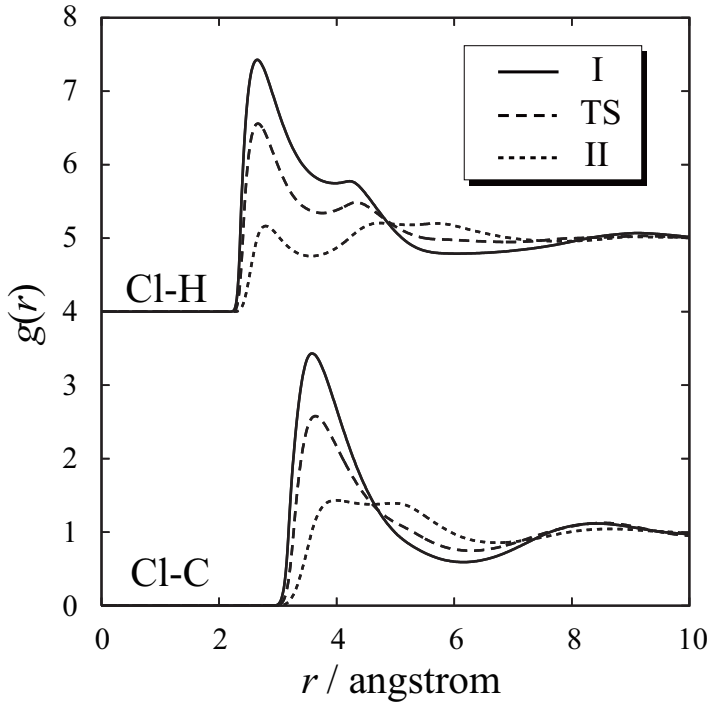

Figure 5.7: RDFs around the Cl atom at I, TS, and II: C and H in DCM

mechanism of S_N2 reaction in ionic liquid from the first principle. Highly sophisticated electronic structure theory, CCSD, was employed coupled with statistical mechanics at molecular level.

The barrier height in DCM obtained by RISM-SCF method is 14.0 kcal mol^{-1}, in reasonable agreement with the experimental value (18.8 kcal mol^{-1}). [2] The value in [mmim][PF_6] is calculated to be 27.3 kcal mol^{-1} (experimental value: 19.7 kcal mol^{-1} in [bmim][PF_6]). The qualitative difference between the two solvent is properly reproduced in the present model, [30] but the barrier in ILs is slightly higher. Note that the S_N2 reaction is simply described by ordinary electronic structure theory thus the present treatment is more than enough. PCM (polarizable continuum model) may not be applicable because dielectric constant (ϵ) seems to be an oversimplified parameter to describe ILs. [3, 28]

A few factors are conceivable: (i) treatment of $[PF_6]^-$ anion as a united site, (ii) inhomogeneity effect on the reaction, and (iii) the difference between $[mmim]^+$ and $[bmim]^+$. To check the contribution from (i), we compared the difference of activation free energy between the united model and all-atom model. But the difference evaluated with RHF method is very small, 1.2 kcal mol^{-1}. For (ii), it is believed that the effects of inhomogeneity is negligible when the length of the side chain is less than 4-5 units. [29] The contribution from (iii) is not quantitatively obvious. At this moment, development of a new theory that can deal with structural flexibility of the chain is now progress. We believe that quantitative description of the chemical reaction in ILs, including $[bmim]^+$, should come close in near future.

5.5 Appendix

Table 5.2: Activation free energy evaluated with the solvation free energy in different forms at RHF level. Zero point and thermal corrections are not included. All units are in kcal mol^{-1}. Relative values to the barrier evaluated in HNC form are in parenthesis.[a]

free energy form	$\Delta\mathscr{A}^{\ddagger}$ ([mmim][PF_6])	$\Delta\mathscr{A}^{\ddagger}$ (DCM)
KH	22.52 (-1.74)	12.59 (-1.39)
GF	27.40 (3.14)	19.74 (5.76)

[a] $\Delta\mathscr{A}^{\ddagger}$ in HNC form is 24.26 kcal mol^{-1} in [mmim][PF_6] and 13.98 kcal mol^{-1} in DCM.

Bibliography

[1] *Ionic Liquids in Synthesis*; Welton, T.; Wasserscheid, P.; VCH-Wiley; Weinheim; 2002.

[2] (a) Lancaster, N. L.; Welton, T.; Young, G. B. *J. Chem. Soc., Perkin Trans.* **2001**, *2*, 2267. (b) Lancaster,N. L.; Salter, P. A.; Welton, T.; Young, G. B. *J. Org. Chem.* **2002**, *67*, 8855. (c) Lancaster,N. L.; Welton, T. *J. Org. Chem.* **2004**, *69*, 5986.

[3] Weingärtner, H. *Angew. Chem. Int. Ed.* **2008**, *47*, 654.

[4] (a) Acevedo, O.; Jorgensen, W. L.; Evanseck, J. D. *J. Chem. Theor. Comp.* **2007**, *3*, 132. (b) Sambasivarao, S. V.; Acevedo, O. *J. Chem. Theor. Comp.* **2009**, *5*, 1038.

[5] Arantes, G. M. ; Ribeiro, M. C. C. *J. Phys. Chem.* **2008**, *128*, 114503.

[6] (a) Chandler, D.; Andersen, H. C. *J. Chem. Phys.* **1972**, *57*, 1930. (b) Hirata, F.; Rossky, P. J. *Chem. Phys. Lett.* **1981**, *83*, 329. (c) Hirata, F.; Rossky, P. J.; Pettitt, B. M. *J. Chem. Phys.* **1982**, *78*, 4133.

[7] Kinoshita, M.; Hirata, F. *J. Chem. Phys.* **1997**, *106*, 5202.

[8] (a) Bruzzone, S.; Malvaldi, M.; C. Chiappe, C. *Phys. Chem. Chem. Phys.* **2007**, *9*, 5576. (b) Bruzzone, S.; Malvaldi, M.; Chiappe, C. *J. Chem. Phys.* **2008**, *129*, 074509.

[9] (a) Ten-no, S.; Hirata, F.; Kato, S. *Chem. Phys. Lett.* **1993**, *214*, 391. (b) Ten-no, S.; Hirata, F.; Kato, S. *J. Chem. Phys.* **1994**, *100*, 7443. (c) Sato, H.; Hirata, F.; Kato, S. *J. Chem. Phys.* **1996**, *105*, 1546. (d) Yokogawa, D.; Sato, H.; Sakaki, S. *J. Chem. Phys.* **2007**, *126*, 244054.

[10] Malvaldi, M.; Bruzzone, S.; Chiappe, C.; Gusarov, S.; Kovalenko, A. *J. Phys. Chem. B* **2009**, *113*, 3536.

[11] Hayaki, S.; Kido, K.; Yokogawa, D.; Sato, H.; Sakaki, S. *J. Phys. Chem. B* **2009**, *113*, 8227.

[12] Chiappe, C.; Malvaldi, M.; Pomelli, C. S. *J. Chem. Theor. Comp.* **2010**, *6*, 179.

[13] Iida, K.; Yokogawa, D.; Ikeda, A.; Sato, H.; Sakaki, S. *Phys. Chem. Chem. Phys.* **2009**, *11*, 8556.

[14] Sato, H.; Sakaki, S. *J. Phys. Chem. A* **2004**, *108*, 1629.

[15] Minezawa, N; Kato, S. *J. Phys. Chem. A* **2005**, *109*, 5445.

[16] Iida, K.; Yokogawa, D.; Sato H.; Sakaki, S. *Chem. Phys. Lett.* **2007**, *443*, 264.

[17] Hayaki, S.; Yokogawa, D.; Sato, H.; Sakaki, S. *Chem. Phys. Lett.* **2008**, *458*, 329.

[18] *Continuum Solvation Models in Chemical Physics: From Theory and Applications*; Mennucci, B.; Cammi, R.; Wiley: West Sussex, England, 2007.

[19] *Molecular Theory of Solvation*; Hirata, F. Eds.; Kluwer Academic Publishers: Netherlands, 2003.

[20] *Computational Biochemistry and Biophysics*, Becker, O. M.; MacKerell, A. D.; Jr. Roux, B.; Watanabe, K. Eds.; Marcel Dekker; New York, 2001.

[21] Kovalenko, A.; Hirata, F. *J. Chem. Phys.* **1999**, *110*, 10095.

[22] Hanke, C. G.; Price, S. L.; Lynden-Bell, R. M. *Mol. Phys.* **2001**, *99*, 801.

[23] (a) Fox, T.; Kollman, P. A. *J. Phys. Chem. B* **1998**, *102*, 8070. (b) Cornell, W. D.; Cieplak, P.; Bayly, C. I.; Gould, I. R.; Jr. Merz, K. M.; Fergunson, D. M.; Spellmeyer, D. C.; Fox, T.; Caldwell, J. W.; Kollman, P. A. *J. Am. Chem. Soc.* **1995**, *117*, 5197.

[24] Kelkar, M. S.; Shi, W.; Maginn, E. J. *Int. Eng. Chem. Res.* **2008**, *47*, 9115.

[25] Yoshida, N.; Ishida, T.; Hirata, F. *J. Phys. Chem. B* **2008**, *112*, 433.

[26] Schmidt, M. W.; Baldridge, K. K.; Boatz, J. A.; Elbert, S. T.; Gordon, M. S.; Jensen, J. H.; Koseki, S.; Matsunaga, N.; Nguyen, K. A.; Su, S. Windus, T. L.; Dupuis, M.; Montgomery J. A. *J. Comput. Chem.* **1993**, *14*, 1347.

[27] Hardacre, C.; Holbrey, J. D.; McMath, S. E. J.; Bowron, D. T.; Soper, A. K. *J. Chem. Phys.* **2003**, *118*, 273.

[28] Kobrak, M. N. *J. Phys. Chem. B* **2007**, *111*, 4755.

[29] Canongia Lopes, J. N. A.; Pádua, A. A. H. *J. Phys. Chem. B* **2006**, *110*, 3330.

[30] The difference in barrier hight in [mmim][PF_6] and in DCM is 9.93 kcal mol^{-1} in the KH form free energy and that in other form such as gaussian fluctuation is reduced (see appendix) but the error in the barrier height difference is not so improved. Thus the error arise from the same reason that the barrier height in ILs is slightly overestimated.

Chapter 6

An *Ab Initio* Study on an Excited-State Intramolecular Proton Transfer Reaction in Ionic Liquids

6.1 Introduction

Room-temperature ionic liquids (RTILs) have been extensively studied as a novel class of solvent. [1–4] The solvation dynamics of RTILs attracts great attention from researchers, and its features have been clarified. In particular, one of interesting features is the wide distribution of solvation time scales [5–13]. Molecular dynamics simulations [14–16] suggested that the fastest component is attributed to translational motions of the ions in the vicinity of the solute molecule.

The solvation dynamics [17, 18] on an excited-state intramolecular proton transfer (ESIPT) reaction of 4′-N, N-diethylamino-3-hydroxyflavone (DEAHF) (Figure 6.1) in RTILs has been studied with steady-state and time-resolved fluorescent spectroscopy [19–21]. Basically, the ESIPT kinetics in RTILs is similar to those in conventional solvent [22–24], the proton-transfer rate shows noticeable dependence on the excitation wavelength [20, 21]. Several other works also report the excitation-wavelength dependence (red-edge-effect) in ionic liquid systems [25–28]. Although the molecular mechanism of this dependence was suggested [21], the role of the solvation on ESIPT reaction is still unclear.

In the field of theoretical chemistry, a hybrid method of quantum mechanics and molecular mechanics (QM/MM) is a straightforward approach to study the electronic structure of a molecule in solution phase. The QM/MM study on ionic liquid system, however, is very

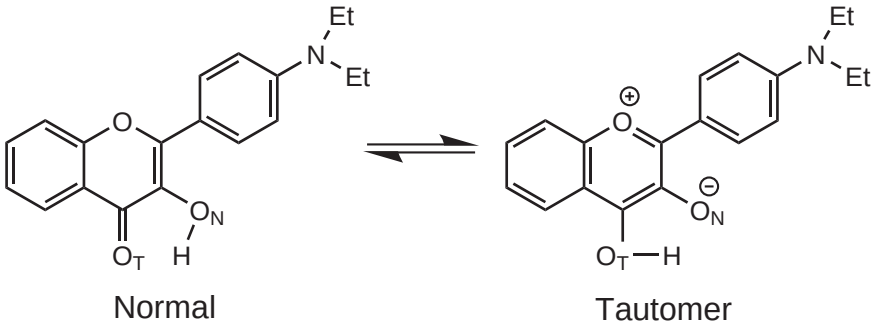

Figure 6.1: Excited state intramolecular proton transfer reaction of DEAHF.

limited so far because the strong Coulombic interactions among ions make it formidable to properly describe RTILs solvation, leading to a large computational demands. Hence semi-empirical methods such as PM3 are mainly utilized to describe chemical reactions in RTILs [29–33], except for one density functional theory (DFT) study [34].

The reference interaction site model (RISM) [35, 36] is an alternative way to tackle ionic liquid systems. Thanks to its analytical treatment on correlation function, RISM is capable of taking into account the long range Coulombic interaction and free from statistical error. RISM-SCF-SEDD [40, 41] is a hybrid of RISM and *ab initio* molecular orbital theory, which enable us to pursue chemical phenomena in RTILs. KS-DFT/3D-RISM-KH [42] is a similar approach combining RISM and Kohn-Sham DFT. These theories have been expanded to multi-component systems [43] and successfully applied to investigate solvation structure [44–46]. The mechanisms of chemical reactions in RTILs were clarified from the first-principle [47–49]. It is also noted that RISM-SCF [37–39] was proved to be a powerful tool to obtain free energy profiles along proton transfer reaction coordinates in solutions [50–54]. The transport and relaxation properties of RTILs were explored using mode-coupling theory based on RISM [55].

In the present article, we wish to report a molecular-level RISM-SCF-SEDD study on the ESIPT of DEAHF in 1-butyl-3-methylimidazolium hexafluorophosphate ([bmim][PF_6]) , which is one of the most widely used RTILs. Two new aspects are introduced: Because the molecular geometry of solvent in the conventional RISM must be fixed at a specific one,

the conformational flexibility of [bmim][PF_6] was not able to be treated. Here, the structural fluctuation such as the rotation of side chains was incorporated with the aid of flexible-RISM theory [56]. The other is the nonequilibrium free energy change due to the solvent fluctuation [57–62] along the ESIPT process. While RISM is basically a theory for equilibrium statistical mechanics, orientational polarization of solvent molecules plays an important role [17, 18]. We focused on the changes in free energy and microscopic solvation to grasp the solvent relaxation of RTILs along ESIPT. To our best knowledge, this is the first *ab initio* study on photochemical reactions in RTILs.

6.2 Computational Details

The Kovalenko-Hirata (KH) type closure was coupled to solve the RISM equation [42]. The number density (ρ) of [bmim][PF_6] was set to 0.002894 molecules $Å^{-3}$ and the temperature T was 298.15 K, which corresponds to the experimental condition [1, 19–21]. The potential parameters of solvent [bmim][PF_6] molecules and Lennard-Jones parameters of solute molecule were taken from the literatures [45, 63–65] and given in Table 6.1 and Table 6.2. For [bmim][PF_6] molecules, we employed the united-atom model, in which hydrogen atoms and fluoride atoms are respectively fused to carbon atoms and phosphorus atom as shown in Figure 6.2. The rotations of three dihedral angles along the butyl chain were taken into account using flexible-RISM theory [56] (see appendix for the detailed procedure).

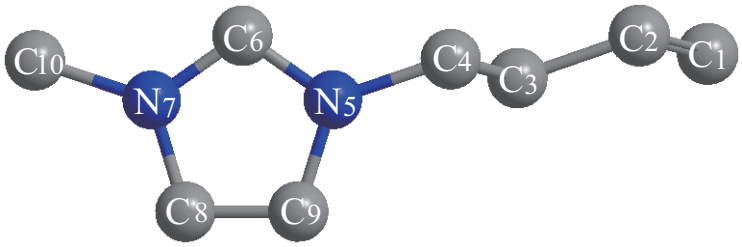

Figure 6.2: $[bmim]^+$ of united-atom model.

Standard 6-31G* basis sets were adopted for carbon and nitrogen atoms, and diffuse function was added to oxygen (6-31+G*). 6-31G basis set was used for H, while polarization function

Table 6.1: Potential Parameters for Solute and Solvent Molecules.

species	site	σ/Å	ϵ/kcal mol^{-1}	$q/\|e\|$
DMAHF[a]	C	3.400	0.086	-
	N	3.341	0.170	-
	O	3.066	0.210	-
	H	2.600	0.015	-
	H_O[b]	1.000	0.056	-
[bmim][PF_6]	C_1	3.905	0.175	-0.047
	C_2	3.905	0.118	0.118
	C_3	3.905	0.118	0.118
	C_4	3.905	0.118	0.024
	N_5	3.250	0.170	0.071
	C_6	3.880	0.106	0.229
	N_7	3.250	0.170	0.133
	C_8	3.880	0.106	0.041
	C_9	3.880	0.106	0.096
	C_{10}	3.775	0.207	0.217
	PF_6	5.600	0.399	-1.000

[a] Electrostatic interactions are determined by RISM-SCF-SEDD procedure.
[b] H_O denotes the hydrogen atom attached to oxygen atoms.

Table 6.2: Torsional Parameters for the Rotatable Dihedral Angles. All Units are in kcal mol^{-1}.

Dihedral angle	V_0	V_1	V_2	V_3
C_1–C_2–C_3–C_4	0.0000	0.7040	-0.1350	1.5740
C_2–C_3–C_4–N_5	0.0000	1.3360	-0.1145	0.2425
C_3–C_4–N_5–C_6	0.0000	-0.6980	-0.2125	0.0000
C_3–C_4–N_5–C_9	0.0000	-0.6980	-0.2125	0.0000

was added to the transferring H. DFT and TDDFT with B3LYP functional were utilized to describe the electronic structure of solute molecule. Ethyl group in DEAHF were modeled with methyl group and we abbreviate the modeled molecule as DMAHF hereafter. Geometry optimizations were performed in the gas phase and all the energy was then evaluated using the same geometries in the gas phase as well as in [bmim][PF_6].

We adopted the difference between the O_N–H and O_T–H distances as the proton coordinate q (Figure 6.1),

$$q = r(\mathrm{O_N} - \mathrm{H}) - r(\mathrm{O_T} - \mathrm{H}). \tag{6.1}$$

For each state, the solute geometry along the proton transfer path was determined by optimizing the other internal degrees of freedom at each q value. In the optimization, no symmetry constraint was applied.

All calculations for electronic structures were performed by GAMESS suite of programs [66] modified by us to implement RISM-SCF-SEDD method and flexible-RISM computations were performed by our program.

6.3 Results and Discussion

6.3.1 Free energy changes

The energy profiles of S_0 and S_1 states in the gas phase and in [bmim][PF_6] along the proton coordinate q are shown in Figure 6.3. In S_1 state two minima are found, which is consistent with the experimental observation of dual emission spectra. DMAHF molecule in S_0 state is more stable in the normal form compared to the tautomer one. The difference between the solid and dotted lines in Figure 6.3 corresponds to the solvation effects in energy. The molecule in the excited normal form is stabilized due to considerable solvation effects in [bmim][PF_6]. As discussed below in details, this can be understood the changes in dipole moment.

The absorption and emission energies are summarized in Table 6.3. Here we assumed that the electronic transition to the final state is fast enough to leave the solute geometry and the

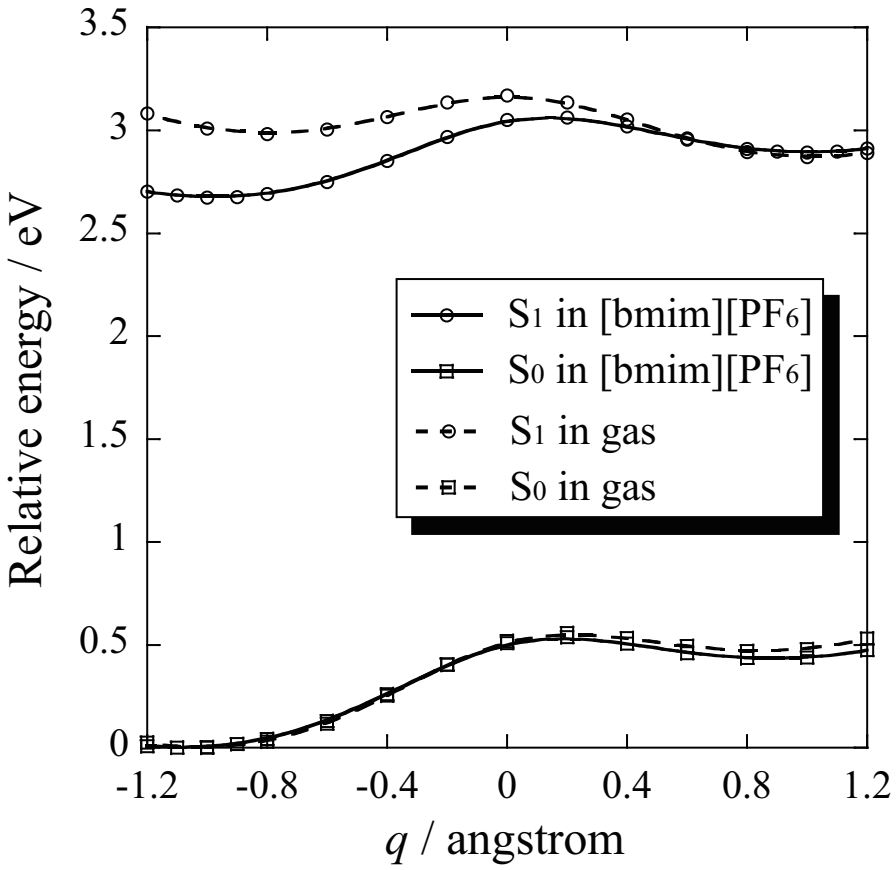

Figure 6.3: Relative energy as a function of the proton coordinate q with respect to the normal form in the ground state. Solid and dotted lines indicate the free energy in [bmim][PF_6] and potential energy in the gas phase, respectively. Lines with squares and circles correspond to the S_0 ground and S_1 excited state.

solvation structure frozen at the initial state of transition. We further assumed that the solvation is equilibrated in the excited state within the observation time-scale of the steady-state spectroscopy. [20] The latter assumption might be invalid in the case of highly viscous RTILs, whose time scale of solvation dynamics is quite slower compared with that of conventional liquids (1-10 ps). [11, 13] It is noted, however, that the observed fluorescent lifetime (ca. 3 ns) [20] is slightly longer compared to the time scale of [bmim][PF_6] (ca. 1 ns). In fact, the obtained results are in good agreement with the experimental ones, while the emission energy from tautomer form is slightly overestimated.

Table 6.3: Absorption and Emission Energies in eV.

	calc.	exptl. [20]
Absorption	2.99	3.02
Emission (normal)	2.34	2.34
Emission (tautomer)	2.37	2.14

6.3.2 Changes in dipole moment

Solvation effects in the free energy profiles can be rationalized in terms of the dipole moment of solute molecule shown in Figure 6.4. The dipole moment becomes larger due to the excitation in the normal form, which increases the solute–solvent electrostatic interaction. The dipole moment in the excited state, however, drastically decreases as the proton transfer reaction proceeds, and thus the dipole moment of the tautomer form in the excited state is comparable to that of the ground state. These results correspond to the CIS calculations performed by Chou and collaborators [23], although the magnitudes of their dipole moments are smaller than those of ours. The distinct solvation effects on the excited state at normal form is consistent with the remarkable increase in the dipole moment.

The change in the dipole moment is consistent with the time-resolved fluorescent spectra [19, 20]. While a drastic Stokes shift was observed at the normal form, no marked shift was found at the tautomer. From the changes of the dipole moment, it turns out that the electron distribution is changed due to the excitation in the normal form and the subsequent proton transfer reaction in the excited state. The changes in the dipole moment due to the excitation can be understood from the viewpoint of molecular orbitals. TDDFT calculations revealed that the excitation was mainly described with a HOMO(π)–LUMO(π^*) transition. Figure 6.5 displays important Kohn-Sham orbitals. This Figure indicates that the excitation is characterized by the electron transfer from the HOMO localized at the aniline moiety (right hand side of DMAHF as shown in Figure 6.5) to the LUMO at chromene moiety (left hand side), giving rise to the drastic increase of the dipole moment upon the excitation.

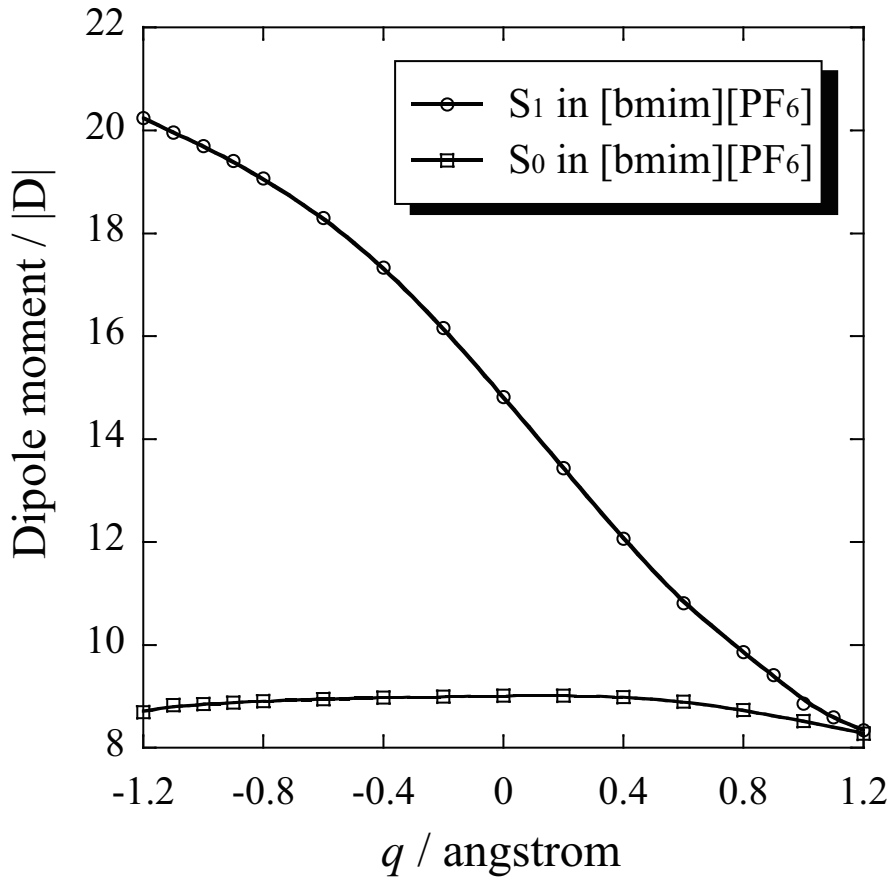

Figure 6.4: Changes in dipole moment along the proton coordinate q. Lines with squares and circles denote the dipole moment of DMAHF in the S_0 ground and S_1 excited state, respectively.

6.3.3 Effects of relaxation of solvation

Nonequilibrium free energy change due to solvent fluctuation

The nonequilibrium free energy is given as the sum of the equilibrium free energy and the deviation from it;

$$\mathscr{A}_{\rm neq}(\mathbf{R},\mathbf{V}) \;=\; \mathscr{A}_{\rm eq}(\mathbf{R_0},\mathbf{V_0}) + \Delta\mathscr{A}(\mathbf{R},\mathbf{V}), \tag{6.2}$$

where $\mathbf{R}$ and $\mathbf{V}$ denotes the solute geometry and the electrostatic potential (ESP) acting on the solute molecule, respectively. The subscript 0 stands for the equilibrium state.

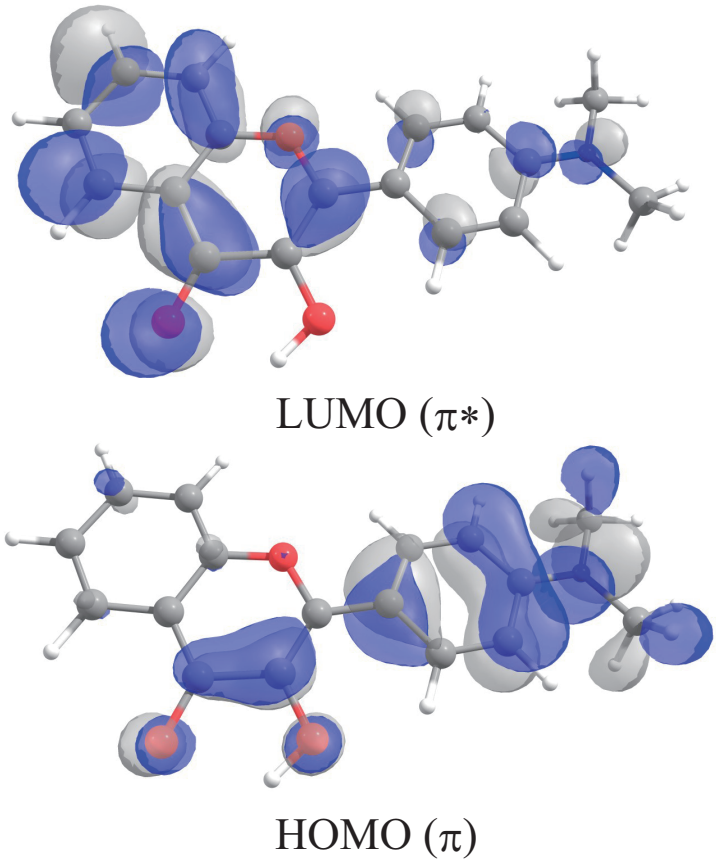

Figure 6.5: Important Kohn-Sham orbitals of the normal form DMAHF in [bmim][PF_6].

The equilibrium free energy defined in the framework of RISM-SCF theory is

$$\mathscr{A}_{\text{eq}}(\mathbf{R_0}, \mathbf{V_0}) = \left\langle \Psi_{\text{sol}}(\mathbf{R_0}, \mathbf{V_0}) \left| \hat{H}(\mathbf{R_0}) \right| \Psi_{\text{sol}}(\mathbf{R_0}, \mathbf{V_0}) \right\rangle + \Delta\mu_0(\mathbf{R_0}, \mathbf{V_0}). \tag{6.3}$$

$\hat{H}$ is the Hamiltonian for a solute molecule in the standard quantum chemical method and Ψ_{sol} is the wave function of the solute molecule in solution. In the framework of RISM with KH closure, solvation free energy $\Delta\mu_0$ is analytically given. [42]

$$\Delta\mu_0(\mathbf{R_0}, \mathbf{V_0}) = \sum_{\alpha}^{\text{solute}} \sum_{\gamma}^{\text{solvent}} \frac{4\pi\rho_\gamma}{\beta} \int \mathrm{d}r r^2 \left\{ \frac{1}{2} \left(h_{\alpha\gamma}(r)\right)^2 \Theta(h_{\alpha\gamma}(r)) - c_{\alpha\gamma}(r) - \frac{1}{2} h_{\alpha\gamma}(r) c_{\alpha\gamma}(r) \right\} \tag{6.4}$$

where $h_{\alpha\gamma}(r)$ and $c_{\alpha\gamma}(r)$ are the total and direct correlation functions, respectively. β is the inverse of the product of Boltzmann constant k_{B} and temperature T. ρ_γ denotes the density of solvents.

Here we assumed that the deviation from the equilibrium free energy can be considered as the change due to the solvent fluctuation. Chong *et al.* have proposed a method to evaluate the nonequilibrium free energy profile in the electron transfer process, which was further extended to quantum mechanical systems. [57–62] We modify the method to evaluate $\Delta\mathscr{A}$ so as to adapt RISM-SCF-SEDD method, in which the charge distribution of the solute molecule is expressed with the expansion coefficient of auxiliary basis sets (ABSs) $\mathbf{d}$. [40,41] To calculate the distribution functions for nonequilibrium process, a hypothetical charge distribution and solute geometry, as a function of linear parameter s, are introduced for describing the solvent fluctuation due to the excitation:

$$\mathbf{d}^{s} = (1-s)\mathbf{d}_{\mathrm{S}_0} + s\mathbf{d}_{\mathrm{S}_1}, \tag{6.5}$$

and

$$\mathbf{R}^{s} = (1-s)\mathbf{R}_{\mathrm{S}_0} + s\mathbf{R}_{\mathrm{S}_1}. \tag{6.6}$$

To express the solvent fluctuation due to the proton transfer, we adopted a coordinate $q^{'}$, which denotes the equilibrium state parameter at a specific proton coordinate:

$$\mathbf{d}^{q^{'}} = \mathbf{d}(q^{'}), \tag{6.7}$$

and

$$\mathbf{R}^{q^{'}} = \mathbf{R}(q^{'}). \tag{6.8}$$

Combining s and $q^{'}$, we generated the solvent configurations corresponding to the fluctuation due to the excitation and the proton transfer reaction in the excited state.

In the model (a schematic illustration is shown in Figure S1), "nonequilibrium" solvent configuration $\mathbf{V}^{s,q^{'}}(\mathbf{d}^{s,q^{'}})$ can be realized as an "equilibrium" state by setting $\mathbf{d}^{s,q^{'}}$ corresponding to hypothetical charge on solute molecules. With the same procedure described in the previous papers, [59–61] the expression of the nonequilibrium free energy change is given by

$$\Delta\mathscr{A}(\mathbf{R}^{s,q^{'}}, \mathbf{V}^{s,q^{'}}) = \Delta\mu^{s,q^{'}} - \Delta\mu_0 - \mathbf{V}^{s,q^{'}}(\mathbf{d}^{s,q^{'}} - \mathbf{d}_0), \tag{6.9}$$

where the solvent ESP $V^{s,q'}$ acting on ABSs can be expressed in the framework of RISM-SCF-SEDD [40, 41] as follows:

$$\begin{aligned}\mathbf{V}^{s,q'} &= \sum_{i}^{\text{ABSs}} V_i^{s,q'} \\ &= \sum_{i}^{\text{ABSs}} \sum_{\gamma}^{\text{solvent}} \rho_\gamma q_\gamma C_i \left(\frac{\pi}{\alpha_i}\right)^{3/2} \int_0^\infty \mathrm{d}r 4\pi r^2 \frac{\mathrm{erf}(\sqrt{\alpha_i} r) h_{\alpha\gamma}^{s,q'}(r)}{r}. \end{aligned} \tag{6.10}$$

C_i and α_i stand for the coefficients and exponents of ABSs. $\Delta\mu^{s,q'}$ can be obtained by substituting the correlation functions calculated with the hypothetical $\mathbf{d}^{s,q'}$ and geometry into Eq. (4). From Eqs. (2), (3), and (9), the final form for the nonequilibrium free energy is given by

$$\begin{aligned}\mathscr{A}_{\text{neq}}(\mathbf{R}^{s,q'}, \mathbf{V}^{s,q'}) = \left\langle \Psi_{\text{sol}}(\mathbf{R_0}, \mathbf{V_0}) \middle| \hat{H}(\mathbf{R_0}) \middle| \Psi_{\text{sol}}(\mathbf{R_0}, \mathbf{V_0}) \right\rangle \\ + \Delta\mu^{s,q'}(\mathbf{R}^{s,q'}, \mathbf{V}^{s,q'}) - \mathbf{V}^{s,q'}(\mathbf{d}^{s,q'} - \mathbf{d}_0). \end{aligned} \tag{6.11}$$

Evolution of proton transfer potential

As a solvation coordinate corresponding to the solvent fluctuation in the ESIPT process, we chose the difference between the electrostatic interaction energies as a standard manner:

$$\Delta H^{s,q'} = \mathbf{V}^{s,q'}(\mathbf{d}_{\mathrm{S}_1}^{\text{normal}} - \mathbf{d}_{\mathrm{S}_1}^{\text{tautomer}}). \tag{6.12}$$

Figure 6.6 shows the free energy surface of S_1 state. [67] The plotted energy is relative value to the equilibrium free energy of the excited state at normal form. Note that the free energy changes with respect to the solvent fluctuation (vertical direction) can be well approximated with quadratic functions (see Supporting Information for the Stokes shift in the normal form), although the method employed here is inherently a nonlinear theory. The linear response regime provides a good approximation for this system, similar to the preceding papers. [68–74] The potential energy change of the proton transfer under the fixed field of the solvent molecules gives us an insight into the evolution of the proton transfer process coupled to the solvent orientational polarization. [53, 75, 76] In particular, we focused on the solvent configurations immediately after the excitation (corresponding to $\Delta H^{s,q'} \simeq 3.9$ kcal/mol^{-1} and $q < 0$: we call the region "A") and equilibrium solvation after the relaxation, which are consistent with

the tautomer form ($\Delta H^{s,q'} \simeq 4.2$ kcal/mol^{-1} and $q > 0$: region "B") and excited normal form ($\Delta H^{s,q'} \simeq 12.2$ kcal/mol^{-1} and $q < 0$: region "C"). Figure 6.7 shows energy change of the transfer in the excited state, corresponding to the cross-sections at fixed $\Delta H^{s,q'}$. In the region A (green), the barrier height of the proton transfer is relatively small because the solvent configuration is unfavorable for the normal form. As the relaxation toward the equilibrium, the solvation configuration becomes consistent with the normal form (red: region C). Eventually, the excited normal form is strongly stabilized while the excited tautomer is apparently unstable. This suggest the barrier becomes higher as the solvent relaxes towards the normal form, corresponding to the dynamic Stokes shift observed in the experiments [19–21]. The energy profile, in which the solvation configuration is consistent with the tautomer form (blue: region B), is rather similar to that in the region A. This can be understood in terms of the dipole moment (Figure 6.4) and the solvation coordinate (Figure 6.7). The dipole moment and $\Delta H^{s,q'}$ in the tautomer are similar to those of the region C.

Although quantitative description of the time-dependent perspectives is not available from the free energy surface, the relation between solvent relaxation and ESIPT process is understood with the aid of experimental observations [19–24]. Experimentally, faster ($\sim$ 3 ps) and slower (20$\sim$30 ps) ESIPT processes were observed not only in RTILs, but also in acetonitrile [20, 23]. The solvation dynamics of RTILs is much slower than the ESIPT process, in ns time scale. Based on these observations, it seems that the proton transfer mostly proceeds under the solvation coordinate with small $\Delta H^{s,q'}$ (corresponding to green line in Figure 6.6). After the completion of the ESIPT in the initial stage, the solvent relaxation to the excited state normal form proceeds along the solvation coordinate. The solvation coordinate near the region A may be dominated by the local translations of the ions in the vicinity of the solute as suggested previously. [14–16]

6.3.4 Solvent configurations

Typically solvation structures are discussed using radial distribution functions $g(r)$. [bmim][PF_6] is, however, composed of many sites and it is difficult to identify solvation structure by ascrib-

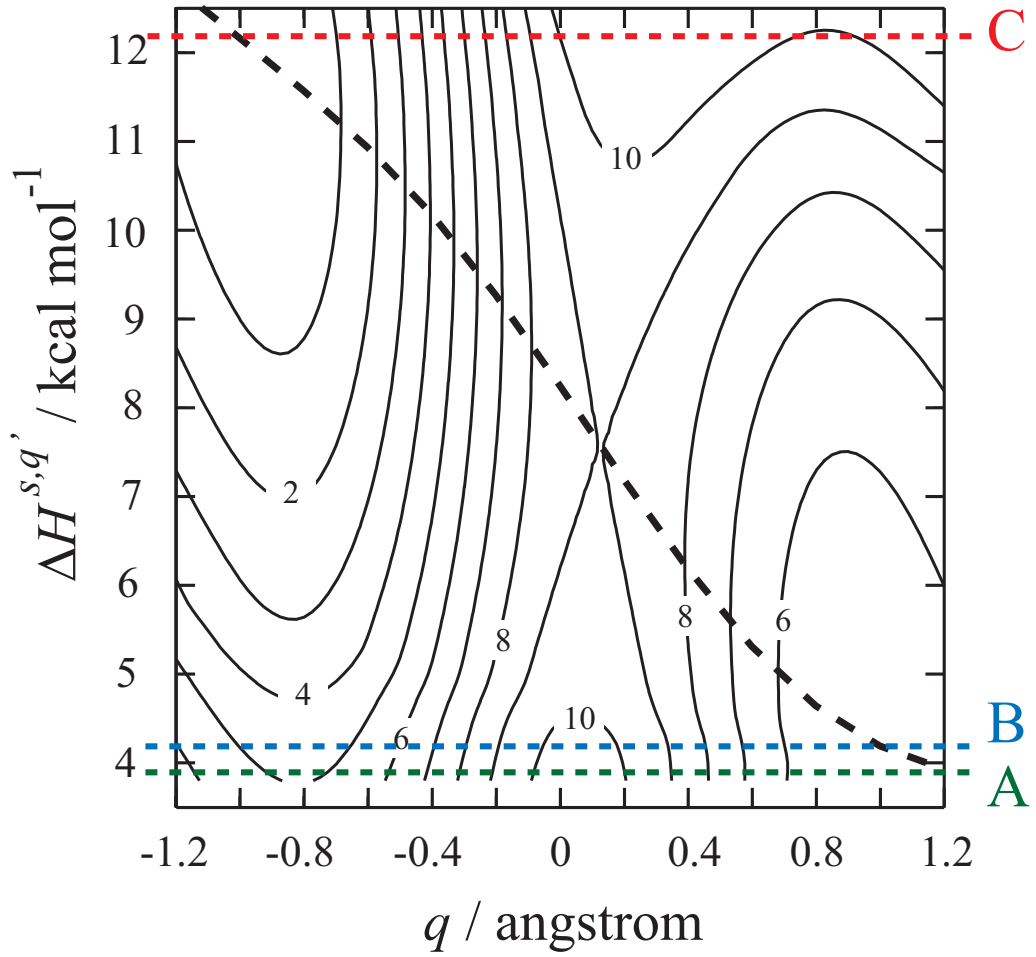

Figure 6.6: Relative nonequilibrium free energy to that of the equilibrium excited state normal form ($\Delta\mathscr{A}_{\mathrm{neq}}$). Contour spacings are 1.0 kcal mol^{-1}. The dotted thick line stands for the equilibrium free energy solvation path, which corresponds to the free energy curve of S_1 state in Figure 6.3. The green, blue, and red lines correspond to the solvation coordinate consistent with (A) the immediately after the excitation, (B) the equilibrium excited state tautomer form, and (C) normal form, respectively.

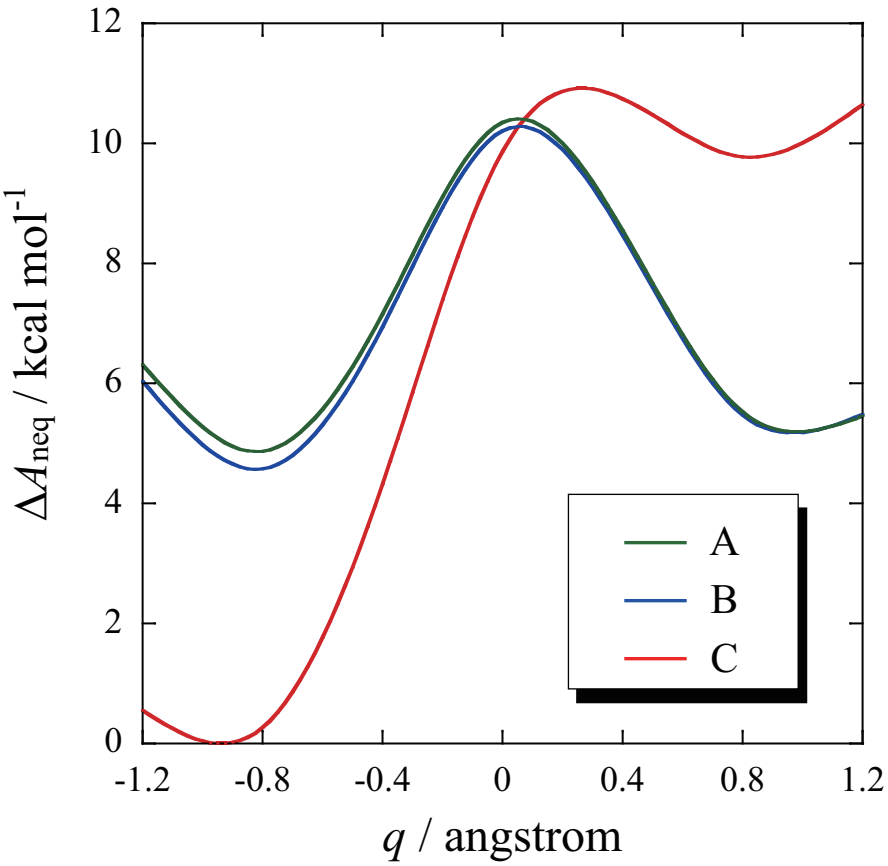

Figure 6.7: Nonequilibrium free energy changes $\Delta\mathscr{A}_{\mathrm{neq}}$ along the proton coordinate q. See the text and Figure 6.6 for the definitions of the curves A, B, and C.

ing specific configurations of solvent. Thus we focused on charge density functions which reduce solvent configurations to distributions of solvent charge,

$$\rho_\alpha(r) = \sum_{\gamma}^{\text{solvent site}} \rho_\gamma q_\gamma g_{\alpha\gamma}(r). \tag{6.13}$$

Figure 6.8 represents changes in the charge density around O_T along the relaxation (a) from the immediately after the excitation to the normal form in the excited state mainly attributed to the change in $\Delta H^{s,q'}$ and (b) from the immediately after the excitation to the tautomer related to the change in q. The positive sign of the functions indicates that contribution from the $[bmim]^+$ is dominant around the distances while the negative sign corresponds to the main contribution from the $[PF_6]^-$. In the charge density functions in Figure 6.8 (a), a sharp positive peak is found at 3.3 Å, indicating the main contribution in the first solvation shell is from the cations which directly contacts to O_T. A small negative peak is found at 4.7 Å, indicating that the anions do not contact with O_T directly. The contribution is attributed to the transferring H. As the relaxation to the normal form proceeds, the positive peak is enhanced while the negative peak diminishes. This is because O_T is more negatively charged due to the charge transfer from the amine moiety. In the charge density functions in Figure 6.8 (b), a sharp peak is found at 3.3 Å too, where the peak height is lowered as the solvation structure relaxes to the tautomer. The peak position and height of a small negative peak found at 5 Å become closer and higher along the relaxation. These changes arise from the formation of a bond between O_T and H.

6.4 Conclusions

In the present paper, we theoretically investigated the ESIPT of DEAHF molecule in $[bmim][PF_6]$ using RISM-SCF-SEDD method in conjunction with flexible-RISM. In order to incorporate the nonequilibrium solvation effects due to solvent fluctuation concomitant with the photo excitation and proton transfer process, a thermodynamic treatment proposed by Chong *et al* was utilized.

The free energy curves along the proton coordinate q exhibited two important features: the normal form is more stable in the ground state and two minima are found in the excited state,

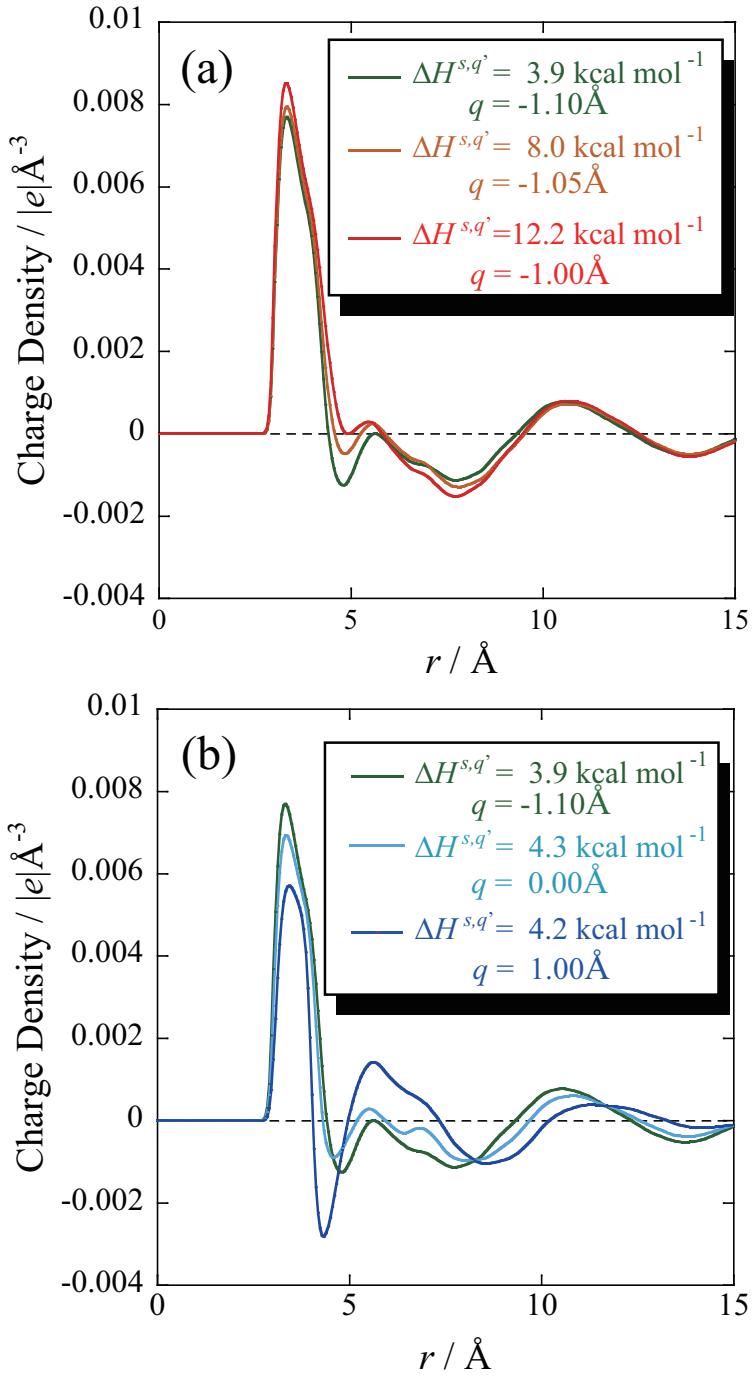

Figure 6.8: Changes in charge density functions around O_T along the relaxation (a) from the immediately after the excitation to the excited state normal form and (b) from the immediately after the excitation to the excited state tautomer. The orange and cyan curves represent the intermediate to the excited normal and tautomer states;see the inset and Figure 6.6 for detail.

which is consistent with the experimental observations. The calculated absorption and emission energy are in good agreement with the experiments. The excitation is mainly characterized by the electron transfer from the HOMO on aniline moiety to the LUMO on chromene moiety, giving rise to the drastic increase of the dipole moment of DMAHF. This corresponds to the observed dynamic Stokes shift of the peak assigned to the excited normal form. The proton transfer in the excited state are also accompanied by drastic changes in the dipole moment. The nonequilibrium free energy contour as a function of the proton coordinate q and the solvation coordinate $\Delta H^{s,q'}$ gives us two insights into this system: (i) the evolution of proton potential and (ii) the validity of linear response approximation. While immediately after the excitation the barrier height of the proton transfer process is relatively small, the barrier becomes larger as the solvation relaxation to the excited normal state proceeds. The experimental observations and the obtained results suggest that the ESIPT process completes in the solvation coordinate near the region A, namely in the initial stage of the photo excitation. The result obtained here and in the preceding papers suggest that linear response free energy, in which the distribution of solvent fluctuation is represented by a gaussian form, [51, 53, 77–79] is applicable to wide range of ionic liquid systems.

Before closing, we draw the readers' attentions to the dependency of the rate of proton transfer on the excitation wavelength. [20, 21] Very recently, the excitation wavelength dependence was explored in relation to the inhomogeneous distribution of the solute in RTILs. [21] It is reported that the inhomogeneous structure [74,80–85] is not crucial for the excitation wavelength dependence since similar effect is observed for the conventional molecular liquids. Further theoretical studies with some improved treatments on the relation between reaction dynamics of the ESIPT of DEAHF and inhomogeneous solvation are highly desired.

6.5 Appendix I: Incorporating Structural Fluctuation of [bmim]$^+$

The solvent-solvent RISM equation, which gives correlation functions for neat liquids, is written as follows, [86]

$$\boldsymbol{h}_{vv} = \boldsymbol{\omega}_v * \boldsymbol{c}_{vv} * \boldsymbol{\omega}_v + \boldsymbol{\omega}_v * \boldsymbol{c}_{vv} * \boldsymbol{\rho}_v \boldsymbol{h}_{vv}. \tag{6.14}$$

Here, $\boldsymbol{h}$ and $\boldsymbol{c}$ are the matrices of total and direct correlation functions, respectively. $\boldsymbol{\rho}$ is that of the number density of solvent and $\boldsymbol{\omega}$ denotes the matrix of intramolecular correlation functions, which is represented with delta functions for rigid molecules. The subscript *v* indicate sol*v*ent. In flexible-RISM theory, the intramolecular structural fluctuation of solvent molecules are treated in terms of intramolecular correlation functions $\boldsymbol{\omega}$, which is decomposed to the ideal gas part $\boldsymbol{\omega}^{\mathrm{ref}}$ and the residual part $\Delta\boldsymbol{\omega}$, as follows:

$$\boldsymbol{\omega} = \boldsymbol{\omega}^{\mathrm{ref}} + \Delta\boldsymbol{\omega}. \tag{6.15}$$

$\boldsymbol{\omega}^{\mathrm{ref}}$ is evaluated with Monte Carlo simulation for an isolated molecule and $\Delta\boldsymbol{\omega}$, which describes many-body effects in liquids, is iteratively determined by solving the developed equations. [56]

In the RISM computations of the ionic liquid, only four dihedral angles were flexible in this model, namely, C_1–C_2–C_3–C_4, C_2–C_3–C_4–N_5, C_3–C_4–N_5–C_6, and C_3–C_4–N_5–C_9. Since the C_3–C_4–N_5–C_6 and C_3–C_4–N_5–C_9 dihedral angles share the C_4–N_5 axis, the degree of freedom is virtually three (see Figure 6.2). The bond lengths and bond angles were fixed at the geometry of $\boldsymbol{\omega}^{\mathrm{ref}}$ determined by optimizing isolated $[\mathrm{bmim}]^+$ at MP2/6-311G(d,p) level. The potential for these dihedral angles $V(\phi)$ is expressed as follows;

$$V(\phi) = V_0 + \sum_{n=1}^{3} V_n[1 - (-1)^n \cos(n\phi)], \tag{6.16}$$

where the parameters employed for four dihedral angles in $[\mathrm{bmim}]^+$ are summarized in Table 6.2. [63,64] The standard Monte Carlo simulation for $\boldsymbol{\omega}^{\mathrm{ref}}$ of isolated $[\mathrm{bmim}]^+$ using Metropolis algorithm was carried out with 300 million configuration generations.

Solvation effects on solute molecules is incorporated through the solute-solvent RISM equation: [86]

$$\boldsymbol{h}_{uv} = \boldsymbol{\omega}_u * \boldsymbol{c}_{uv} * \boldsymbol{\chi}_{vv} \tag{6.17}$$

$$= \boldsymbol{\omega}_u * \boldsymbol{c}_{uv} * \boldsymbol{\omega}_v + \boldsymbol{\omega}_u * \boldsymbol{c}_{uv} * \boldsymbol{\rho}_v \boldsymbol{h}_{vv}. \tag{6.18}$$

The subscript *u* stands for sol*u*te. We can solve the equation by obtaining solvent susceptibility $\boldsymbol{\chi}_{vv}$ with flexible-RISM theory to incorporate solvation effects in flexible solvent molecules.

6.6 Appendix II: Stokes Shift in the Normal Form

A significant dynamic Stokes shift was observed by time-resolved fluorescent measurements and the shifting peak was assigned to the excited state normal form. [19–21] In order to see the free energy changes due to the solvent fluctuation more clearly, we focused on the Stokes shift in the excited state normal form.

To calculate the distribution functions for nonequilibrium process after the excitation, a hypothetical charge distribution **d** and solute geometry **R**, as a function of linear parameter s, are introduced for describing the solvent fluctuation due to the excitation:

$$\mathbf{d}^s = (1-s)\mathbf{d}_{\mathrm{S_0}}^{\mathrm{normal}} + s\mathbf{d}_{\mathrm{S_1}}^{\mathrm{normal}}, \tag{6.19}$$

and

$$\mathbf{R}^s = (1-s)\mathbf{R}_{\mathrm{S_0}}^{\mathrm{normal}} + s\mathbf{R}_{\mathrm{S_1}}^{\mathrm{normal}}. \tag{6.20}$$

By using the same procedure described in the previous papers (Figure 6.9), [59–61] the final expression of the nonequilibrium free energy change $\Delta\mathscr{A}$ is given by

$$\Delta\mathscr{A}(\mathbf{R}^s, \mathbf{V}^s) = \Delta\mu^s - \Delta\mu_0 - \mathbf{V}^s(\mathbf{d}^s - \mathbf{d}_0). \tag{6.21}$$

Thus the nonequilibrium free energy including the electronic term can be obtained,

$$\mathscr{A}(\mathbf{R}^s, \mathbf{V}^s) = \left\langle \Psi_{\mathrm{sol}}(\mathbf{R_0}, \mathbf{V_0}) \left| \hat{H}(\mathbf{R_0}) \right| \Psi_{\mathrm{sol}}(\mathbf{R_0}, \mathbf{V_0}) \right\rangle + \Delta\mu^s(\mathbf{R}^s, \mathbf{V}^s) - \mathbf{V}^s(\mathbf{d}^s - \mathbf{d}_0) \tag{6.22}$$

As a solvation coordinate which corresponds to the solvent fluctuation in the relaxation process, we chose the difference between the electrostatic interaction energies acting on the ground and excited normal form:

$$\Delta H^s = \mathbf{V}^s(\mathbf{d}_{\mathrm{S_0}}^{\mathrm{normal}} - \mathbf{d}_{\mathrm{S_1}}^{\mathrm{normal}}). \tag{6.23}$$

The relative free energies against the solvation coordinate focused on the normal form are shown in Figure 6.9. It is noteworthy that the nonequilibrium free energy changes against

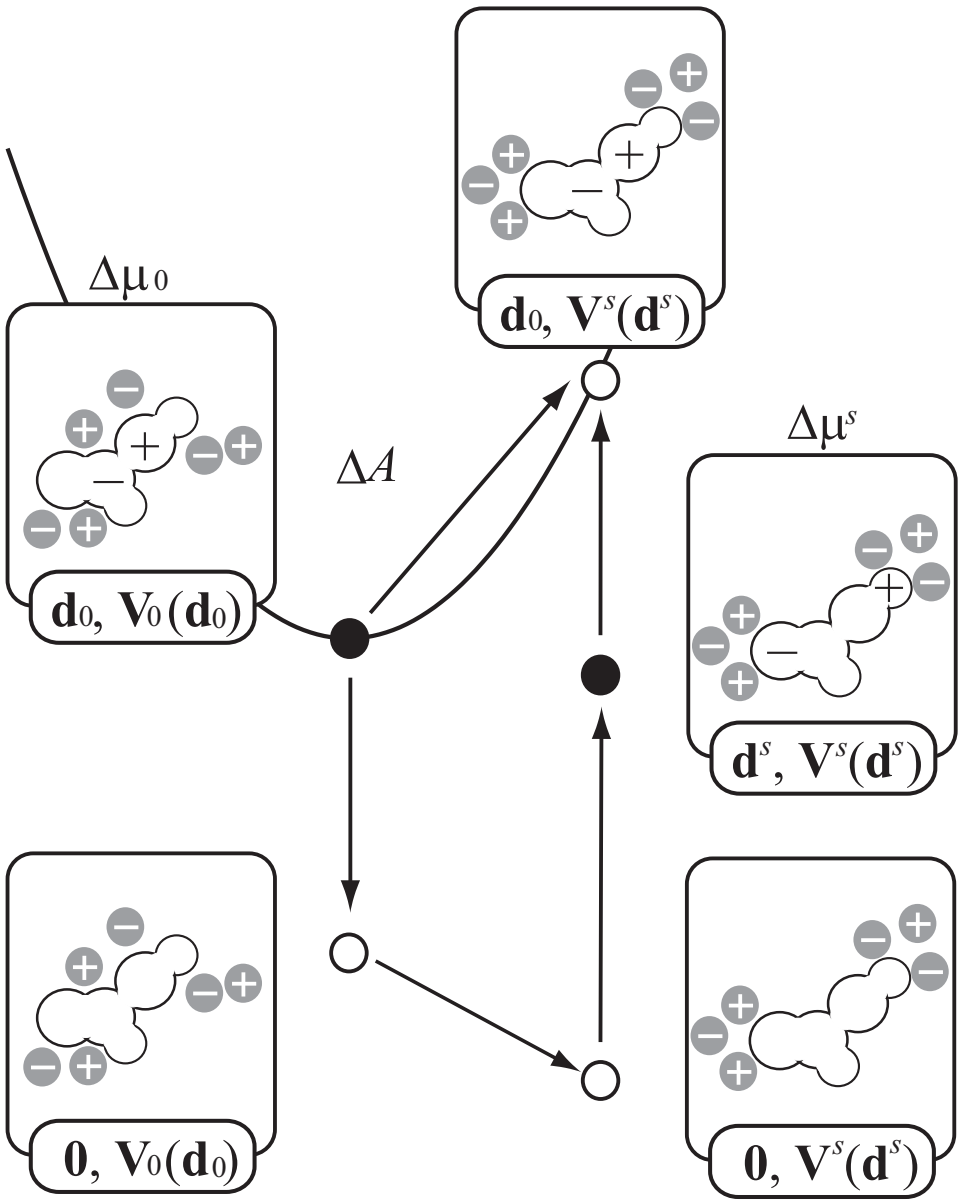

Figure 6.9: Schematic illustration for nonequilibrium free energy due to solvent fluctuation in the framework of RISM-SCF-SEDD based on the thermodynamic cycle model. [59–61] The solvent configuration is schematically represented by gray circles with positive or negative signs. The charge distributions and solvent configurations are denoted by the two variables: $\mathbf{d}$ and $\mathbf{V}(\mathbf{d})$. Black circles mean the equilibrium states obtained by standard RISM calculations.

the solvent fluctuation can be approximated well with quadratic functions. These results indicate linear response approximation is applicable for ionic liquid systems, which is consistent with the articles reported by Lynden-Bell, [68–71] Kim, [72, 73] and Margulis [74] with their coworkers that reaction free energies for electron transfer processes in ionic liquids are quadratic form and Marcus theory can be applied to the systems they investigated.

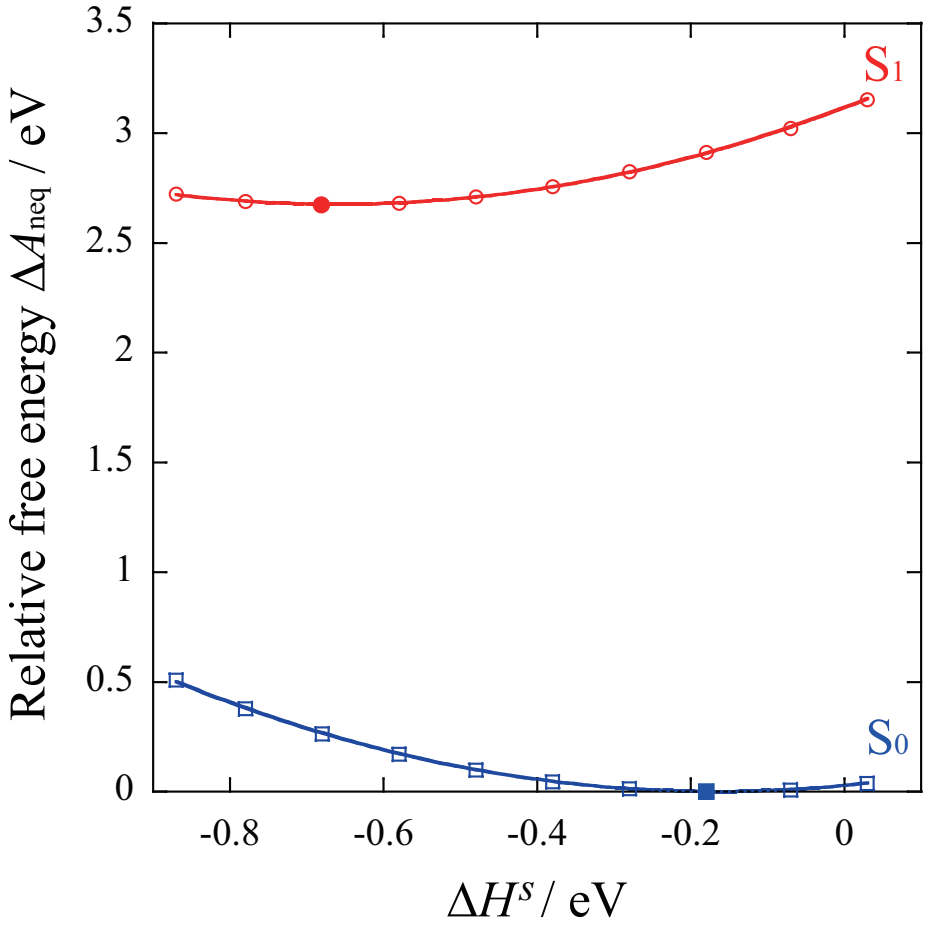

Figure 6.10: Relative free energies against the solvation coordinate ΔH^s. Blue line with squares and red line with circles are free energy of S_0 and S_1, respectively. Filled symbols indicate the equilibrium states. The parabolas are plotted by least-square fitting with the same force constant for S_0 and S_1 curves. Parameter s is changed from -0.4 to 1.4.

Bibliography

[1] *Ionic Liquids in Synthesis* 2nd ed.; Welton, T.; Wasserscheid, P. Eds.; VCH-Wiley: Weinheim, Germany, 2008.

[2] Weingärtner, H. *Angew. Chem. Int. Ed.* **2008**, *47*, 654.

[3] Castner, E. D.; Wishart, J. F. *J. Chem. Phys.* **2010**, *132*, 120901.

[4] Castner, E. W. Jr.; Margulis, C. J.; Maroncelli, M; Wishart, J. F. *Annu. Rev. Phys. Chem.* **2011**, *62*, 85.

[5] Karmakar, R.; Samanta, A. *J. Phys. Chem. A* **2002**, *106*, 4447.

[6] Karmakar, R.; Samanta, A. *J. Phys. Chem. A* **2003**, *107*, 7340.

[7] Paul, A.; Samanta, A. *J. Phys. Chem. B* **2007**, *111*, 4724.

[8] Ingram, J. A.; Moog, R. S.; Ito, N.; Biswas, R.; Maroncelli, M. *J. Phys. Chem. B* **2003**, *107*, 5926.

[9] Arzhantsev, S.; Ito, N.; Heitz, M.; Maroncelli, M. *Chem. Phys. Lett.* **2003**, *381*, 278.

[10] Arzhantsev, S.; Jin, H.; Baker, G. A.; Maroncelli, M. *J. Phys. Chem. B* **2007**, *111*, 4978.

[11] Jin, H.; Baker, G. A.; Arzhantsev, S.; Dong, J.; Maroncelli, M. *J. Phys. Chem. B* **2007**, *111*, 7291.

[12] Seth, D.; Chakraborty, A.; Setua, P.; Sarkar, N. *J. Phys. Chem. B* **2007**, *111*, 4781.

[13] Nagasawa, Y.; Itoh, T.,; Yasuda, M.; Ishibashi, Y.; Ito, S.; Miyasaka, H. *J. Phys. Chem. B* **2008**, *112*, 15758.

[14] Shim, Y.; Duan, J. S.; Choi, M. Y.; Kim, H. J. *J. Chem. Phys.* **2003**, *119*, 6411.

[15] Shim, Y.; Choi, M. Y.; Kim, H. J. *J. Chem. Phys.* **2005**, *122*, 044511.

[16] Kobrak, M. N. *J. Chem. Phys.* **2006**, *125*, 064502.

[17] *Chemical Dynamics in Condensed Phase* 1st ed.; Nitzan, A.; Oxford University Press: New York, United States, 2006.

[18] *Charge and Energy Transfer Dynamics in Molecular Systems* 3rd ed.; May, V.; Kühn, O.; VCH-Wiley: Weinheim, Germany, 2011.

[19] Fukuda, M.; Terazima, M.; Kimura, Y. *Chem. Phys. Lett.* **2008**, *463*, 364.

[20] Kimura, Y.; Fukuda, M.; Suda, K.; Terazima, M *J. Phys. Chem. B* **2010**, *114*, 11847.

[21] Suda, K.; Terazima, M; Kimura, Y. *Chem. Phys. Lett.* **2012**, *531*, 70.

[22] Chou, P. T.; Huang, C. H.; Pu, S. C.; Cheng, Y. M.; Yu, W. S.; Yu, Y. C.; Wang, Y.; Chen, C. T. *J. Phys. Chem. A* **2004**, *108*, 6452.

[23] Chou, P. T.; Pu, S. C.; Cheng, Y. M.; Yu, W. S.; Yu, Y. C.; Hung, F. T.; Hu, W. P. *J. Phys. Chem. A* **2005**, *109*, 3777.

[24] Cheng, Y. M.; Pu, S. C.; Yu, Y. C.; Chou, P. T.; Huang, C. H.; Chen, C. T.; Li, T. H.; Hu, W. P. *J. Phys. Chem. A* **2005**, *109*, 11696.

[25] Mandal, P. K.; Sarkar, M.; Samanta, A. *J. Phys. Chem. A* **2004**, *108*, 9048.

[26] Paul, A.; Mandal, P. K.; Samanta, A. *J. Phys. Chem. B* **2005**, *109*, 9148.

[27] Jin, H.; Xiang, Li.; Maroncelli, M. *J. Phys. Chem. B* **2007**, *111*, 13473.

[28] Kimura, Y.; Hamamoto, T.; Terazima, M. *J. Phys. Chem. A* **2007**, *111*, 7081.

[29] Acevedo, O. ; Jorgensen, W. L.; Evanseck, J. D. *J. Chem. Theor. Comput.* **2007**, *3*, 132.

[30] Sambasivarao, S. V.; Acevedo, O. *J. Chem. Theor. Comput.* **2009**, *5*, 1038.

[31] Arantes, G. M.; Ribeiro, M. C. C. *J. Chem. Phys.* **2008**, *128*, 114503.

[32] Yockel, S.; Schatz, G. C. *J. Phys. Chem. B* **2010**, *114*, 14241.

[33] Li, X.; Schatz, G. C.; Nesbitt, D. J. *J. Phys. Chem. B* **2012**, *116*, 3587.

[34] Klähn, M.; Seduraman, A.; Wu, P. *J. Phys. Chem. B* **2011**, *115*, 8231.

[35] Chandler, D.; Anderson, H. C. *J. Chem. Phys.* **1972**, *57*, 1930.

[36] Hirata, F.; Rossky, P. J. *Chem. Phys. Lett.* **1981**, *83*, 329.

[37] Ten-no, S.; Hirata, F.; Kato, S. *Chem. Phys. Lett.* **1993**, *214*, 391.

[38] Ten-no, S.; Hirata, F.; Kato, S. *J. Chem. Phys.* **1994**, *100*, 7443.

[39] Sato, H.; Hirata, F.; Kato, S. *J. Chem. Phys.* **1996**, *105*, 1546.

[40] Yokogawa, D.; Sato, H.; Sakaki, S. *J. Chem. Phys.* **2007**, *126*, 244054.

[41] Yokogawa, D.; Sato, H.; Sakaki, S. *J. Chem. Phys.* **2009**, *131*, 214504.

[42] Kovalenko, A.; Hirata, F. *J. Chem. Phys.* **1999**, *110*, 10095.

[43] Kinoshita, M.; Hirata, F. *J. Chem. Phys.* **1997**, *106*, 5202.

[44] Bruzzone, S.; Malvaldi, M.; Chiappe, C. *Phys. Chem. Chem. Phys.* **2007**, *9*, 5576.

[45] Bruzzone, S.; Malvaldi, M.; Chiappe, C. *J. Chem. Phys.* **2008**, *129*, 074509.

[46] Malvaldi, M.; Bruzzone, S.; Chiappe, C.; Gusarov, S.; Kovalenko, A. *J. Phys. Chem. B* **2009**, *113*, 3536.

[47] Chiappe, C.; Malvaldi, M.; Pomelli, C. S. *J. Chem. Theor. Comput.* **2010**, *6*, 179.

[48] Hayaki, S.; Kido, K.; Yokogawa, D.; Sato, H.; Sakaki, S. *J. Phys. Chem. B* **2009**, *113*, 8227.

[49] Hayaki, S.; Kido, K.; Sato, H.; Sakaki, S. *Phys. Chem. Chem. Phys.* **2010**, *12*, 1822.

[50] Yamazaki, S.; Kato, S. *Chem. Phys. Lett.* **2004**, *414*, 386.

[51] Yamamoto, T.; Kato, S. *J. Chem. Phys.* **2007**, *126*, 224514.

[52] Aono, S.; Kato, S. *J. Comput. Chem.* **2010**, *31*, 2924.

[53] Aono, S.; Yamamoto, T.; Kato, S. *J. Chem. Phys.* **2011**, *134*, 144108.

[54] Inagaki, T.; Yamamoto, T.; Kato, S. *J. Comput. Chem.* **2011**, *32*, 3081.

[55] Yamaguchi, T.; Koda, S. *J. Chem. Phys.* **2010**, *132*, 114502.

[56] Yokogawa, D.; Sato, H.; Sakaki, S. *Chem. Phys. Lett.* **2010**, *487*, 241.

[57] Chong, S-H.; Miura, S.; Basu, G.; Hirata, F. *J. Phys. Chem.* **1995**, *99*, 10526.

[58] Chong, S-H.; Hirata, F. *J. Chem. Phys.* **1997**, *106*, 5225.

[59] Sato, H.; Hirata, F. *J. Phys. Chem.* **2002**, *106*, 2300.

[60] Sato, H.; Kobori, Y.; Tero-Kubota, S.; Hirata, F. *J. Chem. Phys.* **2003**, *119*, 2753.

[61] Sato, H.; Kobori, Y.; Tero-Kubota, S.; Hirata, F. *J. Phys. Chem. B* **2004**, *108*, 11709.

[62] Yoshida, N.; Ishida, T.; Hirata, F. *J. Phys. Chem. B* **2008**, *112*, 433.

[63] Shah, J. K.; Brennecke, J. F.; Maginn, E. J. *Green Chem.* **2002**, *4*, 112.

[64] Shah, J. K.; Maginn, E. J. *J. Phys. Chem. B* **2005**, *109*, 10395.

[65] Cornell, W. D.; Cieplak, P.; Bayly, C. I.; Gould, I. R.; Merz, K. M. Jr.; Fergunson, D. M.; Spellmeyer, D. C.; Fox, T.; Caldwell, J. W.; Kollman, P. A. *J. Am. Chem. Soc.* **1995**, *117*, 5197.

[66] Schmidt, M. W.; Baldridge, K. K.; Boatz, J. A.; Elbert, S. T.; Gordon, M. S.; Jensen, J. H.; Koseki, S.; Matsunaga, N.; Nguyen, K. A.; Su, S. Windus, T. L.; Dupuis, M.; Montgomery J. A. *J. Comput. Chem.* **1993**, *14*, 1347.

[67] The contour is obtained by cubic spline extrapolation since the ESPs are generated from specific geometries along the restrictive proton coordinate q thus it is difficult to calculate the region nearby $\Delta H^{s,q'} \simeq 3.8$ kcal mol^{-1} and $q = -1.2$ Å.

[68] Lynden-Bell, R. M. *Electrochem. Commun.* **2007**, *9*, 1857.

[69] Lynden-Bell, R. M. *J. Phys. Chem. B* **2007**, *111*, 10800.

[70] Lynden-Bell, R. M. *J. Chem. Phys.* **2008**, *129*, 204503.

[71] Streeter, I.; Lynden-Bell, R. M.; Compton, R. G. *J. Phys. Chem. C* **2008**, *112*, 14538.

[72] Shim, Y.; Kim, H. J. *J. Phys. Chem. B* **2007**, *111*, 4510.

[73] Shim, Y.; Jeong, D.; Manjari, S.; Choi, M. Y.; Kim, H. J. *Acc. Chem. Res.* **2007**, *40*, 1130.

[74] Annapureddy, H. V. R.; Margulis, J. *J. Phys. Chem. B* **2009**, *113*, 12005.

[75] Ando, K.; Hynes, J. T. *J. Phys. Chem. B* **1997**, *101*, 10464.

[76] Ando, K.; Hynes, J. T. *J. Phys. Chem. A* **1999**, *103*, 10398.

[77] Yamazaki, S.; Kato, S. *J. Chem. Phys.* **2005**, *123*, 114510.

[78] Higashi, M.; Kato, S. *J. Phys. Chem. A* **2005**, *109*, 9867.

[79] Mori, T.; Nakano, K.; Kato, S. *J. Chem. Phys.* **2010**, *133*, 064107.

[80] Wang, Y.; Voth, G. A. *J. Am. Chem. Soc.* **2005**, *127*, 12192.

[81] Wang, Y.; Voth, G. A. *J. Phys. Chem. B* **2006**, *110*, 18601.

[82] Canongia Lopes, J. N. A.; Pádua, A. A. H. *J. Phys. Chem. B* **2006**, *110*, 3330.

[83] Shigeto, S.; Hamaguchi, H. *Chem. Phys. Lett.* **2006**, *427*, 329.

[84] Iwata, K.; Okajima, H.; Saha, S.; Hamaguchi, H. *Acc. Chem. Res.* **2007**, *40*, 1174.

[85] Hu, Z.; Margulis, C. J. *Proc. Natl. Acad. Sci. U. S. A.* **2006**, *103*, 831.

[86] For example, *Molecular Theory of Solvation* ; Hirata, F. Eds.; Kluwer Academic Publishers: Netherlands, 2003.

Chapter 7

General Conclusion

In this thesis, the author theoretically investigated solvation effects based on realistic molecular models in complicated solution systems composed of complex solute or solvent molecules: reactions with transition metal complexes and chemical events in ionic liquids. The achievements of this thesis is summarized as follows.

In part I, the author studied solvation effects of a reaction of Pt(II) complexes with methylioide in nitromethane focusing on liquid structure of neat nitromethane and solvation structures around Pt complexes.

In chapter 2, the liquid structure obtained by RISM theory is assigned to two dimer structures given by one of the sophisticated electronic structure theory, MP2. MP2 calculations exhibit the antiparallel and head-to-tail conformations. The distances between atoms in the conformations coincide well with the peak distances in the PCFs of liquid nitromethane. This never indicates the existence of the association pair with certain life time but all the molecules move around the "cluster" geometries. The peak distance in H–O PCFs is longer than typical hydrogen bond. The peak distances in PCFs between heavy atoms (N or C) computed with the charge-removed model differ from those calculated with charged model. From these findings, we can conclude that the liquid structure of nitromethane is governed by not hydrogen bond but the charges assigned to heavy atoms.

In chapter 3, the author investigated solvation effects in an oxidative addition reaction of $PtMe_2(NH_3)_2$ with methyliodide by using RISM-SCF-SEDD method. It is known that the

reaction proceeds via S_N2-like mechanism and the reaction is accelerated by 10 times in polar solvent such as nitromethane. After the nucleophile attack with the electron transfer from d_{z^2} orbital to antibonding orbital in MeI, two different reaction paths are conceivable: (i) the iodide anion dissociates from the cationic Pt complex and solvated separately or (ii) the iodide anion attaches to the Pt complex by strong Coulomb interaction. While in nitromethane the path (i) is favorable compared with (ii), in gas phase the reaction proceeds via the path (ii), indicating that solvation effects play important roles to determine not only the reaction barrier but also the reaction path. From the analysis on solvation structures, we can conclude that since the positive of negative charges are localized on the Pt center and iodide anion due to the electron transfer, these atoms are strongly solvated by oxygen or methyl group in nitromethane, respectively.

In part II, theoretical studies on solvaton mechanisms of chemical phenomena in ionic liquids are presented.

In chapter 4, a theoretical analysis on a Diels-Alder reaction of cyclopentadiene (CP) with methylacrylate (MA) which leads *endo* and *exo* forms in one of the standard ionic liquids, [mmim][Cl], is performed in two respects: mechanisms of modest polarity of ionic liquids and the *endo-exo* selectivity. The *endo-exo* selectivity is sensitive to the solvent polarity and the selectivity in typical ionic liquids is weaker than that of water while it is stronger than ether. Considering the strong Coulomb interaction among constituent ions, the origin of modest polarity of ionic liquids is not apparent. We have established a procedure, in which chemical reactions in ionic liquids can be treated with *ab initio* molecular orbital theories. The obtained selectivity semi-quantitatively reproduces the experimental one. The selectivity is roughly understood by dipole moment of solute molecules; the total dipole moment in *endo*-TS is enhanced because the dipole moments of CP and MA are in the same direction. To assess the magnitude of electrostatic interaction, charge density functions, which express the distribution of electrostatic potential acting on solute site from solvent molecules, are introduced. The order of peak heights in the charge density of each solvent is consistent with that of the selectivity, which indicates that the electrostatic interaction in ionic liquids is weaker than that of

water because the number density of ionic liquids is smaller than that of water. In other words, the modest polarity of ionic liquids stems from that the number of solvent ions directly interact with the solute molecule is small due to the bulkiness of ions.

Chapter 5 describes a study on a menshutkin-type reaction of *p*-nitrobenzenesulfonate (*p*-NBS) with chloride anion in [mmim][PF_6]. The calculated activation barrier in ionic liquids is higher than that of dichloromethane, which is consistent with the experimental observation. From the changes in solvation free energy and solvation structure, it is clarified that the barrier height is governed by the solvation of chloride anion and de-solvation of the anion makes it possible to act as a nucleophile and give rise to the reaction. Regardless of employing a highly sophisticated CCSD theory, the reaction barrier is overestimated compared with the experimental one, suggesting the limitation of the model adopted in this case. This is presumably because the assumption inherent in the conventional RISM theory; because the solvent geometry is fixed at a specific one, effects of the flexibility of side chain seen in most ionic liquids are not incorporated.

In chapter 6, the author investigated an excited-state intramolecular proton transfer reaction of 4′-N,N-diethylamino-3-hydroxyflavone (DEAHF) in [bmim][PF_6]. To overcome the aforementioned limitation in RISM theory, flexible-RISM theory, in which the fluctuation of solvent geometries are incorporated, are utilized. Employing TDDFT method to calculate the free energy curves along the proton transfer reaction, two second minima assigned to normal and tautomer forms are found in the excited state, which is consistent with the experiment that dual fluorescent spectra are observed. The calculated absorption and emission energies correctly reproduce the experimental spectra while the tautomer emission is overestimated by 0.23 eV. The excitation is characterized by charge transfer transition from the HOMO on amine moiety to the LUMO on flavonole moiety. Drastic changes in dipole moment are accompanied with the excitation and excited-state proton transfer. The fast chemical process such as electron transfer and proton transfer reactions are affected by solvent fluctuation. Applying the method to evaluate free energy changes due to the solvent fluctuation, the relation between solvent relaxation and proton transfer process is discussed. From the changes in proton potential, it

is suggested that the barrier in proton transfer process is relatively low immediately after the excitation while the barrier becomes higher as the solvent relaxation proceeds.

The author believes that the thesis offers molecular-level understanding on the solvation mechanisms in complicated solution systems: reactions with transition metal complexes and chemical phenomena in ionic liquids. He is also confident that the real-system model adopted in the thesis is powerful tool to investigate the complex chemical phenomena in solution.

List of Publications

Publications included in this thesis

Chapter 2

"A Theoretical Study of the Liquid Structure of Nitromethane with RISM Method"

Hayaki, S.; Sato, H.; Sakaki, S.

J. Mol. Liq., **2009**, *147*, 9.

Chapter 3

"Solvation Effects in Oxidative Addition Reaction of Methyliodide to Pt(II) Complex: A Theoretical Study with RISM-SCF Method"

Hayaki, S.; Yokogawa, D.; Sato, H.; Sakaki, S.

Chem. Phys. Lett., **2008**, *458*, 329.

Chapter 4

"A Theoretical Analysis of a Diels-Alder Reaction in Ionic Liquids"

Hayaki, S.; Kido, K.; Yokogawa, D.; Sato, H.; Sakaki, S.

J. Phys. Chem. B (*Letters*), **2009**, *113*, 8227.

Chapter 5

"*Ab initio* study on S_N2 reaction of methyl *p*-nitrobenzenesulfonate and chloride anion in [mmim][PF_6]"

Hayaki, S.; Kido, K.; Sato, H.; Sakaki, S.

Phys. Chem. Chem. Phys., **2010**, *12*, 1822.

Chapter 6

"An *ab initio* study on an excited-state intramolecular proton transfer reaction in ionic

liquids”

Hayaki, S.; Kimura, Y.; Sato H.

Submitted.

Other publications

1. “Valence ionization spectra of group six metal hexacarbonyls studied by the symmetry-adapted cluster-configuration interaction method”
   Fukuda, R.; Hayaki, S.; Nakatsuji, H.
   J. Chem. Phys., **2009**, *131*, 174303.

2. “3D-RISM-KH Molecular Theory of Solvation and Density Functional Theory Investigation of the Role of Water in the Aggregation of Model Asphaltenes”
   da Costa, L. M.; Hayaki, S.; Stoyanov, S. R.; Gusarov, S.; Tan, X.; Gray, M. R.; Stryker, J. M.; Tykwinski, R.; Carneiro, J. W. M.; Sato, H.; Seidl, P. R.; Kovalenko, A.
   Phys. Chem. Chem. Phys., **2012**, *14*, 3922.